# HYDROPNEUMATIC SEMI-ACTIVE SUSPENSION SYSTEM WITH CONTINUOUSLY VARIABLE DAMPING

By

André Gerhard Vosloo

Submitted in partial fulfilment of the requirements for the degree

Master of Engineering
(Mechanical Engineering)

in the

Department of Mechanical and Aeronautical Engineering
Engineering, Built Environment and Information Technology

UNIVERSITY OF PRETORIA


June 2019

# SUMMARY


**HYDROPNEUMATIC SEMI-ACTIVE SUSPENSION SYSTEM WITH CONTINUOUSLY VARIABLE DAMPING**

By

**André Gerhard Vosloo**

**Supervisor:** Prof. P.S. Els

**Department:** Mechanical and Aeronautical Engineering, University of Pretoria

**Degree:** Master of Engineering (Mechanical Engineering)

**Keywords:** Semi-active suspension; Hydropneumatic; Variable damping; Skyhook control

A well-known challenge in vehicle dynamics is to design a vehicle that will not only keep the occupants comfortable, but will also ensure safe and stable operation during various manoeuvres over multiple driving surfaces. A soft and compliant suspension is generally required for good ride comfort, while a stiff suspension with a low centre of mass is required for improved handling. These contradicting factors in the design process is commonly referred to as the ride comfort versus handling compromise.

A newly developed semi-active hydropneumatic suspension system is proposed to reduce or negate this compromise by being able to change its characteristics according to the dynamic state of the vehicle. The unit is equipped with two proportional solenoid valves that can provide continuously variable damping. In addition, the valves are able to completely close off flow to compressible gas volumes to provide four discrete stiffness characteristics.

This suspension system is based on a previously developed suspension that had only two state (open or closed) valves, which provided discrete damping characteristics. A thorough investigation of the older system proved that the system was capable of addressing the ride comfort versus handling compromise. The purpose of this study was to investigate whether the updated design could deliver improved performance and to recommend focus areas for future research initiatives.

The suspension system's characteristics were determined experimentally by actuating the unit on a test bench. Results indicated that the unit produced the desired stiffness, low damping and response time characteristics. A mathematical model of the suspension unit was developed and validated against experimental data. The model was used in single degree of freedom simulations to investigate both passive and semi-active controlled performance. Results indicated that the suspension could be semi-actively controlled for improve ride comfort. However, the magnitude of improvements with semi-active control, which includes a suitable response time, proved to be rather insignificant compared to the optimum passive suspension.

The findings proved that the suspension system was capable of successfully reducing the ride comfort versus handling compromise. Compared to the previous model, it is expected to deliver improved ride comfort and handling performance when implemented on the vehicle.

# ACKNOWLEDGEMENTS

I would like to thank the following persons who contributed in various ways to the project:

- Project supervisor Prof P.S. Els from the University of Pretoria for his guidance and patience throughout my undergraduate and postgraduate studies.
- My parents who provided a very privileged upbringing allowing me to study full time. Without your continuous support and motivation this project would not have been possible.
- My girlfriend, Ane Janse van Rensburg whose love and continuous support ensured the successful completion of the project.
- Johann Clark and the Sasol laboratory staff for their assistance during experimental setup and testing.
- The Vehicle Dynamics Group of the University of Pretoria for their support and advice, especially my research colleagues: Devin Johnson, Jacques Jooste, Karthik Poovendran, Odette Scholtz and Nico van der Merwe.

# TABLE OF CONTENTS

# LIST OF FIGURES

# LIST OF TABLES

# LIST OF ABBREVIATIONS

| | |
|---|---|
| $4S_4$ | 4-state semi-active suspension system |
| $4S_4$CVD | 4-state semi-active suspension system with continuously variable damping |
| ABS | Antilock braking system |
| ADAMS | Automatic Dynamic Analysis of Mechanical Systems (Computer software) |
| BWR | Benedict-Webb-Rubin |
| BS | British Standard |
| CES | Continuously controlled electronic suspension |
| CVD | Continuously variable damping |
| DAQ | Data acquisition |
| EE | Energy equation |
| HiL | Hardware-in-the-loop |
| IG | Ideal gas |
| ISO | International Organisation for Standardization |
| LOWESS | Locally weighted scatterplot smoothing |
| LVDT | Linear variable differential transformer |
| MOSFET | Metal-oxide-semiconductor field-effect transistor |
| MR | Magneto-rheological |
| MR$4S_4$ | Magneto-rheological equipped 4-state semi-active suspension system |
| NC | Normally closed |
| NO | Normally open |
| RMS | Root mean square |
| RRMS | Running root mean square |
| SUV | Sports utility vehicle |
| SDOF | Single degree of freedom |

# LIST OF SYMBOLS

## English symbols

| Symbol | Description | Units |
|---|---|---|
| $A$ | Area | $[m^2]$ |
| $a$ | BWR constant | $[\left(\frac{m^3}{kg}\right)^3 \frac{N}{m^2}]$ |
| $A_0$ | BWR constant | $[\left(\frac{m^3}{kg}\right)^3 \frac{N}{m^2}]$ |
| $b$ | BWR constant | $[(m^3/kg)^3]$ |
| $B_0$ | BWR constant | $[m^3/kg]$ |
| $c$ | Damping coefficient | $[Ns/m]$ |
| | BWR constant | $[\left(\frac{m^3}{kg}\right)^3 K^2 \frac{N}{m^2}]$ |
| | Specific heat | $[J/kgK]$ |
| $C_0$ | BWR constant | $[\left(\frac{m^3}{kg}\right)^3 K^2 \frac{N}{m^2}]$ |
| $d$ | Derivative of | $-$ |
| $F$ | Force | $[N]$ |
| $f$ | Frequency | $[Hz]$ |
| | Function of | $-$ |
| $g$ | Gravitational constant | $[m^3/kg \cdot s^2]$ |
| I | Solenoid coil current | $[A]$ |
| $k$ | Spring rate or spring stiffness | $[N/m]$ |
| $m$ | Mass | $[kg]$ |
| $M$ | Refers to the mass of a body in vehicle model (see subscripts) | $[kg]$ |
| $N$ | Specific heat constant | $-$ |
| | Total number of data points | $-$ |
| $n$ | Data point number | $-$ |
| $P$ | Pressure | $[Pa]$ |
| $Q$ | Volumetric flow rate | $[m^3/s]$ |
| $\dot{Q}$ | Heat transfer rate between the system and environment | $[W]$ |
| $R$ | Universal gas constant | $[J/kgK\ ]$ |
| $T$ | Temperature | $[K]$ |
| $t$ | Time | $[s]$ |
| $\dot{U}$ | Change in internal energy of the gas | $[W]$ |
| $\dot{u}$ | Change in specific internal energy of the gas | $[W/kg]$ |
| $V$ | Volume | $[m^3]$ |
| $\dot{V}$ | Change in volume | $[m^3/s]$ |
| $v$ | Specific Volume | $[m^3/kg]$ |
| $\dot{W}$ | Work done on the system (piston on gas) | $[W]$ |
| $W_b$ | Frequency weighting function for seated persons | $-$ |

| Symbol | Description | Units |
|---|---|---|
| $x$ | Displacement | $[m]$ |
| | Suspension deflection | $[m]$ |
| $\dot{x}$ | Velocity | $[m/s]$ |
| | Suspension deflection velocity | $[m/s]$ |
| $\ddot{x}$ | Acceleration | $[m/s^2]$ |
| y | BWR constant | – |

## Greek Symbols

| Symbol | Description | Units |
|---|---|---|
| $\alpha$ | BWR constant | $[\left(\frac{m^3}{kg}\right)^3 \frac{N}{m^2}]$ |
| $\beta$ | Bulk modulus of fluid | $[GPa]$ |
| | Bouc-Wen model parameter | – |
| $\Delta$ | Change or difference | – |
| $\delta$ | Bouc-Wen model parameter | – |
| $\gamma$ | BWR constant | $[(m^3/kg)^2]$ |
| $\sum$ | Sum of | – |
| $\tau$ | Thermal time constant | $[s]$ |
| $\zeta$ | Damping ratio | – |

## Subscripts

| Subscript | Symbol | Description |
|---|---|---|
| $1, 2, \ldots, 9$ | $N$ | Indicates specific heat constant |
| | $P, V$ | Indicates accumulator (1 or 2) and strut (3) property |
| $1to2$ | $Q$ | Fluid flow from accumulator 1 to accumulator 2 |
| $4S_4CVD$ | $F$ | Double accumulator 4S$_4$CVD force |
| $4S_4CVD^*$ | $F$ | Single accumulator 4S$_4$CVD force |
| $acc$ | $P, V$ | Accumulator property |
| $controllable$ | $c$ | Controllable damper damping coefficient |
| $d$ | $F$ | Damper force |
| $f$ | $F$ | Friction force |
| | $\Delta P$ | Final pressure drop after response |
| $frac$ | $P$ | Fraction which defines gradual pressure change |
| | $Q$ | Fraction which defines flow split |
| $g$ | $T$ | Gas temperature |
| $i$ | $\Delta P$ | Initial pressure drop before response |

| Subscript | Symbol | Description |
|---|---|---|
| $n$ | $f$ | Natural frequency |
| $oil$ | $V$ | Volume of the suspension fluid |
| $piston$ | $A$ | Suspension piston rod area |
| $res$ | $t$ | Response time |
| RMS | $\ddot{x}$ | Root mean square of acceleration |
| $s$ | $F$ | Spring force |
| | $T$ | Temperature of the environment |
| | $M$ | Sprung mass |
| | $x$ | Sprung mass displacement |
| $sky$ | $F$ | Skyhook control logic force |
| | $c$ | Skyhook control logic damping coefficient |
| $u$ | $M$ | Unsprung mass |
| | $x$ | Unsprung mass displacement |
| $v$ | $c$ | Specific heat constant |
| $V1, V2$ | $\Delta P$ | Pressure drop over valve 1 or 2 |
| $valve$ | $\Delta P$ | Pressure drop over valve |

## Superscripts

| Subscript | Symbol | Description |
|---|---|---|
| 0 | $c$ | Ideal gas heat constant |

# *Chapter 1:*
# *INTRODUCTION*

This chapter will provide the reader with background to the origin of the problem and why a solution is required. The origins of the suspension system used in the study will briefly be mentioned, as it is essentially a continuation of multiple other studies that form the basis of the design. Application of similar systems in the industry will also be investigated. Furthermore, the chapter will provide the aim and overview of the study.

## 1.1 Background

In vehicle dynamics, the suspension system plays the vital role of establishing the link between the road (through the tyres) and the vehicle body. It not only has to manage the vertical dynamics, but also the rotational (roll and pitch) dynamics induced by the driver and road interface. The fundamental purpose of a vehicle's suspension system can be narrowed down to two functions: first, to provide handling or road-holding that allows the vehicle to be controlled in a safe and stable manner by the driver and, secondly, to isolate the passengers from the road disturbances by providing ride comfort. However, the design of a vehicle's suspension system always involves a compromise between these two functions. Designing for handling requires a stiffer suspension system with low suspension travel, combined with a low vehicle body centre of gravity that will decrease body roll. On the other hand, designing for ride comfort requires a compliant, soft suspension system with more suspension travel that will be able to absorb the road disturbances.

Passive suspension systems, currently equipped on all lower-end passenger vehicles, have fixed stiffness and damping characteristics that cannot be changed during operation. However, some vehicles are used on vastly different terrain, ranging from smooth highways to rough cobblestone or dirt roads. Furthermore, the vehicle could be carrying a load, which also drastically change the optimum characteristics required. It is therefore a huge challenge to design a passive suspension system for such a large operating range and the designer invariably has to make a trade-off by sacrificing one or the other.

A simple example of this is a sports car that will handle well on smooth roads, but is very uncomfortable on rough roads, compared to an off-road vehicle or SUV (sports utility vehicle) that is much more comfortable on a rough road but lacks the handling and stability. Although sedan-type passenger vehicles also sacrifice some handling and stability for comfort, SUVs, pickups and off-road vehicles are most susceptible to the negative effects. This is because they are expected to travel at highway speeds, but also have off-road capabilities where they will experience much rougher roads requiring more suspension travel. Their higher centre-of-mass design make them prone to rollover, which could lead to a fatal accident.

A passive suspension system is evidently not capable of achieving the desired combination of handling and ride comfort characteristics and invariably leads to a compromise. However, controllable suspension systems have the potential to reduce or eliminate this compromise. By using such a suspension system, the spring and damper characteristics could be changed according to the type of road the vehicle is travelling on, the load it is carrying or the dynamic state of the vehicle in order to achieve improved handling and/or comfort.

Controllable suspension systems can be classified according to energy requirements, response time and the variability of its spring and damper characteristics. Various technologies have successfully been incorporated in controllable suspension systems to achieve the variable spring and/or damper characteristics. Each class and technology has specific benefits and drawbacks. For a comprehensive presentation see Els (2006), Savaresi et al. (2010) and Guglielmino et al. (2008).

The proposed controllable suspension that forms the topic of this study, is a newly developed prototype originating from the hydropneumatic 4-state semi-active suspension system, $4S_4$ (Els, 2006). The $4S_4$, appropriately named, since it can provide two stiffness characteristics by selectively blocking flow towards two independent accumulators, as well as two damping characteristics by altering the flow path through or around a damper pack. The $4S_4$ was found to successfully reduce the ride comfort versus handling compromise.

In an attempt to improve the $4S_4$, continuously variable damping was initially investigated through the use of magneto-rheological (MR) fluid technology. Such a system uses an electromagnet to generate a magnetic field, thereby greatly increasing the viscosity of the suspension fluid (now MR fluid). Grobler (2016) investigated this proposition with a new design, referred to as the $MR4S_4$, which replaced the solenoid valves and damper packs with two MR valves controlling the flow to each of the two accumulators. Heymans (2017) further optimised the valve and its design, which showed much improvement and promise, but concluded that the system inherently lacked a few of the desired qualities.

An alternative approach to incorporate continuously variable damping is used in the suspension system that forms the topic of this study. This suspension, which is based on the $4S_4$, can be referred to as the 4-state semi-active suspension system equipped with continuously variable damping ($4S_4$CVD). It makes use of proportional, bi-directional flow-control solenoid valves that can control the flow to provide variable damping or completely block the flow to limit the amount of compressible fluid or gas, resulting in a set of discrete spring characteristics. The $4S_4$CVD will be discussed further in section 2.2.

This study does not include the design process of the $4S_4$CVD. It focus is on investigating the feasibility of the $4S_4$CVD by experimentally determining the suspension characteristics, developing a model and using it in simulation to evaluate its potential performance.

## 1.2 Research objective

The purpose of this study is to investigate whether the newly developed prototype $4S_4$CVD could effectively solve the ride comfort versus handling compromise. The vehicle for which it is ultimately intended is a Land Rover Defender 110. Its performance should also be compared to the previous solutions in order to evaluate if any improvements had been realised. In order to determine this, the suspension system should be experimentally characterised. The data should then be used to develop and validate a model that could be used in simulation to analyse the performance of the suspension system, combined with a suitable control strategy. An accurate model would also be required as it could be a powerful tool for use in future research initiatives investigating other aspects.

Since this is the first investigation into this prototype, the process will be kept as simple as possible and as complicated as necessary. Consequently, the vertical dynamics would primarily be considered. It should be noted that suspension characteristics also affect other ground-vehicle dynamics such as roll, pitch and yaw and therefore complete suspension control would be a matter of global chassis control improvement. These aspects are to be considered once the vertical dynamics have successfully been analysed in order to justify further research.

The study aims to conclude by providing a justified recommendation regarding the feasibility and possible implementation of the suspension system based on the experimental and simulation results. This would include comparing the newly developed prototype to previous versions to determine the improvements, if any. Possible improvements, alternative solutions and areas that would require further investigation should be proposed in order to support the continuation of the research.

## 1.3 Overview of study

This document is organised as follows:

Chapter 1: Introduction

This chapter provided background information to the problem and the suspension that form the topic of the study. The research objective has been defined to help understand and guide research and investigations throughout the study.

Chapter 2: Literature review

A thorough literature review of all relevant topics related to the study is presented to describe the problem in detail, highlight challenges and formulate possible solutions. These topics include ride comfort and handling, controllable suspension and its classification, hydropneumatic suspension development at the University of Pretoria, suspension and vehicle modelling as well as suspension control. The chapter will conclude with a detailed problem statement.

Chapter 3: Characterisation

In this chapter, the experimental setup used to characterise the suspension is presented, along with the testing procedures, experimental results and extracted suspension characteristics. These characteristics would include the spring, damper, response time, friction and flow-block ability.

Chapter 4: Suspension modelling

The extracted suspension characteristics and tests results are used to develop a mathematical model of the suspension unit in this chapter. Each sub-system in the model is discussed and validated according to experimental results. Possible suspension characteristics are presented and compared to previous suspension systems.

Chapter 5: Simulation and control

In this chapter, the mathematical model of the suspension is used in simulation to analyse the potential performance of the unit. The vehicle and suspension model used in simulations is discussed. Passive and actively controlled ride comfort performance is evaluated and compared.

Chapter 6: Conclusions and recommendations

The final chapter concludes the overall study based on the results obtained. Recommendations regarding the capabilities of the current suspension system and focus areas for future research and investigations are discussed.

# *Chapter 2:*
# *LITERATURE REVIEW*

This chapter provides a detailed review of relevant literature to fully comprehend and study the problem the research aims to address. Literature required to reach the research objectives is also identified and discussed.

## 2.1 Ride comfort versus handling

Ride comfort and handling were already briefly mentioned in section 1.1, where the requirements for good ride comfort and those for handling were shown to be opposing design factors. Having a soft suspension for good ride comfort versus a stiff suspension for handling, highlighted the fact that a passive suspension system involves a compromise between ride comfort and handling. This section aims to further investigate the ride comfort versus handling compromise and how it can be used to evaluate the performance of the suspension system. These criteria also play a critical role in the development of a control strategy for the suspension system to achieve the optimum characteristics.

### 2.1.1 Ride comfort

Ride comfort can refer to various factors which can cause discomfort to its occupants such as vibrations, temperature, ergonomics, etc. In this study we consider the vibration based ride comfort. This is predominantly associated with the vertical dynamics of the vehicle, which is caused by the road disturbances exciting the vehicle. According to Gillespie (1992) vibrations ranging from 0-25Hz determines the perceived vehicle ride, while higher frequency disturbances are classified as noise. Ride comfort is fundamentally a description of how comfortable the occupants perceive the ride to be. However, it may be difficult to quantify or compare these subjective perceptions. This is especially challenging as the human body is known to be more sensitive to certain frequencies than to others. Furthermore, other variables such as posture and demographics could also play a role in how comfortable the occupant perceives the ride (British Standards Institution, 1987).

To objectively evaluate ride comfort, the vertical acceleration response of the vehicle subjected to a disturbance is commonly used throughout literature. In simulation and experiments the input disturbance can be a step or bump; a measured road, such as a Belgian paving; or even a frequency sweep to expose the system to an entire range of frequencies (Savaresi et al., 2010). As the human body is more sensitive to excitations at certain frequencies, a weighting function is applied. Ride comfort is described as follows by Harty (2003): “Ride comfort is a frequency weighted measure of vertical acceleration, together with subjective assessments of harshness over lateral features and other secondary behaviours.”

There are a few methods to objectively evaluate ride comfort. However, a comparative study done by Els (2005) concluded that any of the four methods considered by him could be used to objectively determine ride comfort. This study will focus on the assessment of ride comfort according to the British Standard BS 6841 (British Standards Institution, 1987). The method consists of measuring vertical acceleration, applying a frequency weighting function and then calculating the root mean square (RMS) value of the weighted accelerations. The frequency weighting function $W_b$, specified by the BS 6841 for seated persons in the vertical direction, is illustrated in Figure 2.1. This weighting is used by Paddan and Griffin (2002), who stated that maximum passenger discomfort occurs in the frequency range from 4 to 8Hz. Knowledge of human response to different frequency vibrations would

allow the designer to tune or control the suspension system for better ride comfort. After weighting the vertical accelerations, the RMS is determined as in eq. (2-1).

$$\ddot{x}_{RMS} = \sqrt{\frac{1}{N} \cdot \sum_{n=1}^{N} \ddot{x}^2} \qquad \textit{(2-1)}$$

where $\ddot{x}$ represents the acceleration, $N$ the total number of data points and $n$ the data point number. The weighted RMS of the acceleration, $\ddot{x}_{RMS}$ can then be used to determine the harshness of the ride, or alternatively directly compared to data obtained at the same vehicle speed and road conditions in another vehicle or suspension setting.

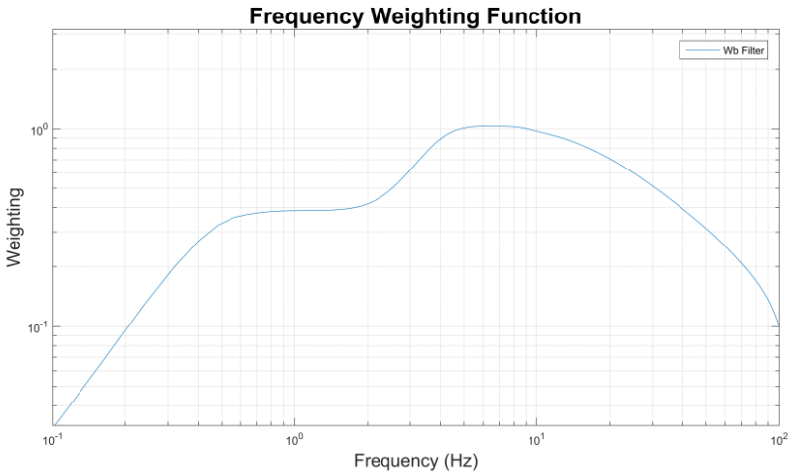


***Figure 2.1: BS 6841 Frequency weighting***

### 2.1.2 Handling

Handling is generally associated with the lateral, yaw and roll dynamics of the vehicle due to steering inputs by the driver. According to Gillespie (1992), handling is associated with the cornering behaviour of a vehicle and implies the responsiveness of a vehicle to driver input or ease of control.

Another property associated with handling in regard to suspension performance is the road-holding capabilities of a vehicle. Road-holding refers to the ability of the vehicle, more specifically its tyres, to keep contact with the road over uneven surfaces and during dynamic vehicle conditions. This is critical, since the longitudinal and lateral forces the vehicle can generate is strongly related to the vertical wheel load (Savaresi et al., 2010). Increased road-holding would therefore result in better overall grip resulting in, among others, improved corning capabilities and stopping distance. Savaresi used tyre deflection or the change in distance between the wheel and the ground to determine the ability of road-holding or handling. The aim is therefore to not only keep the wheel in contact with the road, but to also reduce the change in vertical load.

Although vehicle rollover, where a vehicle tips over onto its side or roof, could be related to handling, it is not necessarily a property of a vehicle's handling capability. Gillespie (1992) defines roll as a function of roll stiffness, which is therefore also a function of suspension stiffness. Excess roll, combined with a high centre of mass during lateral acceleration-generated manoeuvres, could lead to rollover. Consequently, SUVs and off-road vehicles with high centres of gravity are prone to rollover before the limits of tyre side force are generated. Rollover has a higher fatality rate than any other type of vehicle accident. A mere 2.1% of all accidents in the USA in 2010 involved rollover, however, rollover still accounted for 35% of fatalities from passenger-vehicle accidents (National Highway Traffic Safety Administration, 2010). It is therefore paramount that rollover be prevented when considering handling.

Although ride comfort has been extensively researched, a single unambiguous method to objectify handling performance is not as clear in the vehicle dynamics field. Handling tests can be divided into two main categories: steady-state handling tests and dynamic handling tests, which are also referred to as transient response tests (Els, 2006). A constant radius test is the most common steady-state handling test. It compares lateral acceleration to steering angle while the vehicle gradually increases speed while maintaining a constant radius turn (Gillespie, 1992). A severe double lane change manoeuvre (International Organization for Standardization, 1999) is a commonly used dynamic handling test. This test can either be performed closed loop, where the vehicle is corrected to stay on a path; or open loop, where a prescribed steering angle versus time is applied. These steering inputs can be manually applied or computer controlled.

A study conducted by Uys et al. (2006) investigated criteria for handling measurement in order to determine switchover from a ride comfort suspension setting to a handling suspension setting. Their results indicated that roll angle, lateral acceleration and yaw rate were interrelated for several of the manoeuvers considered. They concluded that roll angle, within acceptable limits, was a suitable metric to measure handling in order to determine the moment of switchover.

### 2.1.3 The ride comfort versus handling compromise

Section 1.1 discussed many of the well-known reasons that force engineers to compromise between ride comfort and handling when designing vehicle suspensions. Characteristics required for good ride comfort conflict with those required for good handling and stability. Optimum passive suspension characteristics for ride comfort and handling were investigated on a landmine-protected vehicle (Els and Van Niekerk, 1999) and a Land Rover Defender 110 (Els, 2006). Both studies highlighted that, for all handling cases considered, much higher spring and damper characteristics were required, while all the ride comfort cases considered required soft springs and low damping when compared to the baseline vehicle. These optimum characteristics were used to successfully develop and implement a hydropneumatic semi-active suspension system to effectively reduce the ride comfort versus handling compromise (Els, 2006).

Savaresi et al. (2010) includes various studies which focused on finding the optimal performance of a semi active suspension evaluated in terms of comfort and handling. In these studies a quarter-car model (to be discussed in section 2.5) was used to analyse the effect damping has on the vertical dynamics. Figure 2.2 shows the effect passive damping has on comfort and road-holding: The vehicle chassis resonance can be noted at about 2Hz, while wheel resonance is around 13Hz. When considering road to body height response, it is evident that, at the critical comfort perceiving frequencies (4-10Hz), lower damping would improve ride comfort, however, at low frequencies (<2Hz) high damping would actually be beneficial. The opposite is evident when considering road to tyre deflection. At frequencies below 2Hz and above 13Hz, higher damping would provide better road-holding, while low damping would actually provide better road-holding at the frequencies between these parameters. It was concluded that there is a clear compromise between optimal road-holding and ride comfort. Interestingly, it also shows that designing purely for ride comfort or road-holding would also include a degree of compromise between the frequency ranges. The optimal damping is therefore based on the road disturbance excitation which can either be biased towards ride comfort or road holding.

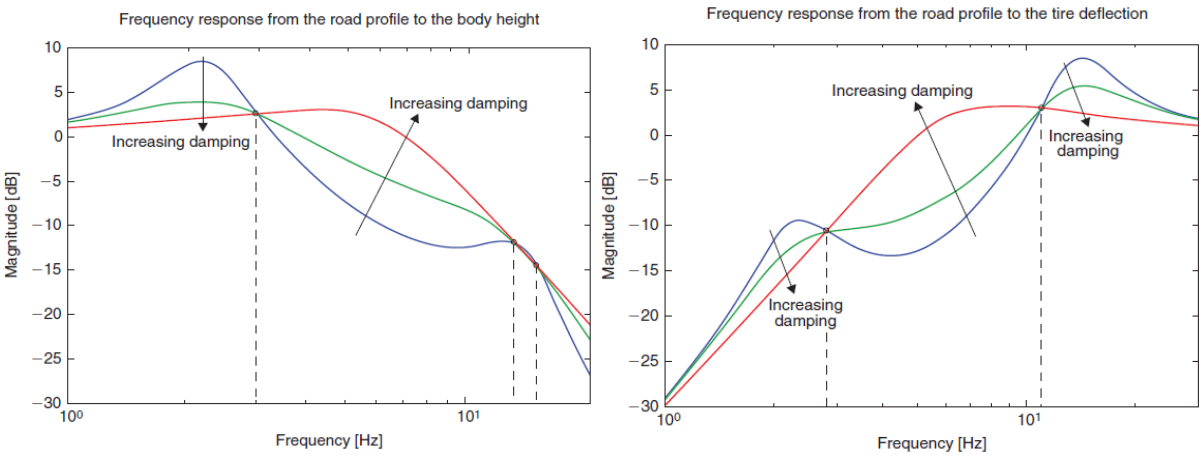


***Figure 2.2: Frequency response of passive suspension (Savaresi et al., 2010)***
***Road to chassis displacement (left), Road to tyre displacement (right)***

## 2.2 Hydropneumatic semi-active suspension development at the University of Pretoria

The investigation into a new prototype suspension that is the topic of this study, is based on multiple other prototypes and studies done at the University of Pretoria. In order to recognise where this system aims to make advancements, the previous systems and their respective studies had to be reviewed. As is commonly used in literature, suspension force resisting compression and relative compressive displacement or velocity is considered negative and extension or rebound considered positive. This convention is used throughout this report.

### 2.2.1 The 4-state semi-active suspension system ($4S_4$)

The University of Pretoria initially developed a semi-active hydropneumatic suspension system with the intent of solving the ride comfort versus handling compromise on a Land Rover Defender 110 (Els, 2006). Els identified the challenge and need for vehicles that offer good off-road capabilities (high ground clearance, large suspension travel and soft springs), but also good handling and stability on smooth roads at high speeds (low centre of gravity and stiff springs). The suspension system focused on wheeled military vehicles and SUVs.

Els (2006) conducted full-vehicle model simulation and determined that, in order to eliminate the ride comfort versus handling compromise, at least two discrete spring and two damper characteristics were required: A stiff spring and high damping suspension for handling, or a soft spring and low damping suspension for ride comfort. The suspension system developed by Els is appropriately called the 4-state semi-active suspension system or simply $4S_4$, as it is capable of two discrete damping as well as two stiffness characteristics, which can be combined to give four different states. The different states is achieved by channelling the fluid flow through the various switching of solenoid valves, as shown in Figure 2.3.

The $4S_4$ design consisted of two pressurised accumulators (with floating pistons), with two state (open or closed) solenoid spool valves that could block or open certain flow paths. With valve 3 opened, both gas volumes could be compressed, which yielded low stiffness, while when closed, only accumulator 1 could be compressed resulting in higher stiffness. The damping states were controlled by having bypass solenoid valves (valves 1 and 2) for each damper leading to the accumulators. With the bypass valves opened, low damping was achieved, while when closed, the fluid was forced through the damper pack resulting in high damping.

Els (2006) characterised the $4S_4$ on a hydraulic test bench, as shown in Figure 2.4. The spring characteristics were extracted by slowly compressing the unit to negate any damping. Similarly, the damping characteristics were extracted by actuating the unit with a constant velocity triangular displacement wave input. The pressure drop over the damper and valve was then measured to derive the force versus velocity characteristic.

To solve the ride comfort versus handling compromise, the $4S_4$ was designed with up to 300mm of suspension travel configured with two modes or settings namely: ride comfort (low damping and a soft spring) and handling (high damping and a harder spring). The valve response time, which determined switching time between these modes, was between 40 and 100 milliseconds. Based on optimisation (Uys et al., 2007) and design limitations, the $4S_4$ had a combined accumulator volume of $0.5l$ for comfort mode or, by closing off flow to the large accumulator, $0.1l$ for handling mode.

The spring characteristics of the $4S_4$ are shown in Figure 2.5. Note that it does not show any hysteresis, since these are model-generated characteristics; the modelling of the pneumatic spring will be discussed in section 2.4. The negative displacement referred to compression, resulting in a negative force that resisted compression and zero displacement was the point where the suspension was in static equilibrium as installed on the vehicle. The damping characteristics due to the pressure drop over the valve are shown in Figure 2.6. The baseline in the graph is the stock rear damper and is included to indicate that the $4S_4$ has much higher damping for handling and similar damping for ride comfort. However, due to the $4S_4$ being mounted vertically rather than at an angle as with the stock damper, it experiences higher velocities, which translates in a higher than expected damping force. The valve block pressure drop was therefore too high and the "low" damping achieved was not low enough to improve the ride. Els concluded that, for significant ride comfort improvements, the low damping of the $4S_4$ should be less than 50% of the baseline value.

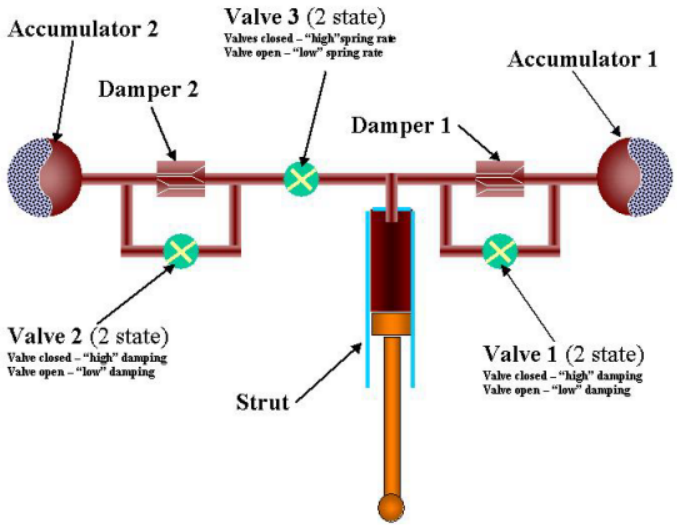


***Figure 2.3: $4S_4$ Design layout (Els, 2006)***

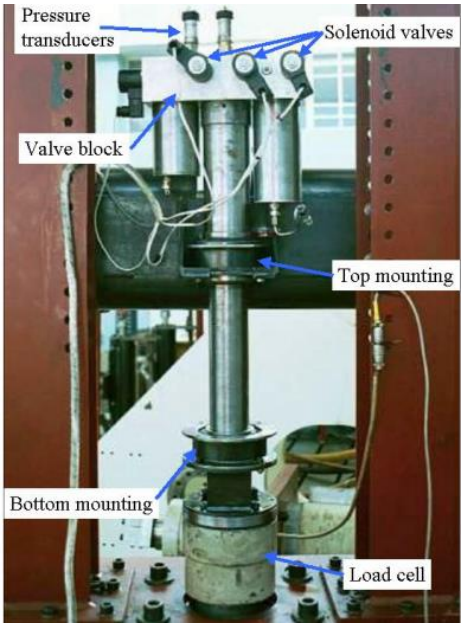


***Figure 2.4: $4S_4$ on Test Rig (Els, 2006)***

To control the switching between the ride comfort or handling modes, a running root mean square (RRMS) of vertical and lateral acceleration were compared. This will be discussed further in section 2.6. The study concluded that the $4S_4$, combined with a suitable control strategy, could successfully eliminate the ride comfort versus handling compromise.

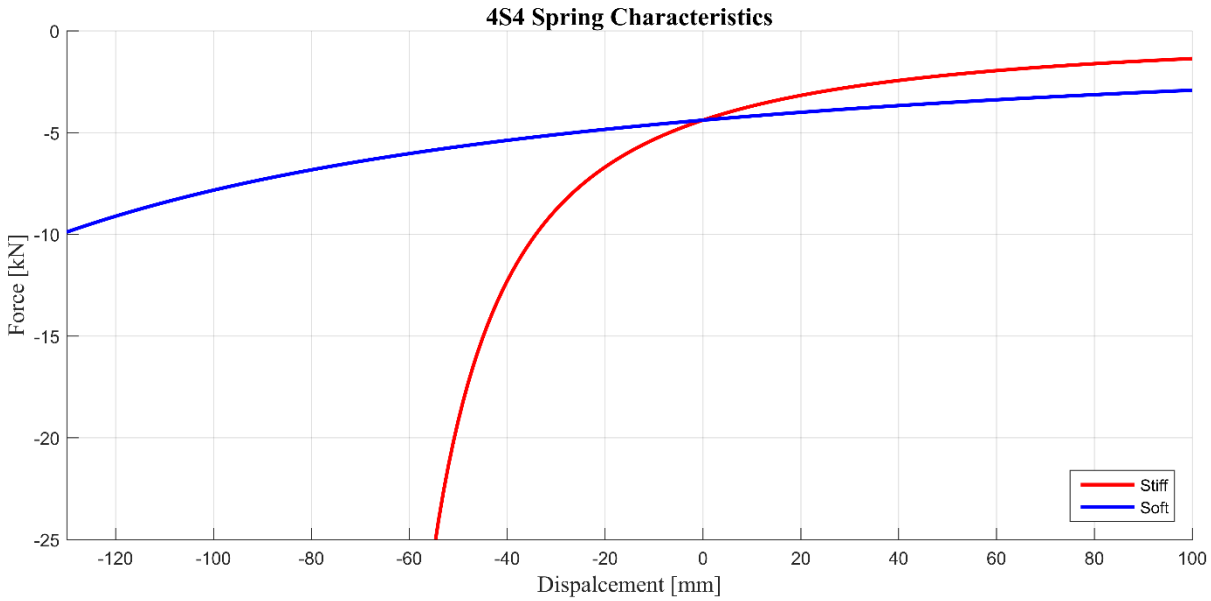


***Figure 2.5: 4S$_4$ Spring characteristics (Els, 2006)***

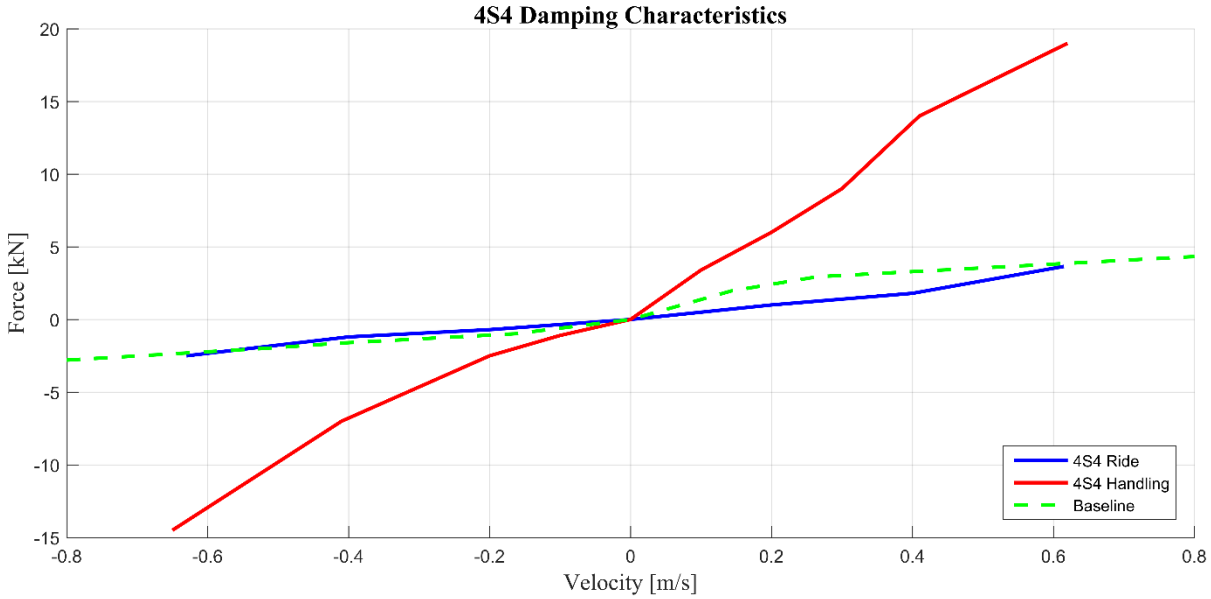


***Figure 2.6: Measured 4S$_4$ Damping characteristics (Els, 2006)***

After successful implementation, Uys et al. (2007) used the 4S$_4$ model in full-vehicle simulations to investigate which spring and damper settings would ensure optimal ride comfort at different speeds on five different road profiles. Optimal spring stiffness seemed to be the softest possible, however, a trend towards increasing stiffness was observable with increasing velocity and road roughness. It was concluded that this was due to preventing bump and rebound stops, which were prone to occur with increasing velocity and road roughness. Optimum damping settings were, however, less predictable or consistent. It was noted that less damping was required as speed increased and more damping was required as the road roughness increased.

Based on this study by Uys et al. (2007), the advantages of being able to continuously change the damping and stiffness characteristics to the suit the road and speed are clear. Obtaining continuously variable stiffness is quite challenging, since it would require a possibly expensive external compressor of some kind. This would add an energy requirement, thereby changing it to an active suspension system. Alternatively, additional accumulators could be added to allow more discreet settings, but this

could raise another challenge due to packaging limitations. Continuously variable damping, on the other hand, showed great promise as literature already indicated multiple methods without greatly increasing cost, complexity or energy requirements. This, along with other advantages of having continuously variable damping, led to an investigation to integrate MR technology into the $4S_4$.

After the successful implementation of $4S_4$ a series of investigations focused on incorporating continuously variable damping based on magneto-rheological (MR) technology (Meeser (2015); Grobler (2016); Heymans (2017)). Heymans ultimately concluded that the MR equipped $4S_4$ ($MR4S_4$) inherently cannot sufficiently further be improved to achieve the desired combination of response time, flow blocking and damping characteristics. Although MR technology in dampers have been proven commercially, these investigations showed that with the current design the technology was unable to meet the demands of a high-pressure hydropneumatic suspension system.

### 2.2.2 Semi-active suspension system equipped with continuously variable damping ($4S_4$CVD)

This study follows an alternative approach to incorporate continuously variable damping within the $4S_4$ design concept (Els, 2006). As previously mentioned, this study does not include the design process of a new hydropneumatic semi-active suspension with continuously variable damping. Most of the design was completed before this study commenced and was manufactured during the initial stages of this study. Therefore, the investigation will focus on the experimental characterisation, modelling and simulation of the unit to form conclusions and recommendations regarding the current design. The newly designed $4S_4$ with continuously variable damping ($4S_4$CVD) is shown in Figure 2.7 and the flow diagram that clarifies the flow path of the suspension fluid in Figure 2.8. The bypass valves, damper packs and shut off valves in the $4S_4$ are essentially replaced by two solenoid flow-control valves. These valves are responsible to restrict flow for increased damping, and blocking flow to decrease the compressible volume for a higher stiffness.

Further changes in the design include a reduction in the piston diameter from 50mm to 32mm. This reduces flow rate and could help by lowering the low damping limit and reduce overall package size as smaller accumulators could be used. Furthermore, the floating piston design is replaced with rolling diaphragms, which could reduce the friction and thus make the system more responsive to smaller inputs. As with the $4S_4$, the accumulators can be charged through a non-return valve with nitrogen gas. Similar to previous designs, nitrogen is used in the pneumatic spring gas as it is an inert gas that is fairly inexpensive and makes modelling much easier as, unlike air, it is a pure substance,. The suspension fluid or oil used is Shell Tellus S2V46 due to its stability across the range of operation. The design allows for fluid pressure measurements in front and behind each valve, as well as measurement of the gas pressure in the accumulators. As with previous designs, the $4S_4$CVD would use spherical bearings on the strut and piston rod to allow the suspension to swivel, the output force would therefore be only in the axial direction with negligible moments that could add considerable friction or cause damage.

The suspension system includes four valves instead of the two used in the $MR4S_4$. The two extra valves is an additional feature to the design, which could allow ride height control or possibly a cross-linked suspension for future investigations. Ride height control would be very beneficial. It would ensure optimal clearance in compression and rebound while in ride comfort mode (higher ride as the soft suspension will use more travel), while lowering the ride height in handling mode (lowering the centre of gravity which has numerous proven benefits for handling). This does, however, not form part of this study.

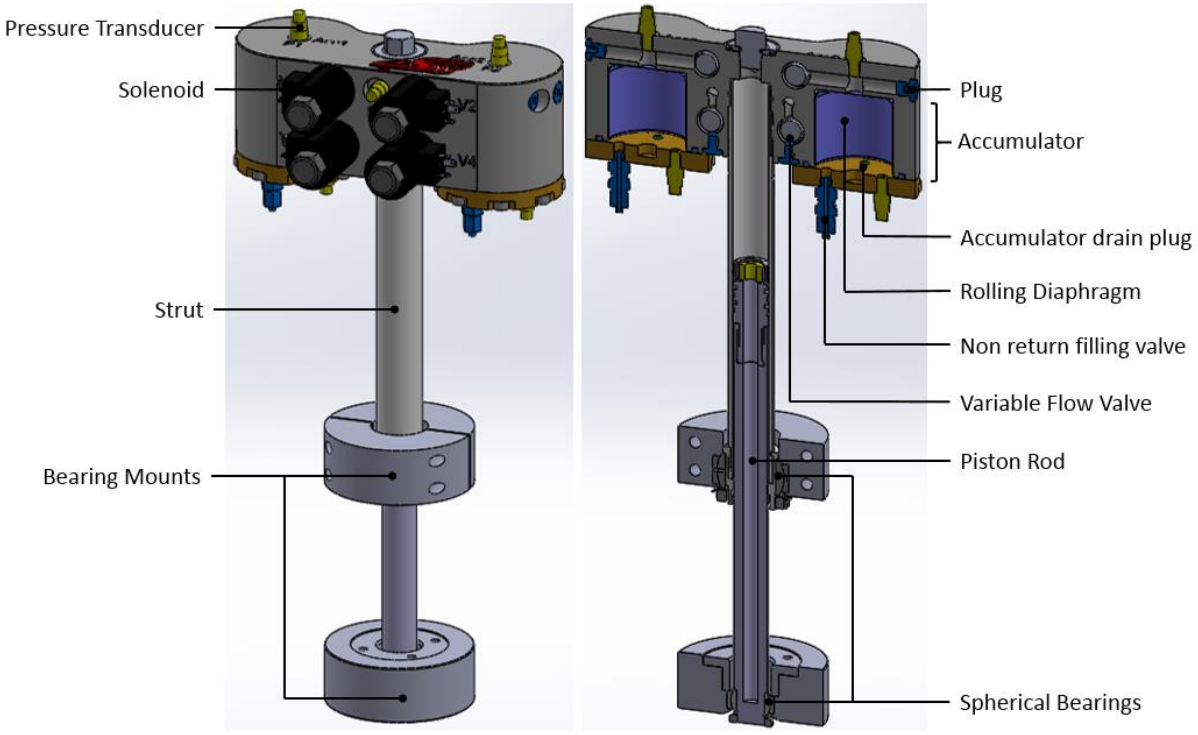


***Figure 2.7: 4S$_4$CVD Design***

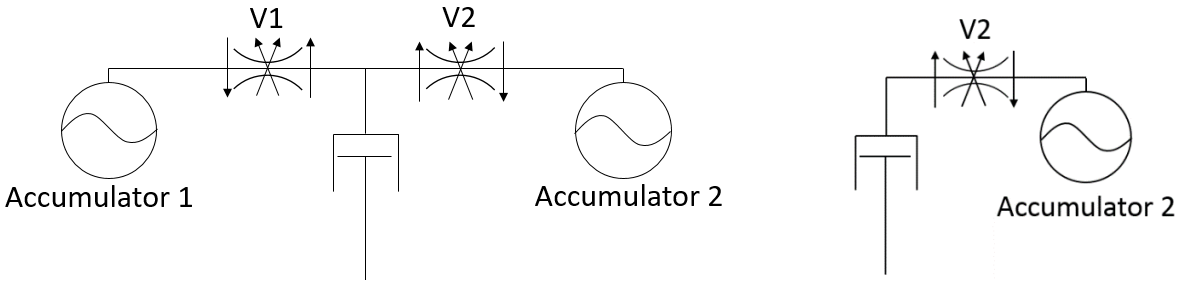


***Figure 2.8: 4S$_4$CVD layout***
***Full design layout (left); manufactured and testing layout (right)***

The valves selected for the design were ZL72-31 and ZL72-30 solenoid, electrically variable, pressure-compensated flow-control, spool valves from Hydraforce (Hydraforce, 2013). The number 31 in the valve code indicates that the valve is normally open while 30 indicates that it is normally closed (as shown in the respective performance diagrams in Figure 2.9). The lines refer to the flow direction, port 3 to 2 refers to flow from the strut to the accumulator and port 2 to 3 vice versa. As indicated, 0-1.5A variable current is required to change the allowed flow and vary the damping. Due to safety and efficiency, valve V2 would be NC, while valve V1 would normally be open. If control of the valves should fail, the suspension would therefore effectively revert to a passive, one-accumulator pneumatic spring that would be quite stiff.

For the purposes of this study, only valve V2's cavity was machined, the suspension fluid could therefore only flow between accumulator 2 and the suspension strut, while flow to accumulator 1 and ports P and R was physically blocked. This was done to reduce the complexity and variables by having only one valve to characterise and model at a time.

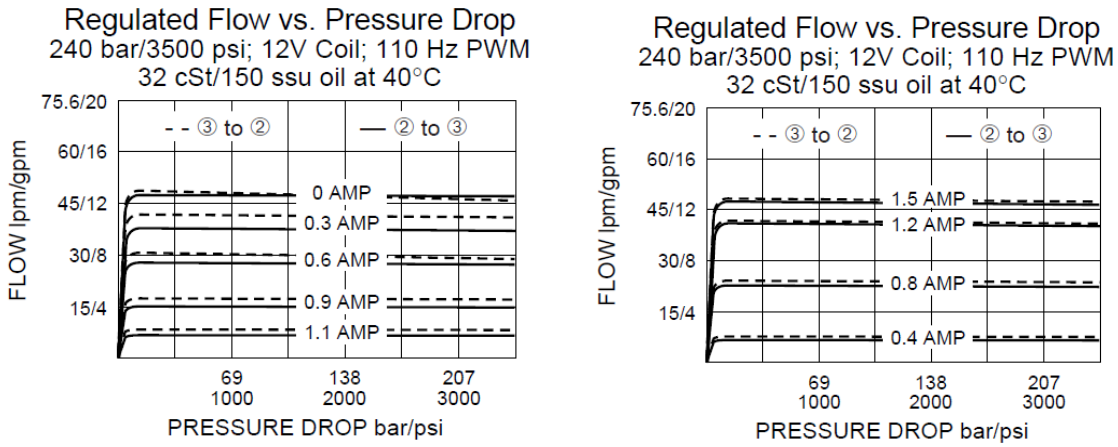


***Figure 2.9: 4S$_4$CVD valve specification (Hydraforce, 2013)***
***ZL72-31 normally open (left), ZL72-30 normally closed (right)***

## 2.3 Response time of semi-active suspensions

Response time is the time required for controllable suspension to transition from the initial damping or stiffness state to 63.2% of the final state, or one time constant. This would also determine the bandwidth of the system (Goncalves et al., 2003). It should, however, be noted that literature sometimes referred to a 95% change (Koo et al., 2006), which rather gives an indication of the time required for the system to fully respond.

Savaresi et al. (2010) described a controllable damper essentially as a combination of an electrical and a mechanical sub-system with the electronic command and deflection speed as input, as shown in Figure 2.10. The current driver (electrical sub-system) turns the electronic voltage command into a physical signal or current that drives the valve. The response time of this system contribute an initial or electrical delay. After the solenoid is charged sufficiently the valve (mechanical subsystem) is actuated which causes a decrease or increase in flow area and results in a damping force, $F_d$ due to deflection velocity, $\dot{x}$. The process of increasing or decreasing pressure drop before settling was defined as the transient response (Els, 2006). The inherent transient response of the valve, combined with the electrical delay, form the response time of a semi-active suspension.

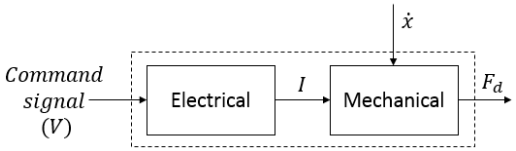


***Figure 2.10: Controllable damper block diagram***

Koo et al. (2006) investigated various aspects that affect the response time of a semi-active MR damper. The driving electronics, which is similar for most semi-active systems, uses a command signal to generate the current needed to power an electromagnet. Koo found that in order to deliver the maximum required 1.5A, the driver response time could be greater than 10ms. He also noted that the larger the current step increase the longer the response time. Koo furthermore studied the effect system compliance had on the response time by adding a rubber layer between the damper and the mount. Results indicated that increased system compliance significantly reduced response time and that it was an important design factor to consider. In his study, the response time of the damper was determined by actuating the unit with a constant velocity and charging the electromagnet halfway through the stroke.

Van Rensburg et al. (2002) did a comprehensive study on the time delay of a semi-active damper that consisted of a pilot valve to open or close a control valve. The system response was determined on a hydraulic test bench that could control the flow and pressure. A physics model with fluid-dynamics simulation software was then developed. It was concluded that the test-bench dynamics greatly influenced both the experimental as well as the simulated values (based on extracted parameters), obscuring actual valve dynamics. Furthermore, the fast-acting sub-systems in hydraulic systems made it difficult to obtain accurate values for use in the model. He suggested that a high-bandwidth test bench and a model thereof could resolve these challenges.

For the $4S_4$, Els (2006) determined the response time by using the test rig shown in Figure 2.4. This was done by blocking the damper orifices and closing the valve, compressing the strut until the required pressure difference was obtained and then opening the valve. It was also done in the opposite direction (extending before opening). Although Els did not model the response time, it was taken into account empirically by interpolating between the initial and final state during the transient response time (as determined experimentally).

This section presents some of the challenges related to accurately determining and modelling the response time of a semi-active suspension and possible solutions used previously. The response time could be influenced by testing equipment having a limited bandwidth. It is also evident that the development of a physics-based model for the complex fluid-flow problem would be no simple task and would require further research. Van Rensburg et al. (2002) and Els (2006) both considered systems where the valves were either open, closed or transitioning between these states. The $4S_4$CVD with continuously variable valves would therefore increase the complexity and could be even more challenging. The significance and effects of response time relating to suspension control will be discussed in greater detail after the control strategies have been discussed in section 2.6.

## 2.4 Suspension modelling

Simulation is vital to ensure the successful design and development of a new suspension system and control strategy. Simulation of the system is a cost-effective and productive method to analyse the characteristics and control strategies in order to highlight shortcomings and to optimise the system by testing possible improvements. In order to obtain meaningful simulations an accurate model of the suspension system is crucial to ensure the simulation results represent that of the actual system. If the model needs to be solved in real time, a trade-off between accuracy and computational efficiency would also need to be considered for vehicle implementation. The model of the $4S_4$CVD should be able to replace the $4S_4$ model, in order to allow full vehicle simulations on a Land Rover Defender 110. This section will present literature related to modelling the $4S_4$CVD and its respective sub-systems.

### 2.4.1 Architecture of models

There has been extensive research and investigation using a $4S_4$ and the vehicle in simulation. Thoresson et al. (2009) developed a full-vehicle model of the Land Rover Defender 110 in MSC Software's Automatic Dynamic Analysis of Mechanical Systems or simply ADAMS suite (Msc Software, 2016). The vehicle model was run in co-simulation with MATLAB/Simulink (Mathworks, 2015), which relied on feedback from the suspension model. This simulation interface and the sub-system in the suspension model (MATLAB M-file) is illustrated in Figure 2.11. It should therefore be noted that a new model, with velocity and displacement as input and the suspension force as output, could simply substitute the $4S_4$ model in order to conduct a full-vehicle simulation.

Van Der Westhuizen and Els (2015) developed the latest model of the $4S_4$ that divided the system into four sub-models to account for the damper, friction, bump stop and spring as shown in Figure 2.11. The damper force is calculated based on the pressure drop over the damper pack or valve, while the frictional force is simply modelled as an external force to account for the friction of the seals in the strut and floating piston. Some damper models would also account for the friction. These sub-models will be discussed further in the sections that follow. The spring force is calculated by a physics based model which determines the pressure of the gas.

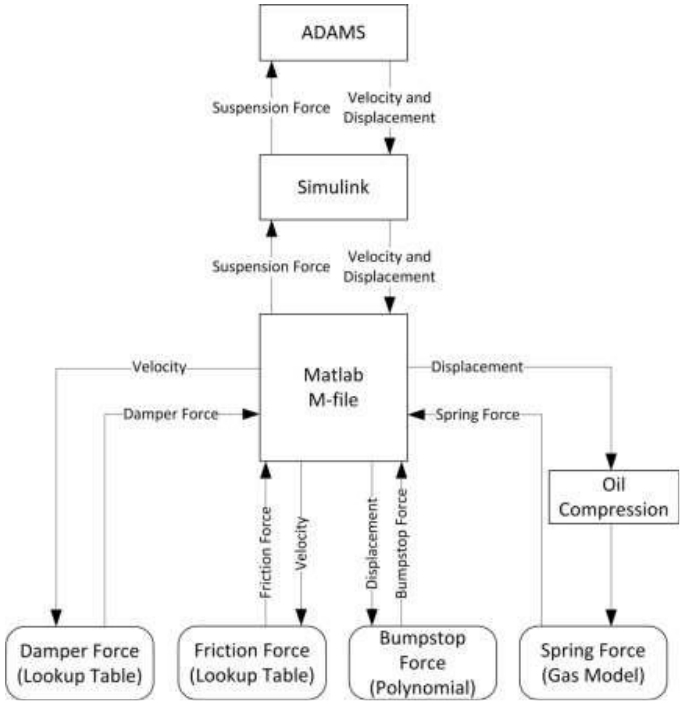


***Figure 2.11: $4S_4$ model interaction (Van Der Westhuizen and Els, 2015)***

## 2.4.2 Hydropneumatic spring

The hydropneumatic spring force, $F_s$ is a function of the gas pressure in accumulator, $P_{acc}$, and the piston rod area, $A_{piston}$:

$$F_s = P_{acc} \times A_{piston} \qquad \textbf{(2-2)}$$

Thus, by determining the gas pressure through a model, the spring force can be determined. A thorough comparative study of five different gas models to calculate the gas pressure in a hydropneumatic suspension has been done by Van Der Westhuizen and Els (2015). The study compared three ideal gas (IG) law variations (isothermal with the energy equation (EE), isothermal and adiabatic) and two real gas approaches (Benedict Webb Rubin (BWR) equation with and without the EE). Figure 2.12b illustrates the response of each model subjected to the input in Figure 2.12a.

The study concluded that the BWR real gas model with the EE gave the best correlation and that it was recommended for high-accuracy applications. However, the IG model combined with the EE was only slightly less accurate than the BWR model. Furthermore, the isothermal model was accurate for low frequency excitations, while the adiabatic model was accurate at higher frequency excitations. A less accurate model would consequently require less computational power. A trade-off might therefore be required for applications where the solve time or computational power is restricted. Since accuracy is of utmost importance for this study and real time implementation was not considered, only the BWR model with the addition of the EE will be discussed. The other gas models could possibly replace the spring force sub-model if needed.

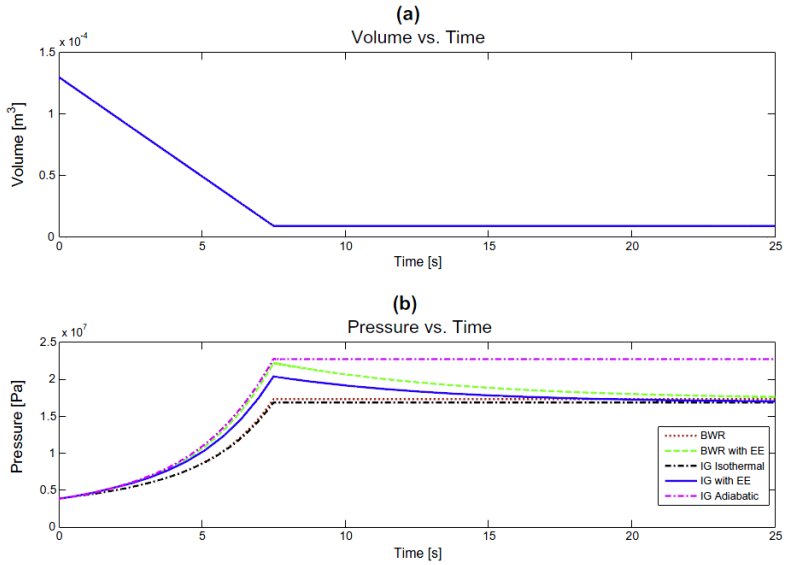


***Figure 2.12: Response of different gas models (Van Der Westhuizen and Els, 2015)***

## BWR real gas approach:

The BWR real gas approach was stated by Els (2006) to be appropriate for use in the typical operating temperature and pressure ranges required for hydropneumatic springs. It adds corrective terms to the IG law to predict the gas characteristics more accurately, as shown in eq. (2-3).

$$P = \frac{RT_g}{v} + \frac{B_0 RT_g - A_0 - \frac{C_0}{T_g^2}}{v^2} + \frac{bRT_g - a}{v^3} + \frac{c\left(1 + \frac{\gamma}{v^2}\right)e^{-\frac{\gamma}{v^2}}}{v^3 T_g^2} \qquad \textbf{(2-3)}$$

The pressure, $P$, is therefore a function of the gas temperature, $T_g$, and specific volume, $v$, with the rest of the variables being BWR constants for nitrogen, as given in Appendix A.

## Energy equation approach to determine gas temperature:

To determine the gas temperature, the heat transfer or EE has to be considered. If there is a significant heat transfer between the gas and its surroundings, it is taken into account using the EE or the first law of thermodynamics for a closed system, as in eq. (2-4).

$$\dot{U} = \dot{Q} - \dot{W} \quad \text{or} \quad m\dot{u} = \dot{Q} - \dot{W} \qquad \textbf{(2-4)}$$

The rate of change in internal energy, $\dot{U}$, is the rate heat transfer, $\dot{Q}$, subtracted by the rate work, $\dot{W}$, done to the system.

In order to apply the method used by Otis and Pourmovahed (1985) to model a hydropneumatic spring, Els and Grobbelaar (1993) made the following assumptions:

- The hydropneumatic suspension system is closed.
- No inertia effects were present during the gas compression.
- The process was seen as a homogeneous, quasi-static gas compression.
- The effect of the thermal capacity of the piston rod and cylinder wall was considered negligible.

The convective heat transfer between the gas and the environment could be approximated by:

$$\dot{Q} = \frac{mc_v\left(T_s - T_g\right)}{\tau} \qquad \textbf{(2-5)}$$

where $m$ the mass of the gas, $c_v$ is a specific heat constant, $T_s$ the ambient temperature and $\tau$ the thermal time constant.

The thermal time constant is a measure of the heat transfer coefficient between gas in a closed container and its surroundings. This could be measured experimentally by subjecting the hydropneumatic system to a step decrease in gas volume. The time it takes for the gas pressure (or temperature) to drop by 63% after initial compression is the thermal time constant (Pourmovahed and Otis, 1990).

Furthermore, the rate of piston work can be defined by:

$$\dot{W} = P\dot{V} \tag{2-6}$$

The change in internal energy due to changes in temperature and volume is given by the thermodynamic relation:

$$du = c_v dT_g + \left[T_g \left(\frac{\partial P}{\partial T_g}\right)_v - P\right] dv \tag{2-7}$$

Equations (2-5), (2-6) and (2-7) can then be substituted into (2-4). After simplification and mathematical manipulation it results in the differential equation as proposed by Otis and Pourmovahed (1985):

$$\dot{T}_g = \frac{T_s - T_g}{\tau} - \frac{\dot{v}}{c_v}\left[\frac{T_g R}{v} + \frac{T_g B_0 R}{v^2} + \frac{2C_0}{T_g^2 v^2} + \frac{T_g bR}{v^3} - \frac{2c}{v^3 T_g^2}\left(1 + \frac{\gamma}{v^2}\right) e^{-\frac{\gamma}{v^2}}\right] \tag{2-8}$$

Equation (2-8) is a first-order differential equation that can be solved by means of the fourth-order Runge Kutta method to determine the needed gas temperature, $T_g$. However, the specific heat, $c_v$ first needs to be determined as given by Otis and Pourmovahed (1985):

$$c_v = c_v^0 + \frac{6}{T_g^3}\left(\frac{C_0}{v} - \frac{c}{\gamma}\right) + \frac{3c}{T_g^3}\left(\frac{2}{\gamma} - \frac{1}{v^2}\right) e^{-\frac{\gamma}{v^2}} \tag{2-9}$$

where the ideal gas specific heat, $c_v^0$, temperature dependence can accurately be approximated by (Jacobsen and Stewart, 1973):

$$c_v^0 = R\left[\frac{N_1}{T_g^3} + \frac{N_2}{T_g^2} + \frac{N_3}{T_g} + (N_4 - 1) + N_5 T_g + N_6 T_g^2 + N_7 T_g^3 + \frac{N_8 y^2 e^y}{(e^{y_-} - 1)^2}\right] \tag{2-10}$$

where $y = N_9/T_g$ and $N_1$ to $N_9$ are constants for nitrogen as listed in Appendix A.

To ultimately determine the gas pressure, eq. (2-10) and then (2-9) needs to be calculated, which is then substituted into eq. (2-8) to determine the changes in gas temperature. Finally, the gas temperature can be derived to solve the gas pressure in eq. (2-3). Note that eq. (2-8) to (2-10) also require the specific gas volume, which will now be discussed.

## Approach to determine specific volume:

The specific volume is merely a function of the amount or mass of nitrogen gas, $m$, and the volume of the accumulator, $V$, that changes relative to the strut displacement.

$$v = V/m \tag{2-11}$$

The volume of the accumulator required in eq. (2-11) can be determined if the suspension fluid was assumed to be incompressible, which would mean that the volume of the fluid displaced by the piston rod would be the same amount by which the accumulator volume changes.

However, by assuming this during the validation of the $4S_4$ model, Els (2006) found that it led to significant errors. He found that the model had to take the compressibility of the fluid into account as shown in Figure 2.13. The compressibility of a fluid can be expressed as:

$$\Delta V = \left(\frac{\Delta P}{\beta}\right) V_0 \qquad \textbf{(2-12)}$$

where $\Delta V$ and $\Delta P$ is the change in fluid volume and pressure between two conditions respectively, $\beta$ the bulk modulus of a fluid and $V_0$ the total volume of the fluid at atmospheric pressure. Thus, the volume of the gas can be compensated by the amount the fluid is compressed as it is a closed system. Figure 2.13 shows experimental data measured by Els (2006) during characterisation of the $4S_4$ compared to an isothermal model with and without accounting for compressibility of the fluid. Since the actuation was at a very low frequency, the isothermal model is expected to be accurate, however, this was established only after accounting for the compressibility of the fluid.

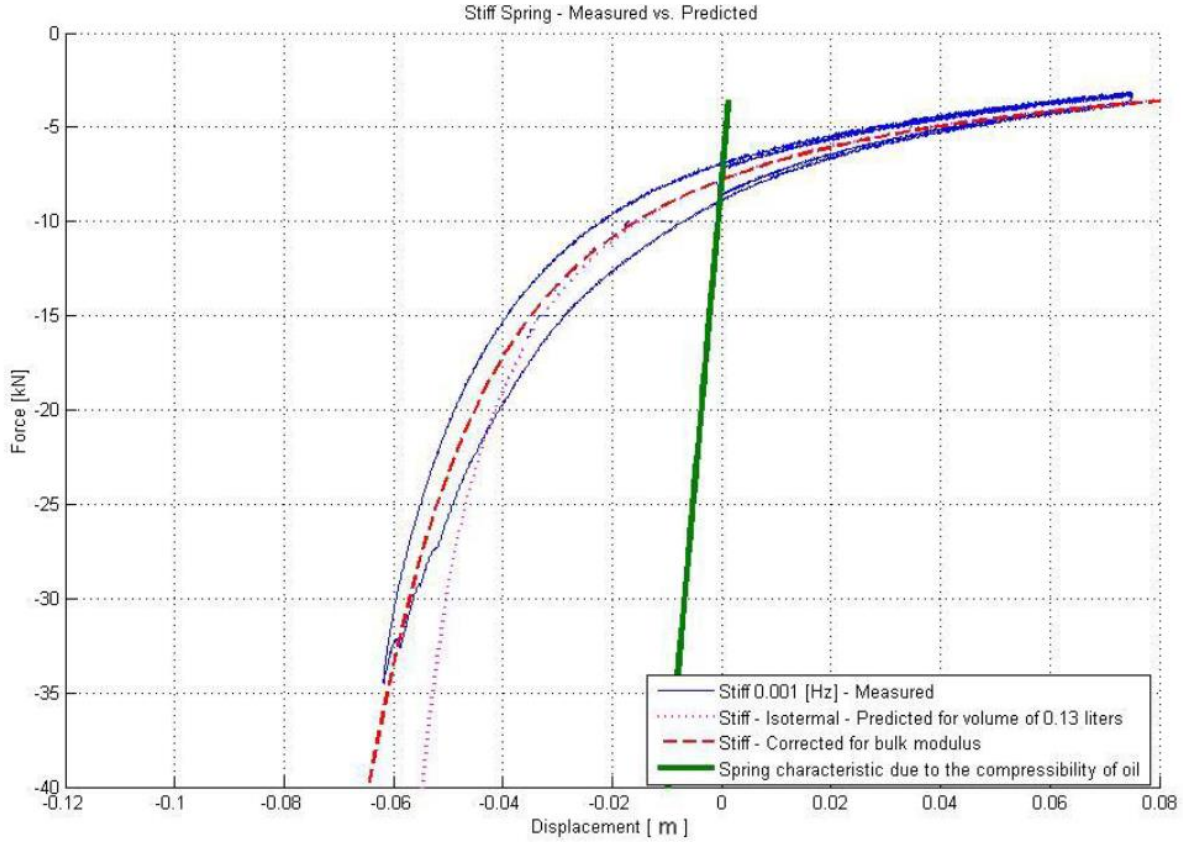


***Figure 2.13: $4S_4$ stiff spring characteristics (Els, 2006)***

## 2.4.3 Controllable damper

The full mathematical modelling of controllable dampers, especially non-linear behaviour, is not a trivial issue and has been an extensively researched topic in the recent past. According to Savaresi et al. (2010), if the semi-active damper exhibits linear force versus velocity characteristic for various commands, it can be approximated by:

$$\begin{gathered} F_d = c(I)\dot{x} + F_0 sign(\dot{x}) \\ c(I) = \gamma I + c_0 \\ 0 \leq I \leq I_{max} \end{gathered} \qquad \textbf{(2-13)}$$

where $F_0$ is a constant that would account for the frictional force that is dependent on the direction of the compression velocity and damping coefficient, $c$, dependent on the current, $I$. However, most dampers do not produce this linear force versus velocity relationship. Literature which is focussed on

control of the suspension systems often uses a simplified linear models, which sacrifices accuracy for controllability, see e.g. Savaresi et al. (2010); Guglielmino et al. (2008). This study focuses on developing an accurate model, therefore, control orientated models would form part of future studies that investigate optimal control strategies.

A popular model used to capture the non-linearity and hysteresis in dampers is the first order dynamic Bouc-Wen model (Savaresi et al., 2010):

$$F_d = c_0(I)\dot{x} + k_0(I)(x - x_0) + \gamma(I)z$$
$$\dot{z} = -\beta(I)|\dot{x}|z|z|^{n-1} - \delta(I)\dot{x}|z|^n + A(I)\dot{x} \qquad \textbf{(2-14)}$$

where $(c_0, k_0, x_0, \gamma, \beta, \delta, A, n)$ are model parameters dependent on the current input, $I$, and $z$ is the internal state that is responsible to model some dynamics and the hysteresis. Through optimisation procedures these parameters can be determined to approximate the experimental results. Variations of the Bouc-Wen model have been developed, such as Spencer Jr et al. (1997), which included more variables to capture the non-linear behaviour of a MR damper. Note that these models have been developed exclusively for a damper unit and not a hydropneumatic suspension unit. Thus, some models, such as in eq. (2-14), accounted for the displacement dependent force due to pressurised gas that would be otherwise be accounted for by the pneumatic spring model in hydropneumatic model. This can be excluded by setting $k_0 = 0$. Various parameters of the Bouc-Wen model are dependent on the command or current input, $I$. From a control design viewpoint, this makes the model difficult to be tractable (Savaresi et al., 2010).

Spencer Jr et al. (1997) further mentioned black-box models, such as neural networks, splines, polynomials, with various degrees of complexities. These models aim to capture the non-linear input-output relationship though various methods:

$$F_d = f(x(t), \dot{x}(t), \dots, I(t), \dot{I}(t)) \qquad \textbf{(2-15)}$$

where, inputs include suspension deflection and velocity, command input and rate, etc. Such a model has been successfully been implemented with control and was validated by Els (2006) in the $4S_4$ model by using a lookup table based on experimental results. This would use suspension setting or command and deflection velocity as inputs to provide the output force.

The response time of the system could essentially also form part of the damper model as it determines the state during the transient change of the damping characteristics. Some of the complex methods of modelling the system, presented in Figure 2.10, was already discussed in section 2.3. In literature (Savaresi et al., 2010), the dynamic behaviour is often neglected or simplified by adding a simple first order delay between the command signal and the resultant output damping force.

Physics based models have also been used to calculate the damping force or valve dynamics. André (2013) developed such a model for a semi-active suspension which relies on a pilot controlled poppet valve system to control the damping. Similarly, Vaughan and Gamble (1996) developed a model that represents the physical dynamics of a proportional solenoid valve. Both of these studies focused on optimising the valve design parameters and the valve controller. This required extensive testing of each subsystem separately rather than a suspension unit as a whole.

This section presented some of the various methods of modelling the damper/valve sub system. The primary focus of this study is to determine the characteristics of the suspension unit and develop a model which can be used in simulation. Modelling and optimisation of the mechanical valve itself or the electrical sub-system (current driver) is therefore not the primary concern. Black-box or fit models as used by Els (2006) have been proven to accurately model and simulate a controllable damper by

capturing non-linear dynamics without requiring extensive testing of each subcomponent. The current driver should, however, be characterised so that the response of the mechanical sub-system (valve) could be determined. It should also respond adequately in order for the response of the mechanical system to not be limited by electrical sub-system. Optimisation and control (e.g. PI or predictive control to reduce response time) of the current driver would further improve the system response time (Savaresi et al., 2010). Nevertheless, this should be considered only after the prototype suspension unit's performance was found to be sufficient.

### 2.4.4 Flow split

For complete analysis of the 4S$_4$CVD a fully defined model that included both accumulators was required. The challenge was in determining the fluid flow through each valve that was restricting flow to the accumulator. For example, if the one valve was set at high damping while the other was set at low damping, the fluid could be flowing through the low damping valve at a higher rate. Furthermore, different flow rates could be due the amount of gas or volume in each accumulator being different, as was the case in the 4S$_4$ that had both a small and a large accumulator. Theron and Els (2007), as well as Heymans (2017), determined the flow rate from and to each accumulator in the 4S$_4$ and MR4S$_4$ models respectively by considering the following equilibrium equation:

$$Q_3 = A_{piston}\dot{x} = Q_1 + Q_2$$
$$Q_3 = \left[\left(Q_{frac} \times Q_3\right) + \left(1 - Q_{frac}\right)Q_3\right] \quad \textbf{(2-16)}$$

where $Q_3$ is the fluid flow rate out of the suspension strut, due to the strut velocity, $\dot{x}$. $Q_1$ and $Q_2$ is the flow through valves V1 and V2 respectively (as depicted in Figure 2.14), which is a function of the flow split faction, $Q_{frac}$. The model therefore used the strut flow rate and estimated an initial flow split to determine the flow through each valve. The estimated flow rates were used to calculate the change in volume of each accumulator, which was used to calculate the pressures, $P_1$ and $P_2$ of each accumulator using the pneumatic spring model. Furthermore, the pressure drop over each valve, $dP_{V1}$ and $dP_{V2}$ could be calculated using the damper model based on the fluid flow rate. These were then used to evaluate whether the equilibrium condition based on the pressure is the strut, $P_3$ was met:

$$P_1 + \Delta P_{V1} = P_3 = P_2 + \Delta P_{V2} \quad \textbf{(2-17)}$$

If this condition was not met, the model iteratively changed the assumed split, $Q_{frac}$, using a gradient-based solver and recalculated the pressures until equilibrium was met or the error was within the defined limits. Once this condition was met, the total suspension force was the product of the equilibrium or strut pressure, $P_3$ and the piston rod area, $A_{piston}$. Heymans (2017) successfully implemented this method and concluded that, when sampling at 1000-2000Hz, the model returned acceptable equilibrium errors. However, he stated that the model was detrimentally affected by large input velocity spikes, such as a step displacement input, since the iterative solver consequently failed to solve the non-linear highly complex system. By including an iterative solver in the MR4S$_4$ model, computational requirements were considerably increased when compared to a simplified lookup table or polynomial as with the 4S$_4$. He showed that sampling at 2000Hz required up to 300 seconds to solve one second of simulation with Belgian paving as input.

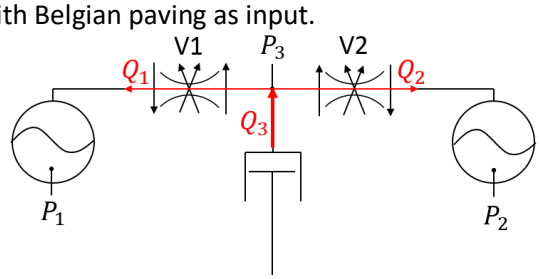


***Figure 2.14: Fluid flow model***

### 2.4.5 Friction

For an accurate model of the $4S_4$CVD, the fictional forces due to sliding between the seals and the piston rod and strut cylinder should also be considered. A vast number of friction models have been developed over the years which can be applied to describe the frictional interaction between two materials, for a comprehensive overview see (Armstrong-Hélouvry et al., 1994). Some models simplify the friction to be a constant force as previously shown in eq. (2-13), while other models such as the Bouc-Wen model in eq. (2-14) capture it empirically. More complex models takes the pre-sliding (stiction), transitional and sliding or coulomb friction into account. For control based models the transition from static to sliding friction is important to reduce the destabilising effect (Guglielmino et al., 2008). Depending on the application the designer can therefore opt for a more or less advanced friction model.

The $4S_4$ (Els, 2006) has been subject to various studies which investigated the friction of hydropneumatic suspension systems. Due to the friction forces generally being quite small relative to the damping and spring forces they are often neglected. Els (2006) neglected friction forces in the model of the $4S_4$ and although a slight offset between the predicted and measured force output could be noted, the simulated and measured force output correlated very well. Therefore, with the frictional force being sufficiently low, the accuracy of the friction model seem to not be critical to ensure representative simulation results.

Van Den Bergh (2014) later investigated how various friction models of the $4S_4$ effect the accuracy of vehicle dynamic simulation. He concluded that neglecting friction has significant impact on the accuracy of the results. Furthermore, it was concluded that complex high computational demand friction models do not yield significant increases in accuracy over a rudimentary look-up table which is based on experimental data. It can therefore be concluded that a look-up table, which approximates test data, will be sufficient for this study.

## 2.5 Vehicle modelling

The spring and damper model needs to be combined with a suitable mathematical model of a vehicle to investigate the dynamic response of the system due to road disturbances. Various vehicle models with increasing degrees of complexity have been developed to provide reliable models for design and performance assessment. Models are selected based on the information, computation power and accuracy required. Frequently used conventional vehicle models will briefly be discussed in this section.

A vehicle can be divided into two main sub-systems: the sprung mass (chassis) and the unsprung masses (wheels, axles and linkages), which is connected via elastic and dissipative elements (suspension, tyres, etc.). This system representing the vehicle is subjected to various inputs from the driver, road or external disturbances (e.g. wind). If the total vehicle body can be assumed to be rigid, the total motion of a vehicle can be described by six degrees of freedom (DOF), three rotational DOF about each axis (pitch, roll and yaw) and three translational DOF (lateral, longitudinal and vertical) (Guglielmino et al., 2008). Vehicle models are often simplified by including motions of interest and disregarding those that do not add value or significant accuracy.

### 2.5.1 Quarter-car vehicle model

As mentioned previously, ride comfort is essentially concerned with the vertical dynamics. The most trivial representation of such a ride model is a 1DOF simplified quarter-car model in which the tyre mass and stiffness are neglected. By incorporating the unsprung wheel and tyre dynamics, the very

popular quarter-car model with 2DOF can be developed, as represented in Figure 2.15. $x_3$ refers to the road disturbance that is the same as the unsprung mass, $M_u$ displacement $x_2$ in the case of the simplified version. The simplified version of the quarter-car reproduces the resonance of the body mass quite well, but the wheel resonance vanishes, as shown in Figure 2.16. According to Savaresi et al. (2010) this model may still be used when the focus is on ride comfort that is defined by the chassis or sprung mass motion with respect to road unevenness. Poussot-Vassal et al. (2010), Guglielmino et al. (2008) and Savaresi et al. (2010) were some of the studies that successfully incorporated quarter-car simulations to analyse the ride comfort and road-holding performance of semi-active suspensions and control strategies. Heymans (2017) also conducted basic quarter-car simulations to assess the performance of the MR4S$_4$.

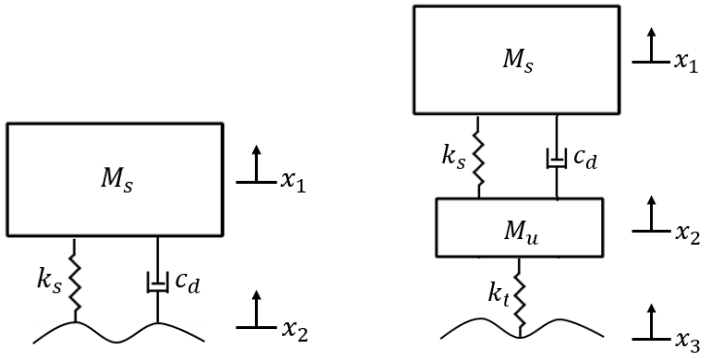


***Figure 2.15: Quarter-car vehicle model***
***Single degree of fredom model (left), Quarter-car model (right)***

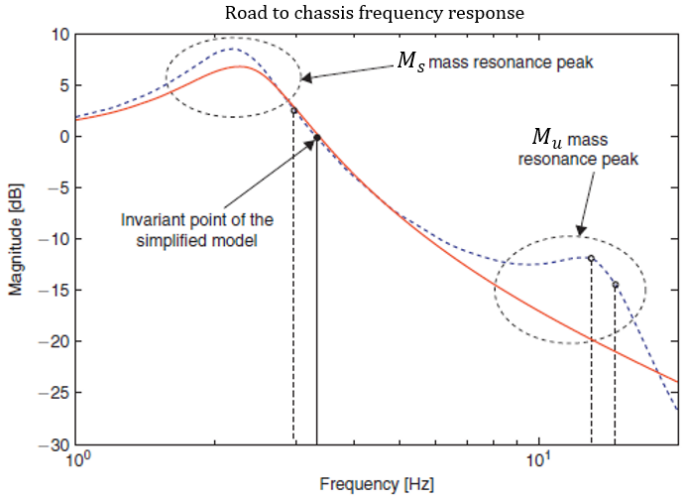


***Figure 2.16: Frequency response comparison of quarter-car models (Savaresi et al., 2010)***
***Quarter-car model (dashed line) and its simplified version (solid line)***

## 2.5.2 Higher-order mathematical models

Quarter-car models are restricted to vertical translation, these models are often extended to 4DOF half-vehicle models to include either pitch or roll of the sprung mass. Dorling et al. (1995) implemented such a model that included roll to study achievable dynamic response with idealised active suspension. The next step is a full-vehicle model that includes the vertical translation of all four wheels, as well as the vertical translation, pitch and roll of the sprung mass, which adds up to 7DOF. The complexity of a full-vehicle model can be increased to include other factors, such as chassis compliance and bushings, which effectively allows an unlimited number of constraints that would all need to be characterised.

Els (2006) developed a model of a Land Rover Defender with 14 unconstrained degrees of freedom to assess the performance of the $4S_4$ and control strategy combination. Thoresson et al. (2009) developed a refined ADAMS model thereof, which was validated against experimental results and used in a suspension optimisation study.

Guglielmino et al. (2008) listed parameter uncertainty and long simulation running time as drawbacks of full-vehicle models. Citing these reasons, he was of the opinion that they were not always the best choice for control design, especially in the early stages of the design. A less complicated model is preferable, reserving the higher-order models for further refinements and optimisation.

### 2.5.3 Conclusion

Based on the literature reviewed it is clear that the vehicle models used is dependent on the design phase of the project, as well as the respective control strategy under consideration. Initial suspension investigations all seemed to favour quarter-car simulations due to their simplicity and unobscured results. Although quarter-car simulation is a valuable tool, care should be taken not to assume simulation results as an accurate representation of the actual response without further investigation. Also note that a validated full-vehicle model of Land Rover Defender 110 has already been developed, which could at least be used in future simulations with the $4S_4$CVD. Simulation models should be developed with regard to the parameters being investigated and should be kept simple but capable of providing acceptably accurate results.

## 2.6 Semi-active suspension control

In order to solve the ride comfort versus handling compromise, the $4S_4$CVD needs to be combined with a suitable control strategy to change the suspension characteristics to suit the situation. The literature on semi-active suspension control is vast. Any measureable parameters, ranging from driver inputs to accelerations, can be used as input to the control strategy to determine which suspension characteristics are most suitable. Furthermore, several strategies, which includes many variations and combinations of known strategies, are developed for specific suspension and vehicle combinations. Although literature on semi-active springs and also hydropneumatic semi-active suspensions are not as common, it can be integrated in the semi-active damper control strategies. There is also a strong tendency to combine control strategies to achieve optimum ride comfort, handling and safety in all circumstances. This is not a trivial exercise as it requires many simulations, tuning and testing for all circumstances (Savaresi et al., 2010).

To assess the feasibility and performance of the $4S_4$CVD, the selected control strategy needs to be kept as simple as possible and as complicated as necessary in order to reflect the capabilities of the suspension. The current focus is on a more fundamental understanding and assessment rather than the development and tuning of a new control strategy. Model-predictive control and other predictive strategies would therefore not be considered, even though literature has shown great promise (Canale et al., 2006).

Some control strategies tries to actively control the high frequency relative suspension deflection, while a more “passive” control strategies determines a suitable characteristic and keeps it uncontrolled until the road condition or dynamic state of the vehicle changes. For example, for a constant sinusoidal road disturbance, active control would change the characteristics during the compression and extension phase, while passive control would determine the best characteristic and keep it until the disturbance changed in magnitude or frequency. Consequently, such active control would theoretically be superior, however, it requires a fast-responding system and preferably continuously changeable characteristics. This will be made clear upon further investigation into

control strategies. The most common suspension control strategies that actively controls the relative deflection are skyhook, groundhook and hybrid control strategies.

Skyhook is a comfort-oriented control strategy that aims to reduce the vertical dynamics of the vehicle body. Groundhook is a handling or, more specifically, road-holding oriented control that aims to reduce the dynamic tyre force. Hybrid control is a combination of both strategies aimed at reducing both body acceleration and dynamic tyre force. However, according to Savaresi et al. (2010) and Guglielmino et al. (2008) the hybrid strategy is not straightforward and requires accurate tuning. Furthermore, it depends heavily on the type of road and is often combined with estimators. In an attempt to simplify and ensure that clear and meaningful results are extracted, such a hybrid control strategy is therefore not considered.

### 2.6.1 Skyhook control

The skyhook control strategy, originally developed by Karnopp et al. (1974) considered a hypothetical damper being connected to a fixed point in the sky in order to reduce vertical oscillations of the sprung mass independent of the input at the base, as shown in Figure 2.17 (left)**.** This system could be modelled as:

$$M_s\ddot{x} = -k(x_1 - x_2) - c_{sky}\dot{x}_1 \qquad \textbf{(2-18)}$$

where $c_{sky}$ is the damping coefficient of the ideal skyhook model. This model is, of course, not physically possible, however, it can be approximated by using a semi-active suspension model, as shown in Figure 2.17 (right), with a controllable damper**.** The controllable damper with damping coefficient, $c_{controllable}$ thus changes to produce the damping force determined by the skyhook controlled system. For example, when the sprung mass and base is moving away from each other and the sprung mass is moving upwards, the dampers in both models would exert a force in the same direction. However, if the sprung mass was moving downwards instead, the controllable damper would be unable to match the direction of the force. In such a case, the damper force would try to approximate the model by minimising its force.

This logic can be summarised by:

$$F_d = c_{controllable}\dot{x} \approx F_{Sky} = \begin{cases} c_{sky}\dot{x}_1 & \dot{x}_1\dot{x} > 0 \\ 0 & \dot{x}_1\dot{x} \leq 0 \end{cases} \qquad \textbf{(2-19)}$$

$F_d$ is force exerted by the damper, $\dot{x}$ refers to the relative velocity $(\dot{x}_1 - \dot{x}_2)$ and the ideal skyhook damping coefficient, $c_{sky}$ is a tuneable parameter determined by the damping ratio, $\zeta$:

$$c_{sky} = 2\zeta\sqrt{k_s M_s} \qquad \textbf{(2-20)}$$

Determining the optimal skyhook parameters is no trivial matter. Poussot-Vassal et al. (2006) developed a reduced order observer model combined with a suitable cost function to implement optimal skyhook control in simulations with great success. Although this control only requires the velocity of the sprung and unsprung mass which is relatively easy to obtain, vehicle implementation it is more challenging as these parameters inevitably also include noise and drift. Savaresi et al. (2010) could successfully implement skyhook control by using measurements from accelerometers on the sprung and unsprung mass, as well as a potentiometer for the suspension deflection. Most of these studies, such as conducted by Poussot-Vassal et al. (2006) and Savaresi et al. (2010), use a linearized spring and damper model which greatly simplifies the numerical problem.

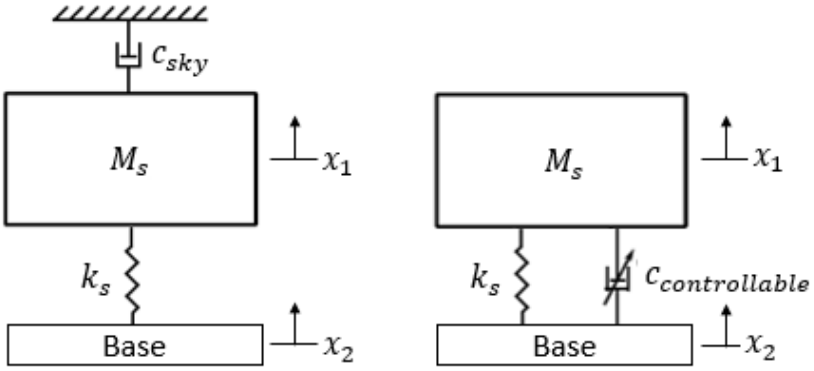


***Figure 2.17: Skyhook model***
***Ideal configuration (left), semi-active suspension configuration (right)***

## 2.6.2 Response time and control

The success of a relative motion control strategy, such as skyhook, relies on a fast-responding suspension system that is able to react promptly to disturbances. Tsampardoukas et al. (2008) assessed the performance of a hybrid control strategy when the response time was incrementally increased from 5 to 20ms. His simulation results showed that the performance deteriorated as the response time increased. Although not investigated further, the unavoidable delay is one of the reasons why designers are actively investigating estimators to reduce, or possibly eliminate, this effect (Canale et al., 2006).

The controllable bandwidth of the suspension essentially limits the efficacy of control at higher frequency disturbances and employing the control strategy outside the bandwidth could have a detrimental effect on the performance. This is not well-documented in literature, as most semi-active suspensions used in literature are ideal zero-delay or fast-responding MR dampers with a reported response time of less than 50ms. With such a system response, the bandwidth stretches over the frequency range of importance. A high-pass filter is also commonly employed to filter the high frequency disturbances or noise, which offer stability to the control strategy (Savaresi et al., 2010).

As discussed previously, the incorporation of MR technology in the $4S_4$ design indicated some limitations, which were to be investigated with use of electro-hydraulic valves in the $4S_4$CVD. The manufacturer did not specify the response time of these valves and they could therefore very well respond slower than the systems considered in literature. In a comprehensive analysis of the response time of MR dampers, Koo et al. (2006) presented results indicating a 20ms response time (for a piston rod velocity higher than 20mm/s). Most of the literature investigating continuous control strategies used this response time of 20ms or even less (Spelta et al., 2008; Tsampardoukas et al., 2008; Sammier et al., 2003). The $4S_4$ (Els, 2006) with a spool valve similar to that used in the $4S_4$CVD had a response time of only 50-100ms. If commercial electrohydraulic dampers were considered, the state of the art continuously controlled electronic suspension (CES) developed by Öhlins (Öhlins Racing, 2018) would arguably be the leader in the industry. In a mostly confidential optimisation study of a recent CES valve by André (2013), some of the results presented showed the valve to have a response time of around 35ms (excluding the driver response). This suggested that the valve would respond slower than those used in control based investigations.

## 2.6.3 $4S_4$ and MR$4S_4$ control

For a comparative analysis of the $4S_4$CVD's performance, the control strategies investigated with the $4S_4$ (Els, 2006) and MR$4S_4$ (Heymans, 2017) and their efficacy is considered.

### $4S_4$ control

As part of the development of the $4S_4$, Voigt (2006) studied several control strategies with the aim of developing an appropriate ride comfort control strategy for a hydropneumatic suspension system consisting of a two-state spring and a two-state semi-active damper. Voigt found that the skyhook control performed unsatisfactory due to the non-linearity of the system (two discrete modes). He also found that the skyhook control performed better at low frequencies, but deteriorated at higher frequencies due to the valve response time. Voigt concluded that it was not possible to notably improve ride comfort by actively controlling the spring and damper when the characteristics had been optimised for ride comfort.

The $4S_4$'s control strategy to switch to ride comfort or handling mode was ultimately determined by comparing the rolling root meat square (RRMS) of the vertical and lateral acceleration. If the lateral RRMS acceleration exceeded that of the vertical, or was higher than 0.3 g, the suspension switched to handling mode. The vehicle would otherwise remain in ride comfort mode. The vehicle-implemented strategy was thoroughly analysed in various situations. Most notably it could successfully deal with a severe double lane change manoeuvre (International Organization for Standardization, 1999) at a speed of 80km/h despite its response time delay. This strategy successfully equipped the $4S_4$ to solve the ride comfort versus handling compromise, yet it was simple enough to implement as it merely required two accelerometers to measure the vertical and lateral acceleration.

### $MR4S_4$ control

As the $MR4S_4$ could continuously vary damping, the implementation of the skyhook control was once again investigated (Heymans, 2017). Although the $MR4S_4$ was never physically tested with a control strategy, the simulations with the validated model provided valuable insights. Heymans found that, with the characteristics of the $MR4S_4$, employing skyhook control deteriorated ride comfort due to the damping being inherently too high. This was verified by artificially decreasing the damping by a factor of 10, which resulted in the skyhook control effectively improving ride comfort by actively controlling the suspension characteristics. This highlights how the skyhook can only effectively be applied if the low damping limit is sufficiently low.

## 2.6.4 Conclusion

The literature review into the background of control strategies indicated that control could become very complex and demanding. However, the classic skyhook control has been identified as a strategy that could be used to assess the performance of the $4S_4$CVD. No conclusive studies were found to investigate maximum allowable response time for improving performance related to specific bandwidths. Reviewing control of the $4S_4$ and $MR4S_4$ revealed how non-linearity, slow response time and a too high lower damping limit could result in the skyhook control not performing adequately. Although the skyhook control is quite unsophisticated, successful implementation thereof could justify exploring other more refined control strategies and combinations thereof in future.

# 2.7 Conclusion and problem statement based on literature review

In chapter 2, a thorough review of literature was presented to explain the fundamental concepts in this research initiative, which formed the basis of the investigation. Ride comfort and handling were shown to have opposing design requirements that involves a compromise. Furthermore, the optimal suspension characteristics continuously change based on the road disturbance and dynamic state of the vehicle. Hydropneumatic semi-active suspension development at the University of Pretoria was

presented which provides background to the 4S$_4$CVD and performance improvements it aims to achieve.

Methods of modelling the suspension and its subsystems as well as vehicle models to analyse the performance of the 4S$_4$CVD in simulation were presented. Lastly, an overview of suspension control was given and important characteristics required for successful control were identified. The knowledge gained through the literature reviewed, could be used to successfully characterise and model the 4S$_4$CVD to analyse its performance in simulation.

Ultimately the problem that the 4S$_4$CVD aims to address is whether the 4S$_4$CVD could be implemented to improve the ride comfort and handling of a Land Rover Defender 110 currently equipped with the 4S$_4$. This guided the decision-making and analysis to allow future investigations to build on the research and findings presented in this study. For example, a full-vehicle model was already available for future use and a suspension model developed in such a way that it could be incorporated in future investigations would therefore be beneficial. This study serves as the preliminary analysis, with the focus on key parameters pertaining to the feasibility and possible improvements, in order to make recommendations.

Based on the literature review, the following parameters requiring further analysis have been identified:

1. Stiffness characteristics provided by the pneumatic spring. Although the pneumatic spring concept in the 4S$_4$ is very similar to that of the 4S$_4$CVD, it has a different accumulator design and a smaller piston area. The 4S$_4$CVD would therefore have to operate under much higher pressures due to the decreased area. The aim is to characterise and model the pneumatic spring of the 4S$_4$CVD and to compare it to the spring characteristics of the 4S$_4$.
2. Damping characteristics, with special attention to the lower damping limit and the ability to at least dynamically block flow to an accumulator and achieve increased stiffness. In previous versions of the 4S$_4$ it was clear that the lower limit of damping was too high, which resulted in sub-optimal ride comfort. The suspension should thus have low enough damping for improved ride comfort. The valves should be able to block flow sufficiently in order to provide dynamic stiffness for handling manoeuvres.
3. The rolling diaphragm accumulator design aimed at reducing the friction. Reducing the floating piston induced friction could result in improved suspension performance, especially with regard to ride comfort as some of the discontinuous force output could be negated. The overall implementation and effectiveness of this design would have to be analysed.
4. The response time of the 4S$_4$CVD to change its characteristics. Although also dependent on a current driver, the main focus of the study is on the inherent dynamic characteristics of the valve, rather than developing an optimised driver. The literature reviewed emphasised some of the challenges related to accurately determining and modelling this complex performance indicator. Without accurately extracting parameters on a high performance flow and pressure controlled test bench, it is apparent that attempting to develop a physics model would be futile. As this is the first study on the 4S$_4$CVD, it would be beneficial to conduct simulation-based analysis before an entire study on the exact response time of the valve was done. For such an analysis, precisely determined response times and models might not be essential to draw meaningful conclusions.
5. It should be investigated whether the new prototype would allow the successful implementation of the skyhook control to improve ride comfort. It was noted that there was a lack of literature investigating slower response systems and the bandwidth that could successfully be applied to in

order to improve ride comfort. Such an analysis could be valuable as it could specify response time requirements and also recommend a cut-off frequency for control. These improvements should be compared to discrete damping used in the past to assess the benefit of having the ability to continuously vary the damping.

The main research question addressed by this study is: *Can the $4S_4$CVD be implemented to significantly improve ride comfort and handling of the Land Rover Defender currently equipped with the $4S_4$?* This also requires addressing other important questions such as: *How does response time affect the performance and what is recommended? Would the current design be sufficient with regard to the damping, stiffness and response time characteristics?* In order to successfully answer these questions the suspension system needs to be characterised and modelled which can then be used to conduct simulation based investigations.

# Chapter 3:
# CHARACTERISATION

The literature review made it clear that characterising the 4S$_4$CVD would be required to achieve the research objective and address the problem statement. Consequently, this chapter describes the process of complete characterisation of the 4S$_4$CVD. Although most of the 4S$_4$CVD was essentially designed before this study was initiated, it was manufactured only during the initial stages of this study. In order to ensure relevant information, manufacturing is not discussed. However, relevant modifications of the initial design are included as it affects or limits future results. All the design modifications, experimental setup and testing procedures used to ultimately obtain and present the experimental results are discussed.

## 3.1 Design modification

During the initial assembly and charging of the 4S$_4$CVD it was found that the rolling diaphragm was prone to tear or even burst when it was forced (due to pressure differential) into the machined flow ports which can be seen in Figure 2.7 previously shown. Furthermore, as shown in Figure 3.1, the diaphragm did not have a piston on the inside to support it and ensure it rolls as recommended by the manufacturer. Without such implementation, the diaphragm could crush or buckle instead of smoothly rolling to retain its shape and form. Due to these reasons, the design was slightly modified to include an extrusion preventer and cover plate. These modifications reduced the maximum volume of a single accumulator from 0.270 litres to about 0.19 litres. Consequently, the smaller gas volume reduced the actuation displacement range or stroke that could be utilized during experimental characterisation due to the maximum operating pressure now being reached at a smaller displacement. The design specification of 300mm travel was therefore not achieved and some of the results such as response time were limited which is further discussed in section 3.3.3. The volume could simply be increased in the second design iteration by using a larger diaphragm and a valve block with a larger accumulator volume.

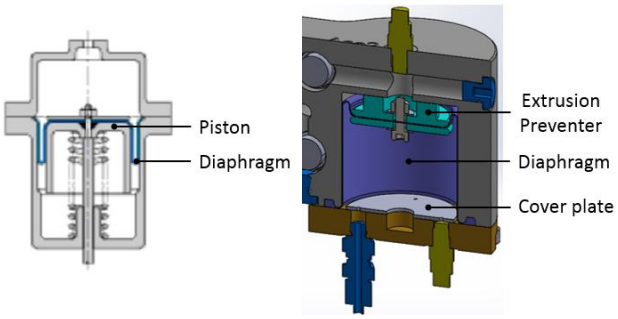


***Figure 3.1: Diaphragm accumulator design***
***Manufacturer specification (Freudenberg, 2017) (left), modified 4S$_4$CVD design (right)***

## 3.2 Experimental setup

Characterisation of the 4S$_4$CVD requires an experimental setup that could support the suspension unit and subject it to predetermined dynamic inputs. Furthermore, it requires electronic systems for control, data acquisition and signal conditioning. The following section describes the experimental setup.

### 3.2.1 Valve block

A critical part of characterisation involves knowing the fluid flow through each valve in order to quantify the damping each valve is responsible for. Due to the lack of flow sensors with the required dynamic response and operating pressure, directly measuring the flow through each valve was not possible. To calculate the fluid flow due to compression or extension the piston speed and area can be used by assuming the oil to be incompressible or compensating for compressibility by means of the bulk modulus. However, with the designed system of two flow paths (one to each accumulator), the flow due to piston displacement splits up between the valves based on the resistance of each flow path which could be different. In order to simplify the setup and to ensure that accurate results could be extracted, the fluid flow was restricted to one flow path (see Figure 2.8 for flow path). This was done by machining only one of the valve cavities, as shown in Figure 3.2, which left all the other flow paths physically blocked until they could later be machined. The suspension fluid would therefore flow from the suspension strut to the accumulator side through the valve, as indicated in Figure 3.3.

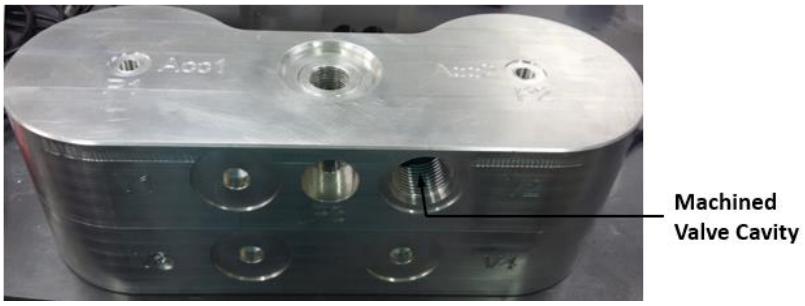


*Figure 3.2: Machined valve block*

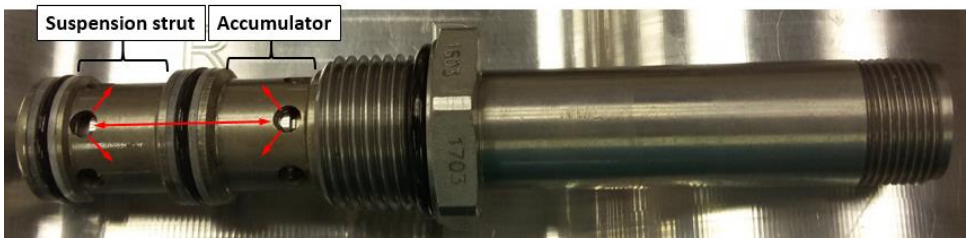


*Figure 3.3: Proportional valve (without solenoid)*

### 3.2.2 Charging procedure

After manufacture and assembly, the $4S_4$CVD could be charged with the suspension fluid and accumulator gas. The chosen suspension fluid is Shell Tellus S2V46 due to its low cost, availability and stability across the range of operation. As with mostly all hydropneumatic suspension systems, nitrogen is used as accumulator gas, since it is inert with well-defined properties.

The spring characteristics are primarily dependent on the volume and the mass of gas in the accumulator. The compressibility of the oil can be taken into account by using the bulk modulus of the fluid. However, there are other unavoidable compressible elements in the system due to air mixing and diffusing into the fluid during filling or possibly getting trapped behind seals and the valve. This makes it is difficult to accurately determine the exact volume of gas which is representative of the whole system. The $4S_4$ (Els, 2006) encountered similar challenges, however, characterisation of the $4S_4$ could still be sufficiently performed. The volume in the proven spring model was iteratively changed until it matched the results, it is therefore not critical to know the exact volume. As the composition of air is predominantly nitrogen, and the air in the system is so small in comparison to the nitrogen it was included in the volume of nitrogen without inducing noticeable errors. By “tuning” the gas volume, the volume can be matched while also compensating for other compressibility that is

not included in the model. Based on the specifications and measurements, the filled accumulator volume was calculated as 0.19 litres. It is therefore expected that a representative volume to be slightly more than this by compensating for any trapped air. Although applying a negative pressure to the fluid could reduce some of the air in the system, the current charging procedure was found to be sufficient for the purposes of this study.

The charging procedure started by removing a filling bolt on top of the valve block and a bleed bolt on the accumulator cap and then fully extending the suspension strut. The suspension was filled with fluid through the top of the valve block. The filling bolt was reinstalled and the suspension was fully compressed, which caused the fluid to flow through the valve and compress the accumulator to release any air. This also forced enough fluid to flow to the accumulator side of the valve, thereby ensuring that this volume was filled with fluid when the accumulator was charged. The accumulator drain bolt was then reinstalled, the strut extended and the filling bolt was removed. The accumulator was charged with nitrogen through the non-return filling valve to 100kPa, which caused the diaphragm to expand fully and push the excess fluid through the valve and out of the top of the valve block. The unit was then tilted and tapped to remove any of the trapped air in the system while adding additional fluid and was then left fully extended in a vertical position overnight. The unit was given a final top-up before reinstalling the filling bolt. The final step was to charge the accumulator from 100kPa to the required pressure. The maximum static vertical wheel load for the fully laden Land Rover Defender test vehicle is 800kg (Els, 2006). Based on this, 7MPa was selected as a suitable charge pressure, which requires 5.63kN of force before the unit starts to compress. Although the optimal gas pressure and volume for the $4S_4$CVD had not yet been determined, this pressure combined with the smaller gas volume (which results in a larger pressure gain per displacement input) would allow for characterisation of the $4S_4$CVD across its range of operation.

### 3.2.3 Test rig setup

To accurately characterise the $4S_4$CVD, a rigid support frame and mountings were required to limit results from being influenced by deflection in the frame. The fully charged unit was installed on an existing test rig, as shown in Figure 3.4. The whole support frame was fitted to the top of a 25kN Schenck hydropulse actuator, which was fixed to a vibration isolation test block. The top mounting of the $4S_4$CVD was fixed to the support frame, while the bottom mounting was fixed to the actuator piston via a load cell to record force. The various displacement inputs were provided by the actuator, which vertically translated the bottom mounting and piston rod while the rest of the system was fixed to the frame. Both mountings still allowed the spherical bearings to rotate freely to avoid inducing any additional forces and moments due to slight misalignments. The actuator also had an internal linear variable differential transformer (LVDT), which could be used to measure the actuator displacement. Three 50MPa KYOWA PLG-A pressure transducers were used to measure the accumulator gas pressure as well as the fluid pressure before and after the valve. The solenoid that was installed onto and controls the valve was powered by the current driver. The test rig setup shown in Figure 3.4 therefore relied on actuator displacements and current powering the solenoid as input.

### 3.2.4 Current driver

As mentioned previously, the valve response time is influenced by the electric circuit that switches the valve. However, the valve could start to respond before the driver transience have passed and some overlap could therefore occur. This could obscure results, since the main focus is on the valve response time rather than on a combination of both the driver and the valve. Ideally, a current driver with a zero response time would allow the precise determination of the valve response time. However this is not possible due to the inductance of the solenoid, current takes time to build up to generate the

necessary force to actuate the valve. The response should therefore be fast enough to reduce or possibly eliminate this overlap in order to allow an accurate valve response time to be determined.

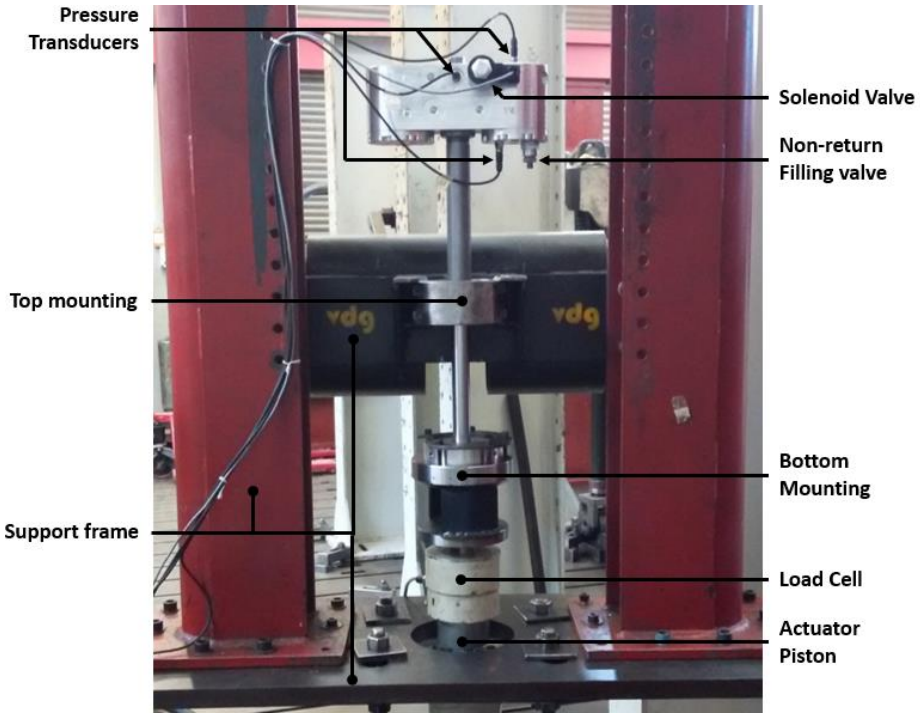


***Figure 3.4: 4S$_4$CVD test rig setup***

It was initially investigated whether a Hydraforce EVDR-0101A current driver would have sufficient response time and accuracy to power the solenoid and control the valve. The current driver can be controlled continuously with a user-defined voltage or a digital command signal. The current through the solenoid directly relates to the magnetic force which actuates the valve. Therefore, the faster the desired current through the solenoid is achieved, the faster the valve can be actuated. To evaluate the driver, a current sensing circuit was developed as in Figure 3.5. The current can be determined by measuring the amplified voltage across a 10milliohm low-side sensing resistor. The voltage due to a maximum of 1.5A through the sensing resistor was amplified by an AD620 instrumentation amplifier up to 10V. A data acquisition (DAQ) module generates the voltage control signal and also records the measured voltage of the current sensing circuit as shown in Figure 3.6.

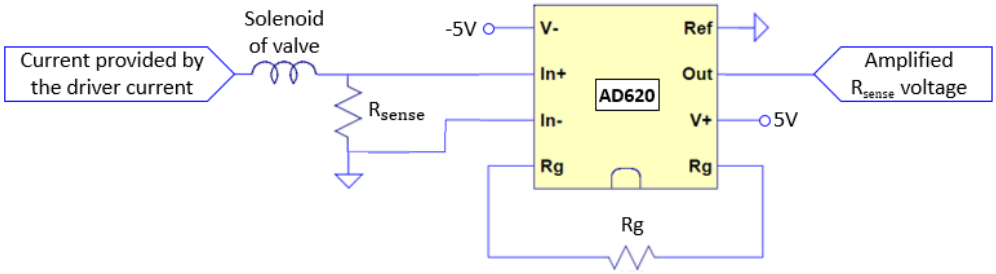


***Figure 3.5: Current sensing circuit***

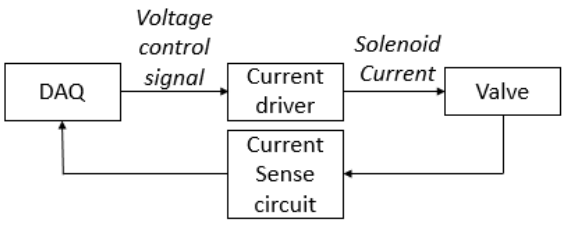


***Figure 3.6: Current driver command and output logic***

## Instrumentation delay

There are inherent delays in the instrumentation between generating the command signal and recording a measured signal. This delay, shown in Figure 3.7, was captured by connecting the voltage command signal that would switch the current driver directly to the DAQ to be recorded. This delay was therefore a combination of generating, sending, receiving, filtering and recording the signal. The same delay would be included when recording the response time of the current driver. Thus, in order to extract the true response time of the current driver, this instrumentation delay should be subtracted. For the 1kHz sampling rate that was used the 40ms delay was larger than expected. However, according to the specifications of the DAQ used (National instruments, NI4472) the anti-aliasing filter is responsible for a delay of 39 samples, which translates to 39ms, therefore the 40ms is simply 1 sample delay which is reasonable.

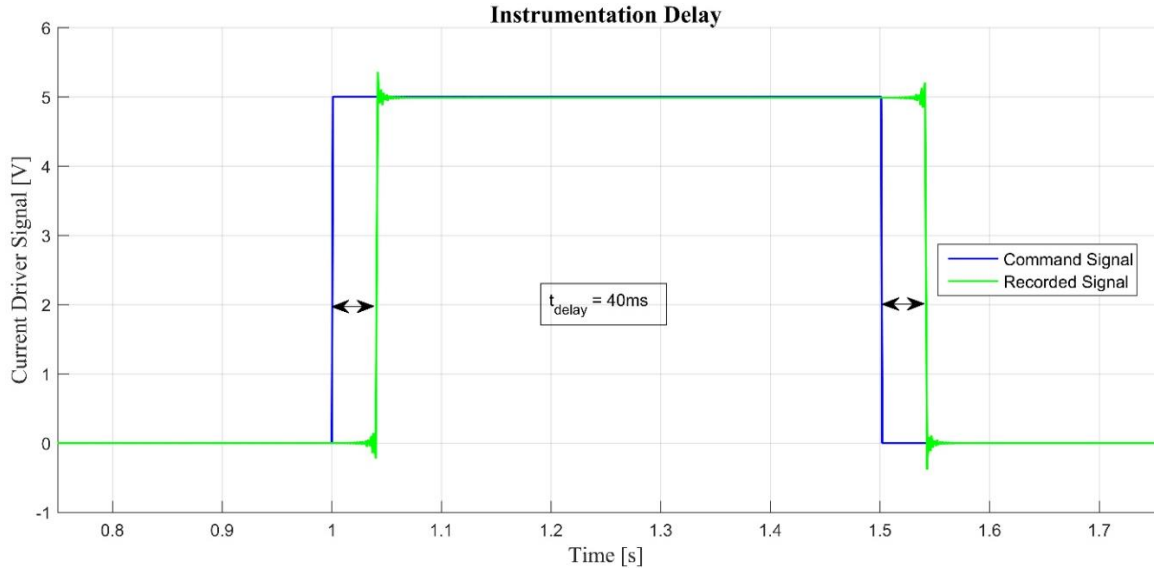


***Figure 3.7: Delay between command and recording signal***

## Hydraforce current driver performance

The response time of the Hydraforce current driver was investigated by comparing the user-defined command signal with the recorded current as derived from the voltage across the sensing resistor. The Hydraforce current driver was configured to deliver 1.5A for a voltage command above 9.5V and 0A for a command below 0.5V. Any voltage signal between these limits delivers current proportionally. Step command signals were given to charge or discharge the solenoid and the time it took for the current to reach 63% of its final value was used to determine the response time. An example of charging the solenoid from 0A to 1.5A is given in Figure 3.8. The current measurements recorded were shifted by -40ms to account for the instrumentation delay, shown in Figure 3.7, to enable comparison with the user-defined command signal.

The extracted response time of the current driver for the various charging and discharging current steps is shown in Figure 3.9. The response time of charging the solenoid ranges from 103ms down to 98ms for a larger step, while discharging ranges from 61 to 70ms for larger steps. This is far larger than expected, and literature (Koo et al., 2006) also mentioned response times of 10ms. This would likely add an additional delay to the valve response and obscure the performance of the valve. Thus, a fast-responding new current driver, had to be developed to extract the response time of the valve. Further investigation into why this driver responded in such an undesirable manner was not conducted.

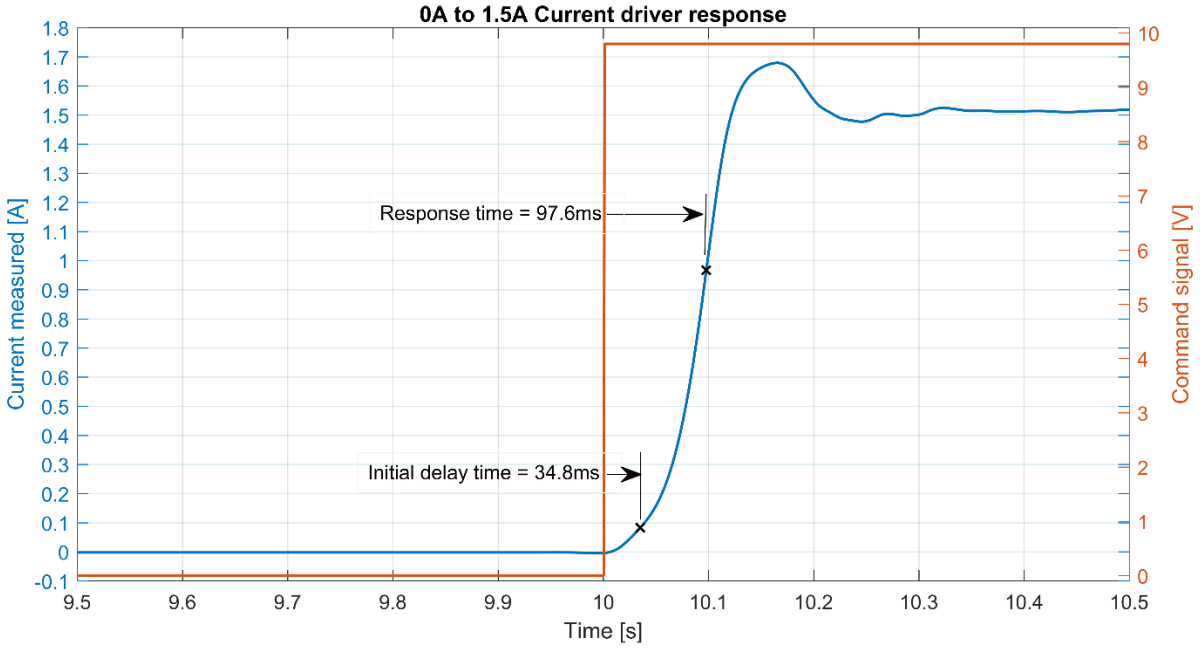


*Figure 3.8: Example of current driver response*

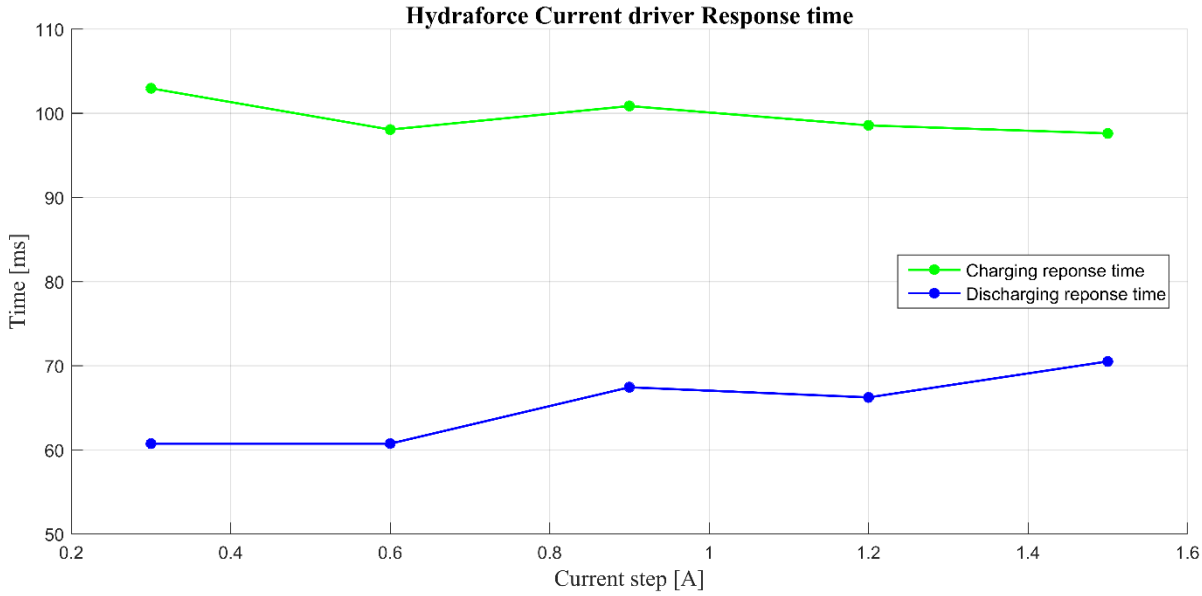


*Figure 3.9: Hydraforce current driver response times extracted*

## Alternative current driver

Since the focus of this study was primarily on the suspension unit itself, a basic fast-responding current driver that could provide a step-up or step-down current was developed. A dual output bench power supply with current and voltage regulation (Rs Components, 2018) was combined with a metal-oxide-semiconductor field-effect transistor (MOSFET) controlled switching circuit, as shown in Figure 3.10. Consequently, this current driver could not deliver a continuously variable current for a given command signal as was possible with the Hydraforce current driver. NMOS is an N-channel MOSFET that can be saturated or switched by a 5V command signal that, in turn, switches the P-Channel MOSFET, PMOS. R2 and R3 are pull-up and pull-down resistors respectively, which ensured that the MOSFET operated appropriately. The command signal was therefore able to connect a secondary current-controlled output in parallel with the other, yielding a step increase in current or a decrease when it was revoked. Resistor R1 was required for power dissipation when both supplies were

connected with a possible voltage difference between them, while having a common ground. As the MOSFETs used are specified to switch within 1ms, the success of this current driver depended on the ability of the power supply to generate and maintain the selected current.

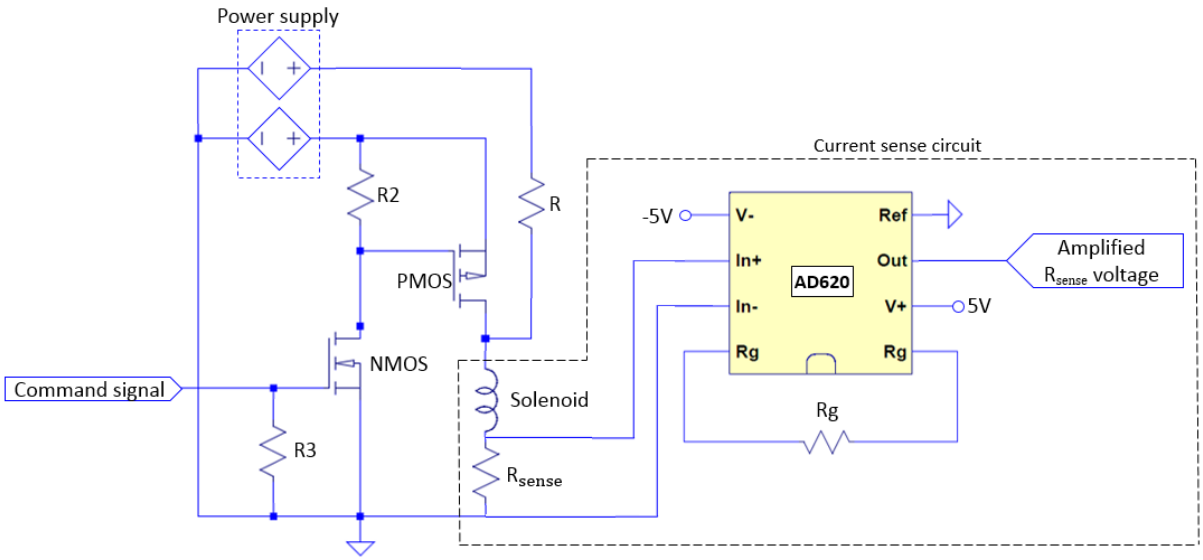


***Figure 3.10: Dual output power supply current driver and sensing circuit diagram***

The response time and accuracy of the dual output power supply current driver was also investigated by comparing the user-defined command signal to the recorded current as derived from the voltage across the sensing resistor. One channel of the power supply was continuously connected to the solenoid, while the other could be connected by saturating the MOSFET with the command signal. One channel was thus always in current-controlled mode, while the other was initially in voltage-controlled mode since it was not connected to the solenoid. When the MOSFET is saturated and the solenoid connected, the other channel transitions into current-controlled mode by reducing the voltage to match the set current. An example of the response time tests results is shown in Figure 3.11. The response was therefore influenced by the voltage the channel was set at before the MOSFET is saturated. In order to minimise the delay and variables, the voltage was set at 24V for all the tests. The slight current overshoot should not affect the damping response times as the current driver settled to the required current much faster than the valve. This was later confirmed to be the case.

The extracted charging and discharging response time of the current driver, compensated for the instrumentation delay, is shown in Figure 3.12. These results showed response times for charging the solenoid from an initial current of 0A and discharging to a final current of 0A. The results showed satisfactory response times with less than 1.5ms for discharging the solenoid, while charging took 1.5ms to 5.7ms. Charging response time is therefore dependent on the current step size. This should be sufficiently faster than the valve, which would later be confirmed and corresponds to reviewed literature. Tests were also conducted where the initial charge current was more than 0A. The results showed that the response time still corresponded to those presented for an initial current of 0A.

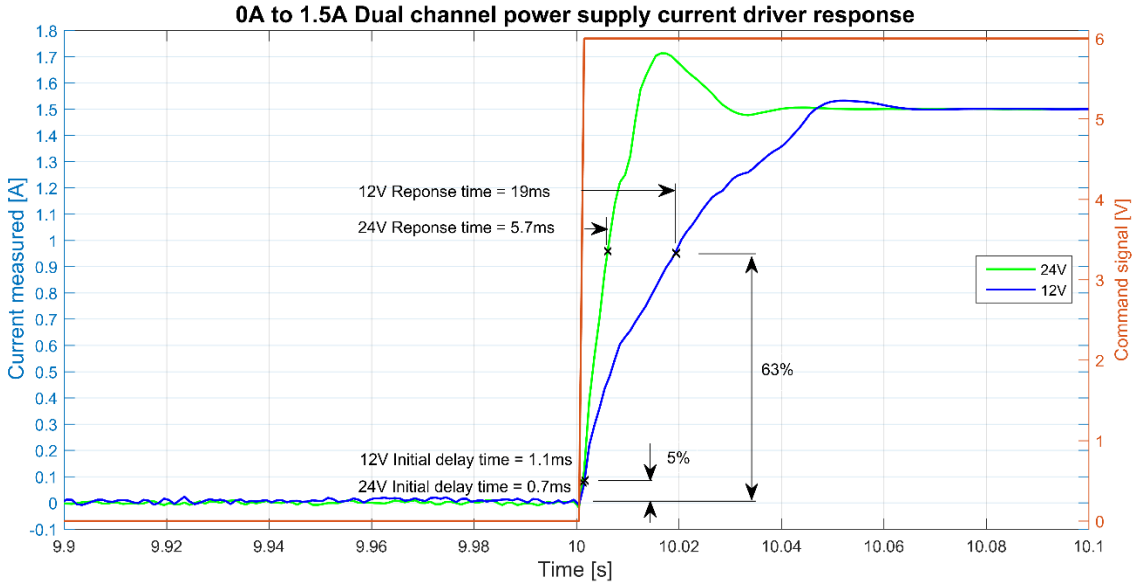


***Figure 3.11: Example of dual output power supply current driver response time test results***

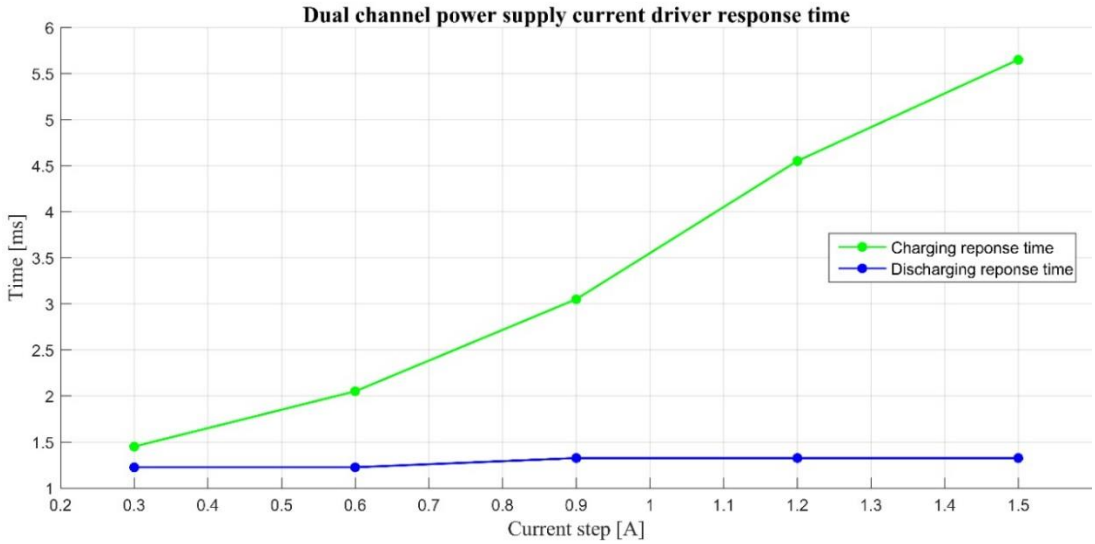


***Figure 3.12: Dual output power supply current driver response time***

## 3.2.5 Control, data acquisition and signal conditioning

The experimental setup consisted of recording six analogue input channels and controlling two output channels sampled at 1kHz, as shown in Figure 3.13. The two output signals for the actuator and current driver were created in MATLAB on the computer system and a modular National Instruments signal generator then converted the digital signal to an analogue signal. The actuator signal was sent to a Zwick K7500 servo controller (Zwick Roell, 2018), which relied on displacement and force feedback from the LVDT and load-cell to accurately and safely control the actuator's two MOOG valves. The current driver signal was a 5V switching signal that connected the additional power supply output.

The six input channels were captured by a National Instruments data acquisition (DAQ) module with a -10V to 10V input range that converted the analogue signals to digital data stored on the computer. The pressure transducer signals were amplified by an AD620 and filtered with a LTC1062, 280Hz low-pass filter. The load-cell and LVDT force and displacement feedback signals that were sent to the servo-controller were also amplified and filtered with a 400Hz low-pass filter before they were sent to the DAQ. These digital signals were converted to their respective units by using their respective conversion

factors. To avoid large phase shifts, relatively high cut-off frequency filters were used. Some channels still required some additional filtering, in which case a zero-phase-shift low-pass filter was implemented in post-processing. Filtering was, however, limited during the response time tests to avoid inducing any time shifts.

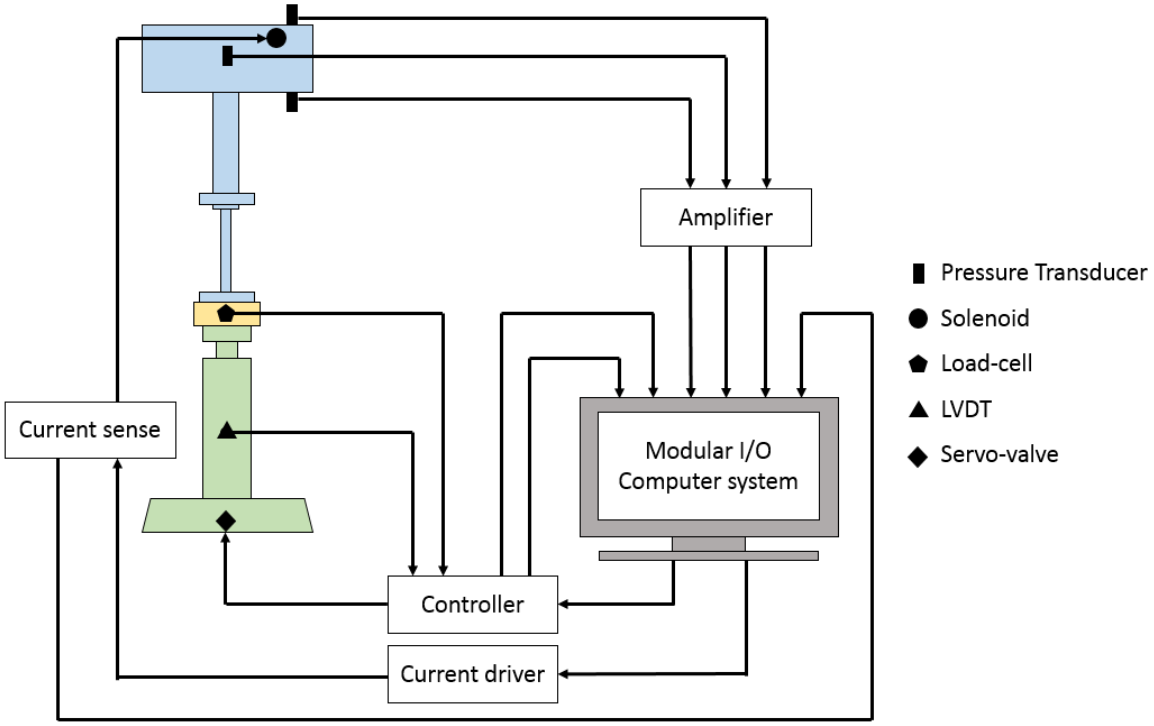


***Figure 3.13: Experimental setup schematic***

Before conducting experiments, all the transducers and measuring equipment were calibrated and zeroed to ensure accuracy of the results. Force and displacement limits were also set to protect the suspension unit and pressure transducers from the unnatural and possibly dangerous actuator output.

## 3.3 Experimental results

This section presents and discusses the results extracted during experimental testing of the $4S_4$CVD. The input or method of extraction is also mentioned. Results include the characterisation parameters required to develop an accurate model. All tests data were recorded at a 1kHz sampling rate.

### 3.3.1 Spring characteristics

The spring characteristics of the $4S_4$CVD were determined by using a triangular-wave displacement input with a frequency of 0.005Hz or period of 200s, resulting in a velocity of 1mm/s. A very slow constant velocity input was used to avoid including any damping effects, with 0mm referring to the fully extended state; for a single cycle the strut was compressed to -115mm and then extended to -15mm. The range of -115mm to -15mm was used to safely avoid physical restrictions and high pressures. A sequence of three cycles were repeated to extract the spring characteristics of the $4S_4$CVD. Figure 3.14 shows the load-cell measured force and the force derived from the accumulator pressure for the strut displacement. The one-accumulator stiffness of the $4S_4$CVD was then compared to that of the $4S_4$ (Els, 2006).

The hysteresis in the pressure-derived force could be attributed to the heat transfer between the gas and the surroundings. The load-cell measurement was also susceptible to this effect. However, friction in the seals and, possibly to a lesser extent, the resistance provided by the diaphragm rolling could be

the reason for the larger hysteresis captured by the load-cell. These frictional forces were not captured by the pressure measurement. Although the test frame is reinforced and extremely stiff, hysteresis in the test frame could possibly also be a contributing factor, but was assumed to be negligible. Overall, the two forces corresponded very well. A very slight offset could be attributed to the frictional force not being symmetrical for extension and compression. This will be investigated further in section 3.3.4.

When comparing the $4S_4$CVD and $4S_4$, it was evident that the current one-accumulator $4S_4$CVD resulted in a stiffness that was between the soft and stiff setting of the $4S_4$. This was, to some degree, expected, since a volume of $0.19l$ was less than both the $0.1l$ for the stiff $4S_4$ setting and $0.5l$ for the soft setting. However, the piston rod diameters between the two units differ and equal volumes would therefore not result in the same stiffness characteristics. Due to making the decision of focusing on characterising a single accumulator, it was not deemed critical for the single accumulator $4S_4$CVD to have similar stiffness characteristics to the already optimised $4S_4$. A validated $4S_4$CVD model could instead be used to find the exact combination of accumulator volumes which would produce similar soft and stiff settings. The one accumulator would have to have a smaller gas volume to exclusively produce the stiff setting that could be combined with the other larger accumulator to produce the lower stiffness. The exact accumulator volumes will further be investigated in section 4.7.

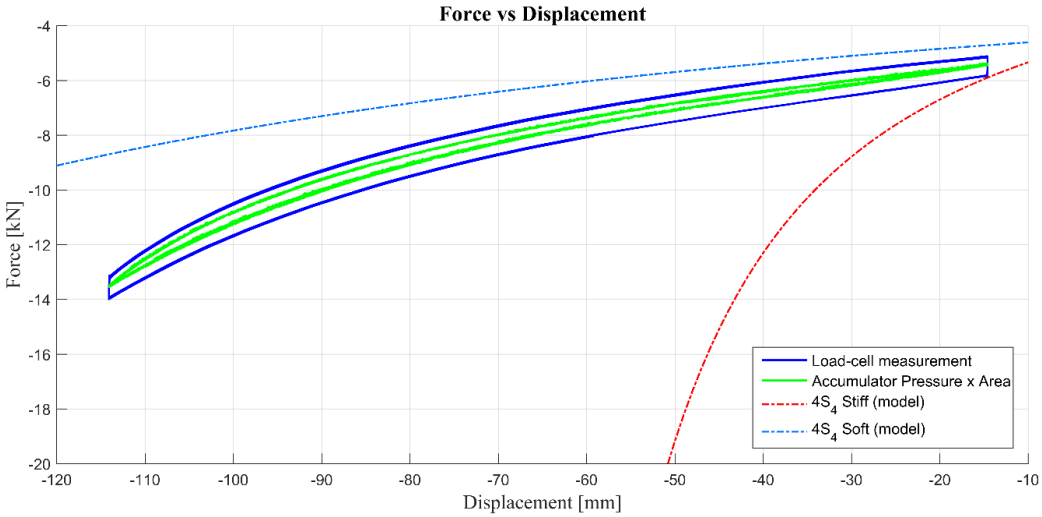


***Figure 3.14: $4S_4$CVD force versus displacement characteristic***

## 3.3.2 Damping characteristics

The damping characteristics of the $4S_4$CVD essentially comprises of the pressure drop over the valve and the valve block channels or ports. This is dependent on the flow rate and current applied to the solenoid. Consequently, to extract the damping characteristics, the flow rate and current were kept constant for each test run. Different frequency triangular wave displacement inputs were used to obtain the various constant velocity inputs. For each current setting, the suspension unit was subjected to constant velocity inputs, as shown in Figure 3.15. The derivative of the measured displacement input was used to represent the velocity input. Although the command was an ideal triangular displacement wave, it was evident from the velocity input that the actuator needed some time to respond, that it overshot slightly and only then achieved the desired constant velocity. To ensure this did not affect the results, only data within an upper and lower displacement limit was used to extract the damping characteristics for a specific velocity.

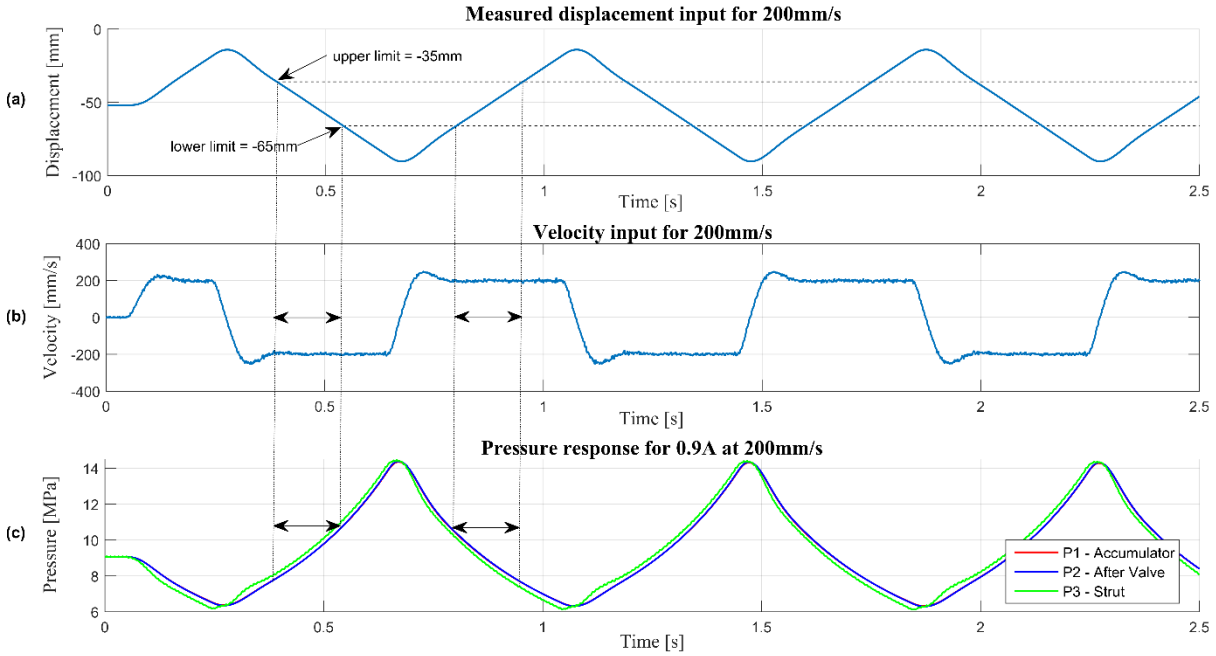


***Figure 3.15: Example of recorded data used to extract damping characteristics (a) Displacement input, (b) Velocity input, (c) Pressure response***

As previously discussed in section 2.2.2, the 4S$_4$CVD design consists of a normally open (NO) and a normally closed (NC) solenoid valve. This is to incorporate a safety aspect where if the control system would fail only the 1 valve would be open, therefore resulting in a stiffer spring better for handling and stability. Both valves were installed and characterised separately.

## Normally open valve damping characteristics

To extract the damping profile with the NO valve installed, the solenoid current was varied from 0A to 1.2A in 0.3A increments. At each of the five current settings, the velocity was increased after each test run until a sufficient pressure drop could be recorded. The pressure-compensated flow-control valves produced exponentially increasing damping as the flow increased. In addition, there was a slight delay in the control electronics to immobilize the actuator after the imposed force limit was exceeded. This, combined with the illustrated velocity overshoot, meant that the maximum pressure drop was limited to ensure the pressure remained well below the 50MPa limit of the pressure transducers. The pressure response for 0.9A at 200mm/s is shown in Figure 3.15 (c). The accumulator pressure, P1, and pressure after the valve, P2, were virtually identical, indicating no pressure drop over the diaphragm. The damping of the unit could therefore be defined by the difference between P2 and the strut pressure, P3, which accounted for the pressure drop over the valve as well as the ports and channels.

The various velocity and currents tested to obtain the force versus velocity characteristic for the NO valve are shown in Figure 3.16, along with the baseline (stock) dampers and 4S$_4$ damping for comparison (Els, 2006). As expected, the flow-control valve provided progressive damping, increasing exponentially as the absolute velocity increased for each current setting. These results could be used to fit and validate a model to determine the resultant pressure drop or damping force for any given velocity and current combination. The manufacturer's low resolution flow versus pressure drop specifications, shown in Figure 2.9, could also be used to generate a force versus velocity curve for comparison. However, the viscosity of the oil used during testing was 46mm$^2$/s, while the manufacturer used oil with a viscosity of 32mm$^2$/s. This, combined with the additional restrictions of the valve block ports and channels, made such a comparison challenging.

When comparing the damping characteristics of the 4S$_4$CVD, it was evident that the 4S$_4$CVD was capable of a much lower damping setting than the 4S$_4$ which was known to be too high (Els, 2006). Figure 3.16 compares the damping a single valve would have. However, the two-accumulator design in ride comfort mode would allow flow through two valves, which would decrease the damping of the 4S$_4$CVD even further (up to a factor of 2). Based on the recommendation made by Els (2006), which stated that damping should be 50% less than the baseline value for significant ride improvements, the results therefore indicated the desired low damping that should yield improved ride comfort. Testing of the 2 accumulator version of the 4S$_4$CVD is required to prove this. In terms of the hard setting, the 1.2A setting was slightly lower than the hard setting of the 4S$_4$. However, the valve could proportionally increase the damping up to being fully closed; a higher current setting of about 1.3A should therefore provide similar or even higher damping.

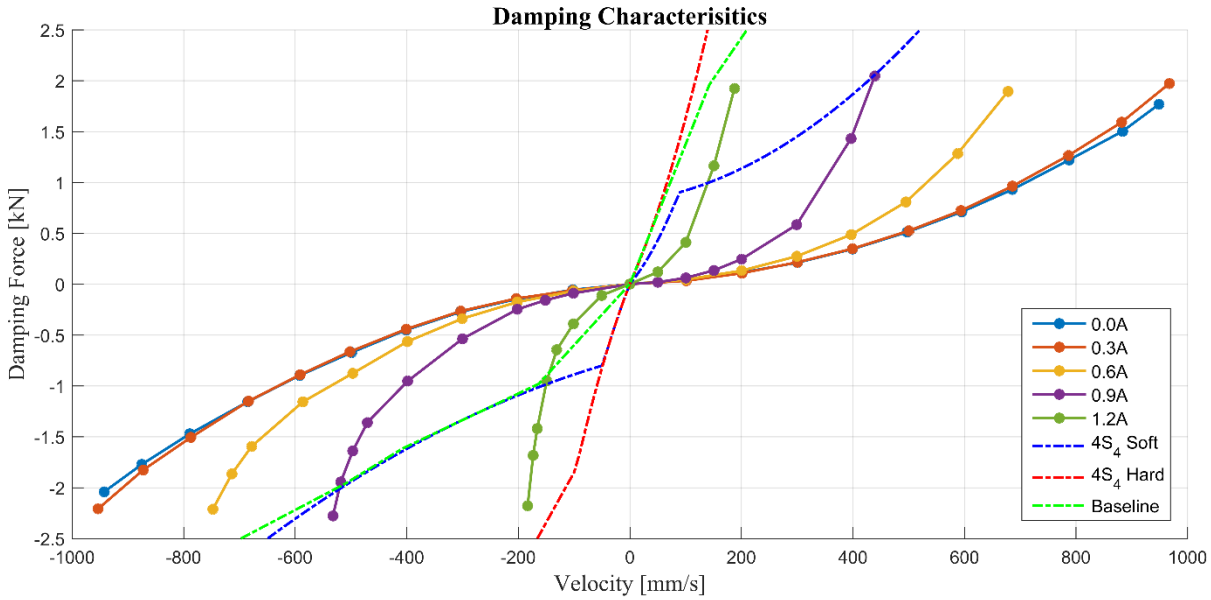


***Figure 3.16: 4S$_4$VD force versus velocity characteristic with the normally open valve***

## Normally closed valve damping characteristics

The pressure drop over the NC valve is inversely proportional to the current, however the maximum flow rate is the same as the NO valve, as previously shown in the manufacturer specifications (Figure 2.9). Therefore, by altering the current, both valves should be able to achieve similar damping characteristics throughout their operating range. The same method used to extract the NO valve damping characteristics in Figure 3.16 was used to determine the NC valve damping characteristics presented in Figure 3.17. The results indicated that both valves do indeed produce the same low damping characteristic. However, increasing the damping with 0.3A current steps, shows that the damping with the NC valve increases more when compared to the NO valve that was also changed at 0.3A steps. The shape defining the force vs velocity relation remains similar and consequently, the current could be manipulated so that both valves could produce the same force versus velocity characteristics. For example, applying 0.8A with the NC valve would produce similar characteristics to 0.9A with the NO valve.

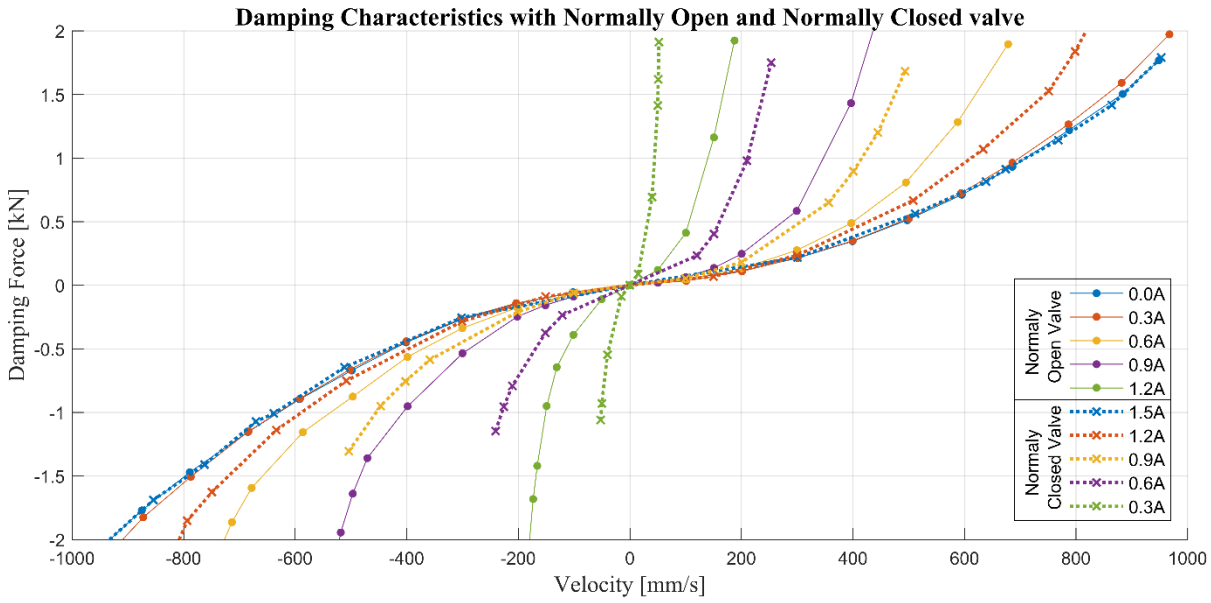


***Figure 3.17: 4S$_4$VD force versus velocity characteristic with the normally open and normally closed valve***

## High and low pressure damping comparison

Even though the valves are pressure compensated, the accumulator was charged at a different pressure and retested to confirm whether the damping characteristics were indeed independent of the pressure. This was done to ensure that the 4S$_4$CVD's damping characteristics were still applicable when changing the accumulator charge pressure is changed. The same method used to produce the previous damping characteristics (Figure 3.16) was used to determine the characteristics for 7MPa accumulator charge pressure which was then be compared to 5MPa previously used. The results, as presented in Figure 3.18, confirms that the damping is independent of the charge pressure. This is to be expected, as the valves are pressure compensated. Only a few tests were therefore conducted to confirm this and to justify the applicability of the damping characteristics for different charge pressures.

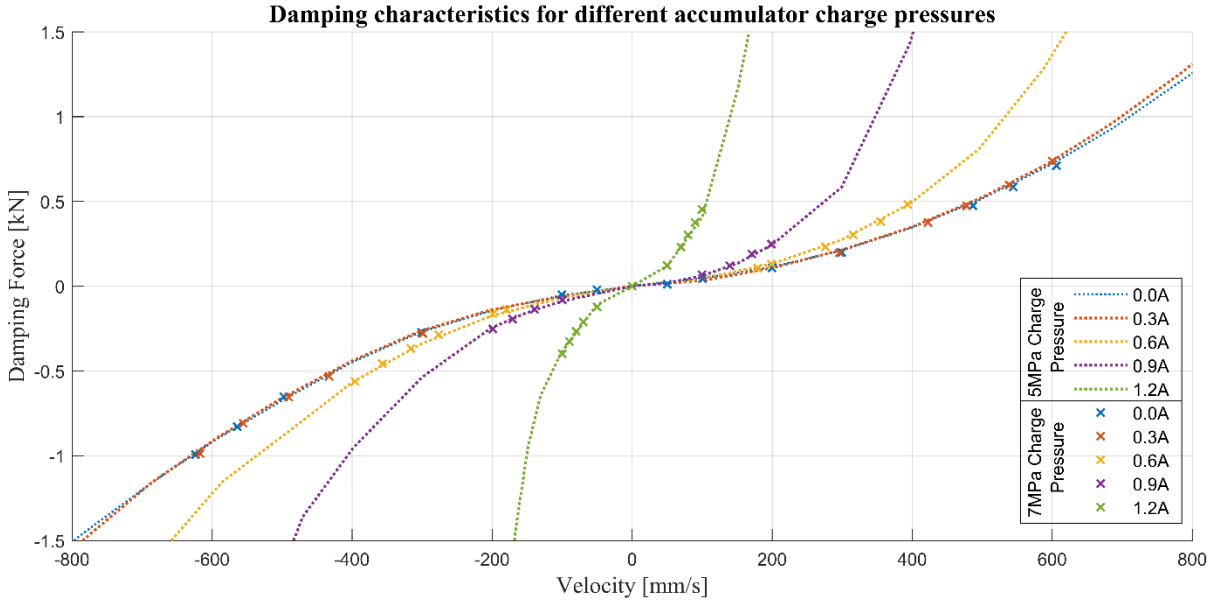


***Figure 3.18: 4S$_4$VD force versus velocity characteristic for different charge pressures***

### 3.3.3 Response time

To accurately extract the true response time of the 4S$_4$CVD, all aspects causing delays in the recorded measurements had to be considered. Comparing the user-defined command signal to measured response signals could include a combination of delays from the instrumentation, actuator, current driver and valve. Implementing a constant velocity input, as previously shown in Figure 3.15, eliminated the effects of the actuator response time. However, the remaining instrumentation, current driver and actual valve response time had to be investigated separately in an attempt to quantify the delay of each component. As mentioned previously, the main focus of this study was the response time of the solenoid and valve combination to generate the desired damping force. A suitable current driver could be developed and optimised in future. The instrumentation delay along with the newly developed current driver and its response time has previously been sufficiently investigated and quantified in section 3.2.4. The current driver delivers the desired current within 6ms for extreme cases (0A to 1.5A) and discharges within 1.5ms for all cases. All the data presented here has been shifted by 40ms to compensate for the instrumentation or recording delay.

In this section the valve response time, with reference to the pressure drop over the valve rather than the physical valve displacement is presented. As the literature indicated, accurately extracting the full response time profile of the valve proved to be challenging. To extract the response time, the 4S$_4$CVD was actuated by a constant velocity input and the command signal actuating the valve was sent effectively halfway through the stroke, as shown in Figure 3.19. To account for the response time, the command signal was advanced by 50ms. The measured pressure drop before and after the valve was switched evidently needed to settle in order to effectively determine the response time. Figure 3.20 shows an example of the tests results and how the response time was determined.

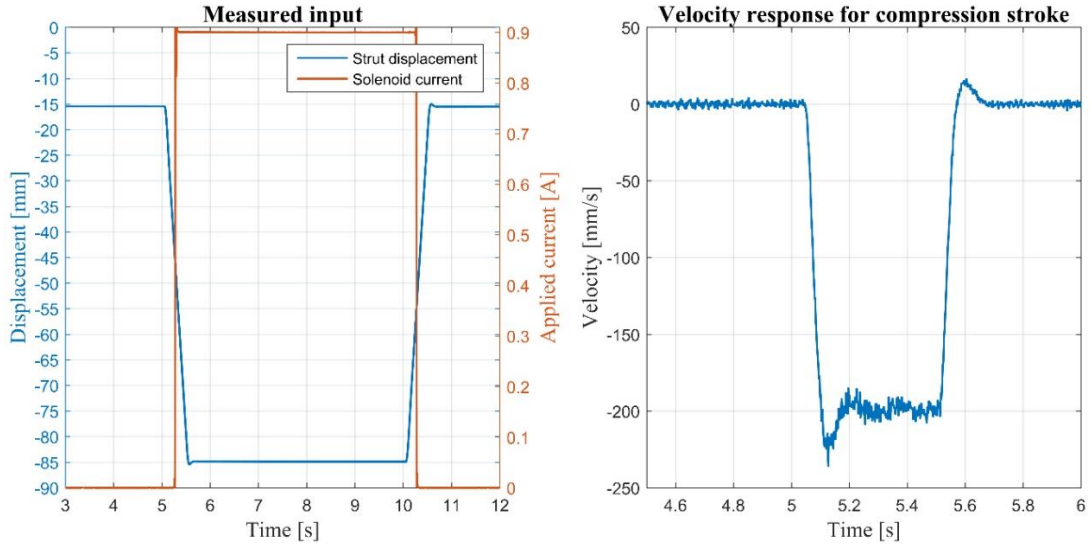


***Figure 3.19: Valve response time input***

However, by using this method it was not possible to determine the response time of the valve to fully close by means of displacement control, since the pressure drop would continuously rise at a dramatic rate that could possibly damage the unit. To determine the response time of the valve closing, a bypass channel could be implemented, as used by Els (2006) for the 4S$_4$ and Van Rensburg et al. (2002) in his tests. Another possibility was to control the actuator in force rather than displacement control. This would raise other challenges. Closing the valve needed to be timed so that the valve was closed before the end of stroke was reached. Evidently, this has the danger of also causing damage. It was therefore decided to determine the response time to a high damping or nearly closed state that still allowed some flow. This should also give a clear indication of what the response time to fully close would be.

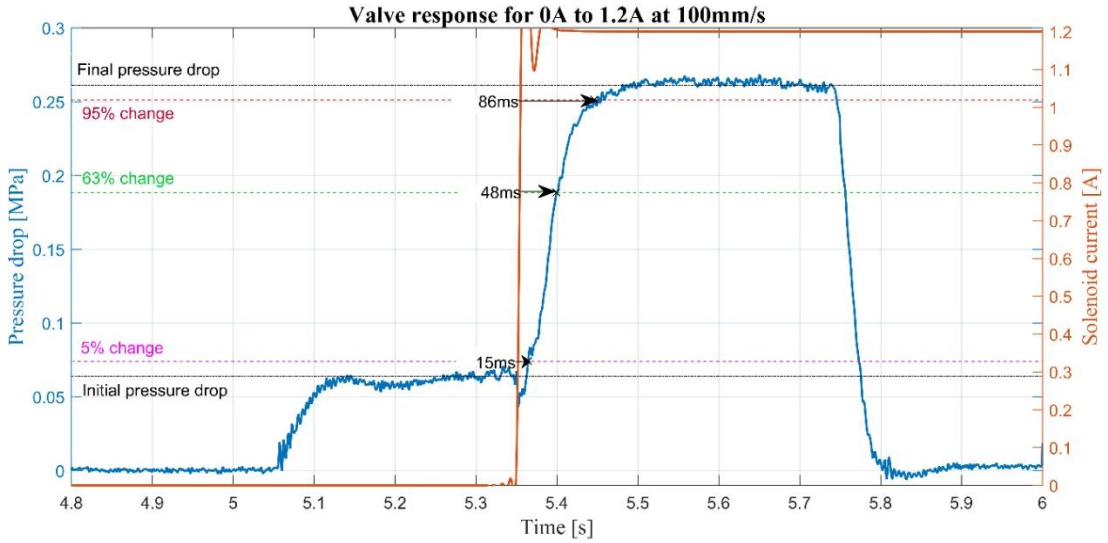


***Figure 3.20: Illustration of extracting valve response time***

Because of the relatively short usable stroke of the 4S$_4$CVD, it became quite difficult to achieve the steady pressure drop before and after switching at higher velocities. Not only did the total time completing the stroke decrease, but the higher the required velocity became, the more the actuator overshot. Figure 3.19 shows a velocity input determined by differentiating the measured displacement input, which indicates the overshoot. The displacement overshoot also translated into a pressure overshoot, which first had to settle, as shown in Figure 3.21. This became a problem when attempting to extract the response time at low damping, since it required higher velocities to generate a noticeable change in pressure drop after switching. In an attempt to account for this, the command signal was slightly delayed to allow the pressure drop to settle before switching. As the actuator control was already tuned and increasing the gas volume requires redesign, the only other solution was to decrease the input velocity. However, this resulted in a reduced pressure drop and could obscure the results for low current settings (low damping) that required higher velocities.

Figure 3.22 shows the test results of attempting to extract the response time of charging the solenoid from 0A to 0.6A with an input of 200mm/s. Even with the fairly low velocity, the combination of overshoot and a mere 50kPa difference between the initial and final pressure drop made it impossible to extract a representative response time. The decision was therefore taken to focus on determining the response times charging the valve to higher damping (0.9A and 1.2A).

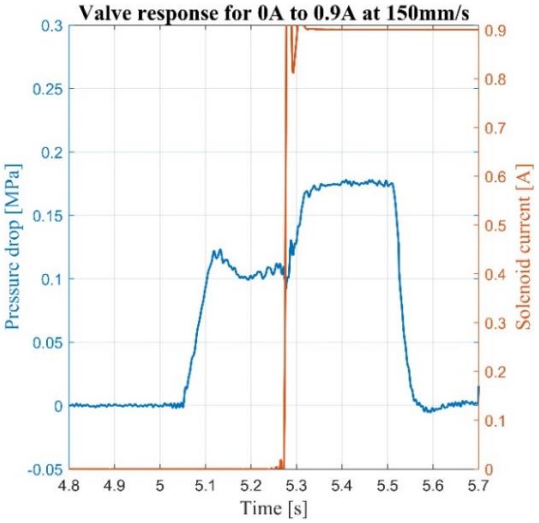


***Figure 3.21: Valve response with overshoot***

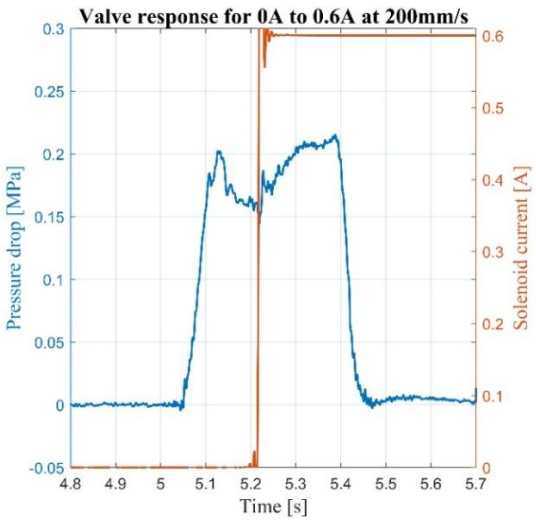


***Figure 3.22: Unclear valve response***

Figure 3.23 shows the response times extracted using the same input method illustrated in Figure 3.19 for various pressure differences between the initial and final pressure drop. The excitation velocity was increased for a higher pressure difference and decreased for a lower pressure difference. Only limited results could be extracted for the 0.9A state, due to the above-mentioned reasons. It can be noted that closing the valve to the 1.2A state responded under 50ms, while the 0.9A state was faster at about 37ms. Opening from 1.2A and 0.9A to 0A damping state was much faster at under 8ms and 12ms respectively. From the results it was evident that closing the valve took notably longer than opening it. The response time when closing the valve increased slightly as the pressure difference increased, however when opening the valve the response time decreased as the pressure difference increased. This could be attributed to the pressure drop resisting to close the valve, but assisting to open the valve. Therefore, increasing the pressure drop (closing the valve), the solenoid valve had to work against the force due to the pressure drop, while when opening, the force assisted the valve.

The response time could be influenced by the initial current or the step size, consequently the current dependent response time was also investigated. Figure 3.24 shows the response time closing the valve to the 1.2A state from different initial states (ranging from 0 to 0.9A) and then opening it from 1.2A to the same initial state. These response times were all recorded at a pressure difference of about 190kPa. When closing the valve, the response time increased the lower the initial current state was. Closing from the 0.9A to the 1.2A state only required 17ms, while from 0A it required about 48ms. This was to be expected, since larger steps required the valve to physically move more. However, when opening the valve, the response time decreased the lower the final current state was. Opening from the 1.2A to the 0.9A state required 14ms, while to 0A it required only about 6ms. Interestingly this was opposite to closing the valve, since a smaller current step resulted in longer response times. Upon further investigation it was found that this could be attributed to the current driver taking slightly longer to respond in such cases.

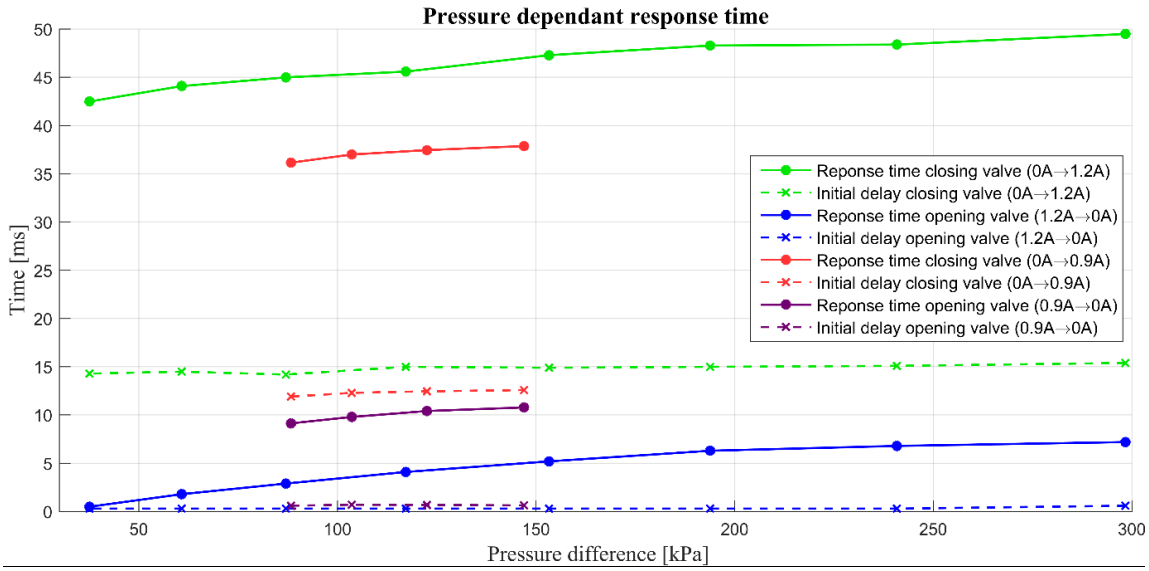


***Figure 3.23: 4S$_4$CVD pressure dependant response time***

Preliminary response time tests were also conducted with the NC valve installed in the 4S$_4$CVD. Results indicated response times very similar to the NO valve. Both valves took roughly the same time to close or increase the pressure drop, while opening or decreasing the pressure was rapid. More tests could be required to fully extract the response time profile for the various dynamic conditions to confirm this.

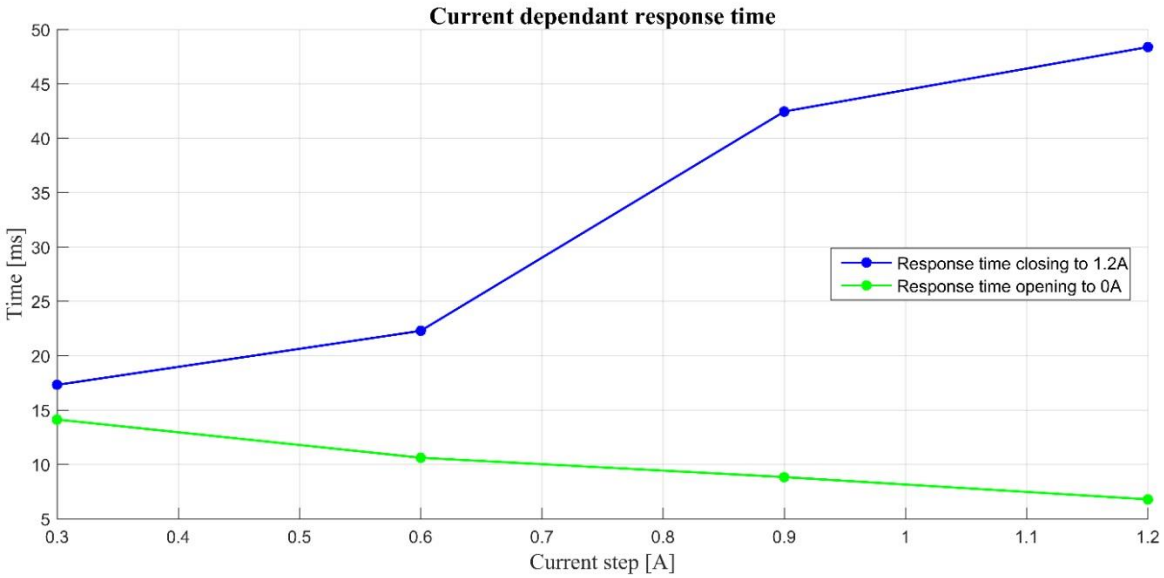


***Figure 3.24: 4S$_4$CVD current dependant response time***

### Concluding remarks

Tests were conducted in order to create a profile and extract the response time for various dynamic states. It remained clear that the response time was also dependent on the test system, as suggested in literature (Van Rensburg et al., 2002). It was noted that, the higher the input velocity and the larger the force variance became, the more difficult it became for the actuator to accurately maintain the defined input. Without being able to control the pressure drop over the valve and sufficient flow it was not possible to extract the full response time profile. Thus, to accurately determine the response time for such a complex continuously variable valve a more controlled environment, such as a high bandwidth test bench, would be required to produce the dynamic states. The current driver in this study was developed only for testing purposes. It is therefore advised to use the current driver which would be implemented with the vehicle setup in future testing to determine the response times, since it would produce the most representative results. However, the results presented should be sufficient to develop a model and analyse the performance of the 4S$_4$CVD.

## 3.3.4 Friction characteristics

The spring and damping characteristics previously presented were derived from pressure measurements that excluded the friction-induced force. To determine the total force output of the unit and analyse the friction of the new design, the friction characteristics had to be determined.

The friction characteristics were extracted by various triangular displacement, constant velocity inputs ranging from 0.5mm/s to 200mm/s. The measured load cell force included the spring and damping component. Although it was possible to eliminate the spring-force component by removing the accumulator bleed bolt so that the pressure was at atmospheric, the high internal pressure acting on the seals affects the friction. Breytenbach (2009) proved this friction and strut pressure dependence by characterising the friction of the 4S$_4$ at various charging pressures. He noted that the frictional force increases with pressure and that it is likely caused by hydraulic pre-loading of the seals in the system. He however concluded that the friction pressure-dependence in the working range off the system is small enough to be considered negligible. In an attempt to minimize the pressure-dependence affecting results, the friction was extracted when the suspension was compressed by 50mm with the accumulator charged as previously (7MPa).

The previously determined spring and damping forces were subtracted from the measured force to yield the friction force, as shown in Figure 3.25. The $4S_4$ friction profile (Van Den Bergh, 2014) is presented alongside the results for comparison. It was noted that the maximum friction of 380N or 40kg occurred during compression at a velocity of 0.3mm/s and settled at just above 100N or 11kg for velocities above 200mm/s. The friction was slightly higher during the compression stroke, which corresponds to the pressure and force results presented for the stiffness characteristics in Figure 3.14.

The results showed that there was still stiction, or stick slip friction, that could hamper the performance. However, when comparing the results to the $4S_4$ with a floating piston design, it could be seen that the kinetic friction at higher velocities was considerably less: About 50% less for compression and 30% less for rebound. The larger peak friction of the $4S_4$CVD could be attributed to the actuation velocity being less than the minimum velocity used during the $4S_4$ testing. Additionally, the higher pressures associated with the $4S_4$CVD, different seal tolerances and designs could also be contributing factors. The rolling diaphragm design resulted in lower kinetic friction, however, the friction at low velocities (stick-slip) did seem to be marginally more.

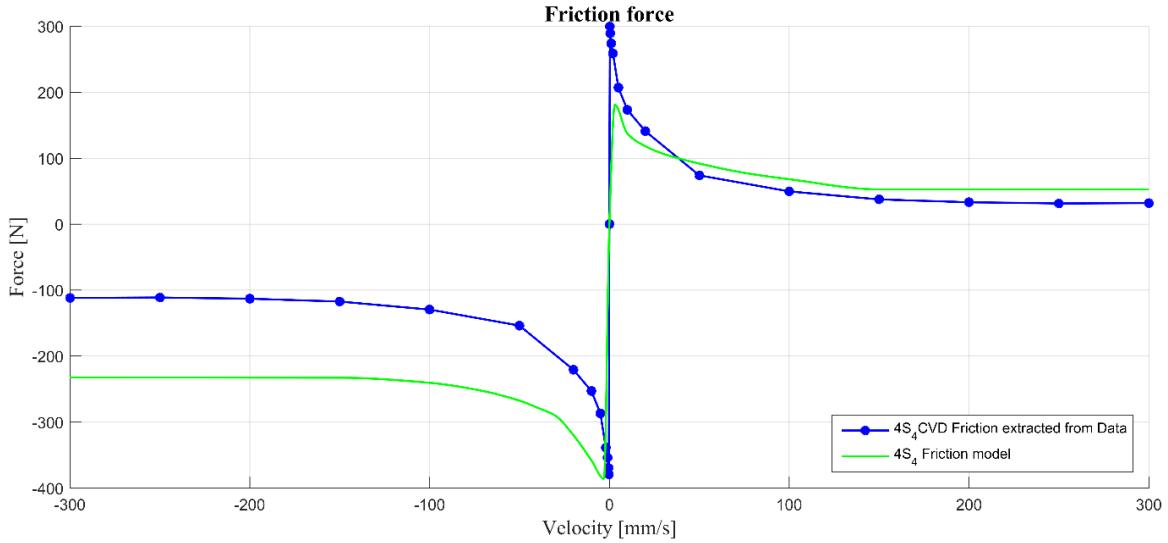


***Figure 3.25: Friction characteristics of $4S_4$CVD***

## 3.3.5 Flow blocking

The success of the two-accumulator design of the $4S_4$CVD relies on the ability of the valve to successfully block flow to decrease the compressible gas volume. Emphasis was placed on determining if the valve had the ability to sufficiently block flow rather than accurately quantifying it. This was done by compressing the unit at maximum velocity for a 3mm step input so that negligible fluid was leaked during compression, as shown in Figure 3.26. A conservative approach was used by not increasing the step size further, since the pressure increased drastically and could damage the unit. The pressure increase shown was due to the fluid being compressed and, as the fluid leaked past the valve, the pressure dropped. The pressure drop over the valve, $\Delta P$, could be used to account for the volume decrease, $\Delta V$, due to compressible fluid using eq. (2-12) where the bulk modulus is 1.4GPa as specified by manufacturer (Shell, 2016) and $V_0$ derived from the CAD model as 275ml.

With the total volume of leaked fluid being equal to the volume decrease, $\Delta V$, the valve leakage rate could be determined by taking the derivative thereof to produce the data shown in Figure 3.27. A maximum leakage of marginally less than 0.2ml/s was noted at a pressure differential of 5.5MPa. To put this into perspective, a mere 100mm/s input produces a flowrate of about 80ml/s. Hydraforce (2013) specifies a maximum internal leakage of 6ml/s, however, one can assume that this is at its

maximum operating pressure of 24MPa, which is essentially three times more than what was tested in this instance.

Accurately quantifying the flow block ability would again present the same challenges discussed during the valve response results in section 3.3.3. However, the preliminary results indicated that the valve would be more than capable to sufficiently block the flow to one accumulator and provide the dynamic stiffness required in manoeuvres. Results presented still included uncertainties, since air in the fluid might have affected the bulk modulus of the fluid and the volume of fluid being compressed was an estimate based on the CAD model rather than an accurate measurement.

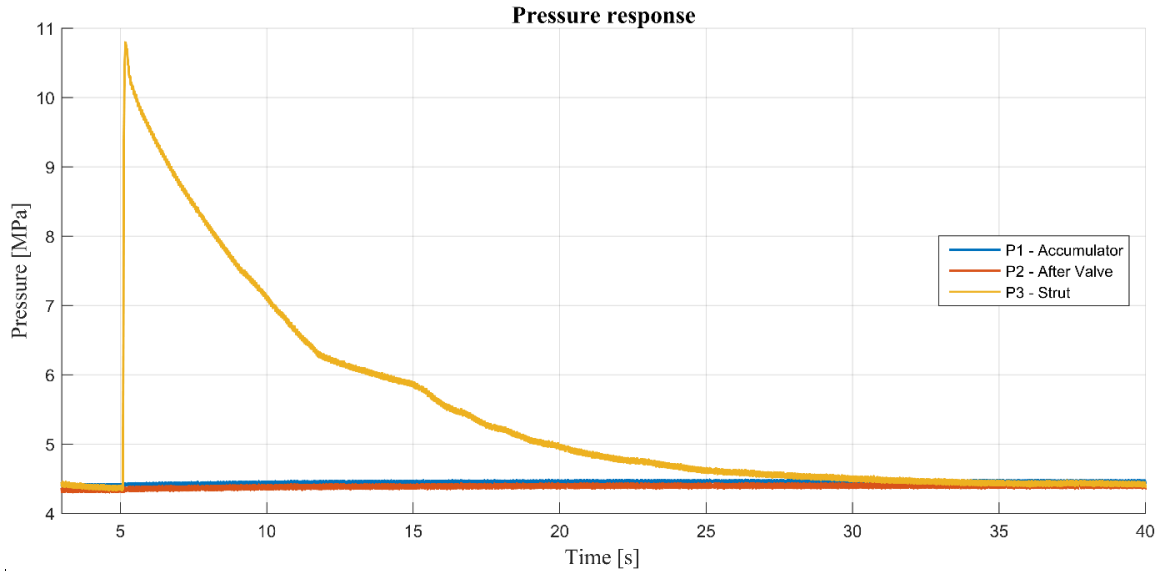


***Figure 3.26: Pressure response for a step input with the valve closed***

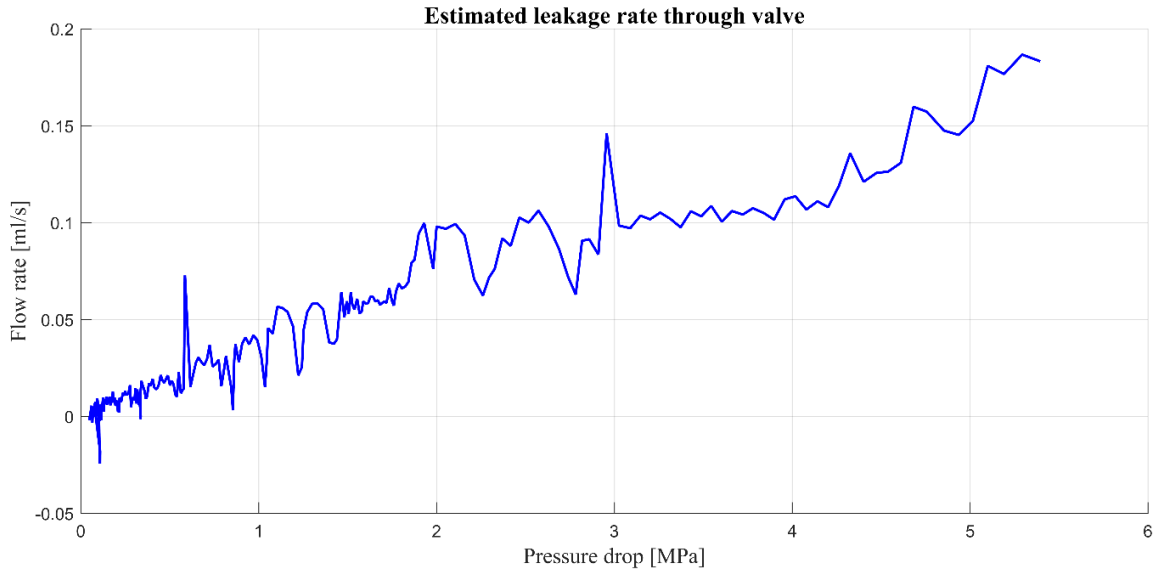


***Figure 3.27: Approximate valve leakage for step input***

## 3.3.6 Thermal time constant

The thermal time constant was required for the pneumatic spring model incorporating the energy equation, as discussed in section 2.4.2. This was determined experimentally by displacing the strut with a step input at the maximum achievable velocity to approximate adiabatic compression. This compression leads to an increase (or decrease in the case of rebound) in temperature, which then

takes time to return to ambient temperature. The time required for the temperature to change by 63% constitutes the thermal time constant. This was determined by using pressure measurements that is analogous to the temperature based on the ideal gas assumption. An example of the test results is shown in Figure 3.28. Various tests were conducted and summarised in Table 3.1. The thermal time constant was greatly influenced by various factors, such as the step size and also the initial and final pressures. However, Els and Grobbelaar (1993) suggested that value differences of up to 30% still resulted in acceptable predictions. The average value of 4.13 seconds was therefore assumed as the future thermal time constant for the $4S_4$CVD model.

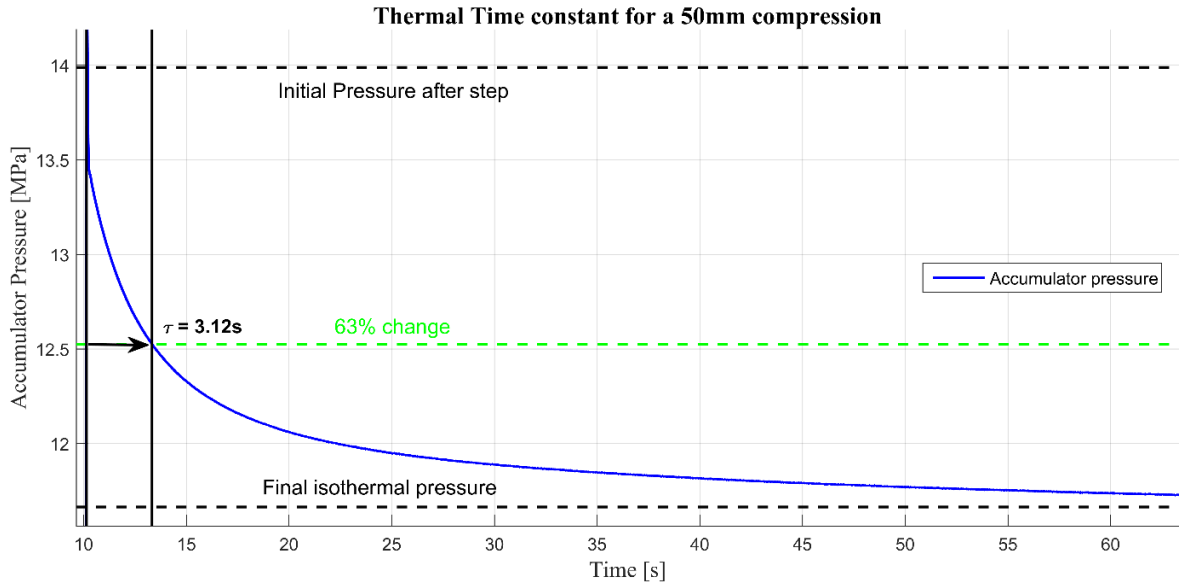


***Figure 3.28: Example of $4S_4$CVD thermal time constant test***

***Table 3.1: Thermal time constant results***

| Stroke Type | Step size [mm] | $P_{initial}$ [MPa] | $P_{final}$ [MPa] | ΔP [MPa] | 63% change [MPa] | $\tau$ [s] |
|---|---|---|---|---|---|---|
| Compression | 50 | 13.99 | 11.67 | 2.32 | 12.53 | 3.19 |
| Compression | 25 | 12.59 | 11.38 | 1.21 | 11.83 | 3.51 |
| Compression | 25 | 10.7 | 9.68 | 1.02 | 10.06 | 4.31 |
| Rebound | 50 | 6.49 | 7.85 | 1.36 | 7.35 | 4.42 |
| Rebound | 25 | 8.26 | 9.16 | 0.9 | 8.83 | 4.24 |
| Rebound | 25 | 7.38 | 8.07 | 0.69 | 7.81 | 5.12 |

## 3.4 Conclusion

This chapter explained the experimental setup to characterise the $4S_4$CVD and presented the results along with a discussion. The results indicated that the unit was capable of the desired stiffness and damping characteristics. However, to accurately determine the correct accumulator volumes, a model is required for further investigation. Although it was concluded that further testing would be required to accurately extract the full response time of the valve, the results justify further investigation of the performance in a simulation-based analysis. The rolling diaphragm design successfully reduced the kinetic friction compared to the floating piston design, however, stick-slip friction remained a factor that could hamper ride performance. The results also showed that the valve is capable of sufficiently blocking flow, however, further testing would be required to accurately quantify the performance. Consequently, sufficient results were extracted to pursue the development of a model that can be used in simulations.

# Chapter 4:
# SUSPENSION MODELLING

Chapter 3 described the experimental characterisation of the components of the 4S$_4$CVD where the spring characteristics, damper characteristics, friction and valve dynamics have been measured. This chapter discusses the development of the mathematical model of the 4S$_4$CVD and its sub-systems. The models of the individual components (accumulator and valves) are validated against test data to quantify the accuracy of the results. A model of the full 4S$_4$CVD, with two accumulators and two valves are developed using these components.

## 4.1 Model philosophy

The aim was to develop a mathematical model that could be used in vehicle dynamic simulations to investigate the performance of the 4S$_4$CVD and the effects of changing certain parameters. A validated full-vehicle model of the 4S$_4$-equipped Land Rover Defender, which is also the intended subject vehicle for the 4S$_4$CVD, has been developed by Thoresson et al. (2009). Consequently, the model is developed with the intent of replacing the 4S$_4$ model and integrating it into the full-vehicle model in future. The model could therefore be developed in MATLAB, which similarly requires strut velocity and displacement but, in addition, also the current command signal as input. The current command signal could either be user-defined or determined by a suitable control strategy. With these three inputs, the force is calculated for each time step.

The layout and operating principles of the 4S$_4$CVD were discussed in section 2.2.2, which showed the manufactured and testing layout along with the final design layout in Figure 2.8. The model was initially developed with a one-accumulator testing layout so that it could be validated by comparing predicted force output with the measured results. The force output is directly related to the pressure of the suspension fluid in the strut cylinder. This pressure is determined by a combination of the accumulator pressures, as well as the corresponding pressure drop, $\Delta P_{valve}$, over the valves and channels due to the fluid flow rate. The accumulator pressure depends on the gas volume of the accumulators that changes relative to the strut displacement, while the damping depends on the fluid flow that changes relative to the strut velocity. The output force could be determined by combining the frictional force, $F_f$, with the product of the strut pressure and piston-rod area. For the single-accumulator 4S$_4$CVD, the force output of the model, $F_{4S_4CVD^*}$ can be described mathematically as:

$$F_{4S_4CVD^*} = -[A \times (\Delta P_{valve} + P_{accu})] + F_f \qquad \textbf{(4-1)}$$

where $A$ is the piston rod area, $\Delta P_{valve}$ the pressure drop over the valves, $P_{accu}$ the accumulator pressure and $F_f$ the friction force. This modelling approach and its sub-models can be described as in Figure 4.1. The suspension model, the 4S$_4$CVD Matlab-file, can be integrated in the desired vehicle model. Each sub-model will be discussed in the sections that follow.

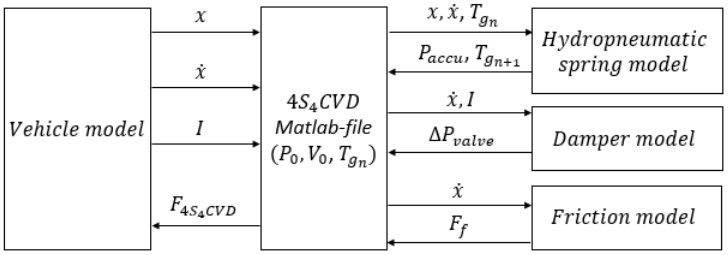


***Figure 4.1: 4S$_4$CVD model layout and interaction***

The validated single- accumulator and valve model will be extended to a full, two-accumulator model of the 4S$_4$CVD, as previously discussed in section 2.4.4. The full model can be used to investigate accumulator volumes and control strategies for optimal performance. Experimental testing of the full, two-accumulator 4S$_4$CVD does however, not form part of this study and some uncertainty regarding the accuracy of the full model remained.

## 4.2 Accumulator pressure

The accumulator pressure was proven to be accurately determined by the BWR real gas model combined with the energy equation, as discussed in section 2.4.2. The following steps were followed to calculate the pressure for every time step in this model. To accurately determine the volume of the accumulator, $V$ for a given displacement input, $x$ the compressibility of the oil is taken into account as:

$$V = V_0 + xA + \Delta V_{oil} \tag{4-2}$$

where the volume decrease of the oil, $\Delta V_{oil}$ due to its compressibility is determined by using the bulk modulus, $\beta$ of the oil:

$$\Delta V_{oil} = \left(\frac{\Delta P}{\beta}\right) V_{0,oil} \tag{4-3}$$

$\Delta P$ refers to the difference in pressure of the oil between filling which is assumed to be the same as the current accumulator pressure. $V_{0,oil}$ is the volume of the oil which the unit was filled with. The mass of the nitrogen, $m_g$, that the accumulator is charged with, can be determined by using the ideal gas law, defined as:

$$m_g = \frac{P_0 V_0}{R T_s} \tag{4-4}$$

where $P_0$ and $V_0$ is the pressure and volume the accumulator is charged with, at an ambient temperature, $T_s$ and $R$ the universal gas constant for nitrogen. The specific volume of the nitrogen can then be determined by:

$$v = V/m_g \tag{4-5}$$

The rate at which the oil volume changes, $\Delta \dot{V}_{oil}$ is assumed to be negligible, thus the rate of specific volume change of the nitrogen is determined based on the strut velocity, $\dot{x}$:

$$\dot{v} = \dot{x}A/m \tag{4-6}$$

This is then used to calculate the specific heat, $c_v$, using eq. (2-9) and (2-10). The change in gas temperature, $\dot{T}_g$, is then determined by the first-order differential equation in eq. (2-8). Finally, this is used to calculate the accumulator pressure, $P_g$, using eq.:

$$P_{accu} = \frac{RT_g}{v} + \frac{B_0 R T_g - A_0 - \frac{C_0}{T_g^2}}{v^2} + \frac{bRT_g - a}{v^3} + \frac{c\left(1 + \frac{\lambda}{v^2}\right) e^{-\frac{\lambda}{v^2}}}{v^3 T_g^2} \tag{4-7}$$

Thus, ultimately, $P_{accu} = f(V_0, P_0, T_g, x, \dot{x})$. For the one-accumulator validation model this sequence of calculations is executed once for every time step, before moving on to determine the pressure drop over the valve. As illustrated in Figure 4.1, with the initial conditions $V_0$ and $P_0$ specified, $T_g, x$ and $\dot{x}$ is given to the model which calculates the accumulator pressure. With $T_{g_1}$ assumed as 25°C the model calculates the gas temperature which is used as input for the next time step, $T_{g_{n+1}}$.

## 4.3 Pressure drop over valve

For an accurate physics-based model to determine the pressure drop over the valve, it is advised that each sub-component of the valve and the channels or ports is tested and modelled separately. Since the suspension system as a whole was tested, such a model therefore does not form part of the study. A continuous model capable of calculating the pressure drop for any velocity and current combination within the operating conditions is required for simulation and control. It was decided to develop a pressure drop versus velocity and current model and to then account for the dynamic behaviour in the form of response time, which will be discussed in the section that follows. Various methods were investigated, however, it was found that using the thin-plate spline method for interpolation and smoothing achieved the best results. Linear, cubic and thin-plate spline interpolation, along with locally weighted scatterplot smoothing (LOWESS), were compared and is discussed in Appendix B.

Figure 4.2 shows a surface plot of the model along with the data points extracted during the experimental testing, as previously shown in Figure 3.16. The thin-plate spline interpolation method was applied to the experimental data to create a surface plot for all the current settings, ranging from 0 to 1.2A. Due to the large pressure drop differences between the 0.9A and the 1.2A setting, some undulations could be noted on the surface plot at -200mm/s, which would not be representative of the actual damping. Overall, the data did, however, seem to be predicted adequately. To analyse this more carefully, the model output and test data is presented in a pressure versus velocity plot in Figure 4.3.

As the model is based on an interpolation method, it approximates the test data very accurately. More importantly, the pressure drop for current settings between the tested values, such as 0.45A and 0.75A, provided representative results. The model seems to slightly “flatten out” the predicted pressure drop at higher velocities (i.e. made it less exponential) as indicated by the red arrows in Figure 4.3. To analyse the previously noted undulation between 0.9A and 1.2A, 1A and 1.1A are presented. In this instance, it is evident that the model does not effectively preserve the shape of the pressure drop and subsequently becomes less accurate. This can be attributed to the sharp increase in pressure drop at 1.2A. To develop a more refined model, extra data points are required and it is recommended that additional testing should be conducted in this region. However, it is expected that the valve would not continuously operate within this region, as it represents fairly high damping. Therefore, the model is assumed to be sufficient for this application. This fairly basic method of predicting the pressure drop over the valve does yield adequate results. After validating the model, it should provide representative simulation results.

By providing a current and velocity input, this model can therefore determine the pressure drop over the valve. This can be added to the pressure determined by the pneumatic spring model to increase or decrease the force output of the $4S_4$CVD. When the suspension is compressed (negative velocity), the resultant pressure drop is positive, irrespective of the applied current. This can be subtracted from the pressure determined by the pneumatic spring model to increase the force output. For extension of the suspension, the output force would consequently be less.

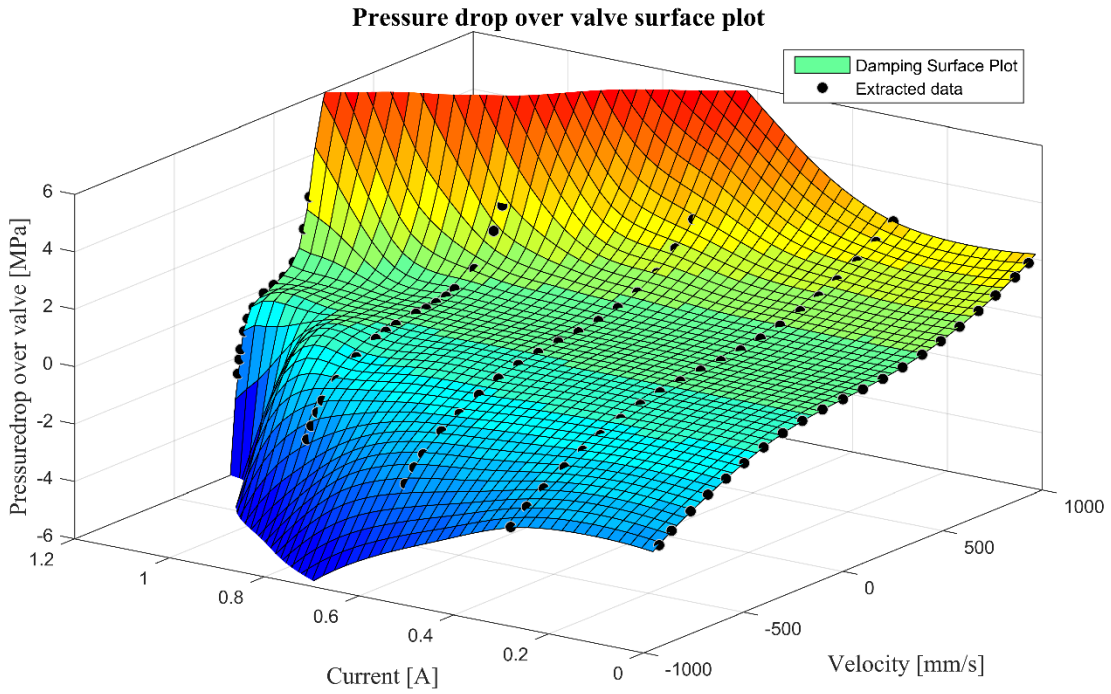


***Figure 4.2: Surface plot of model and data pressure drop over valve***

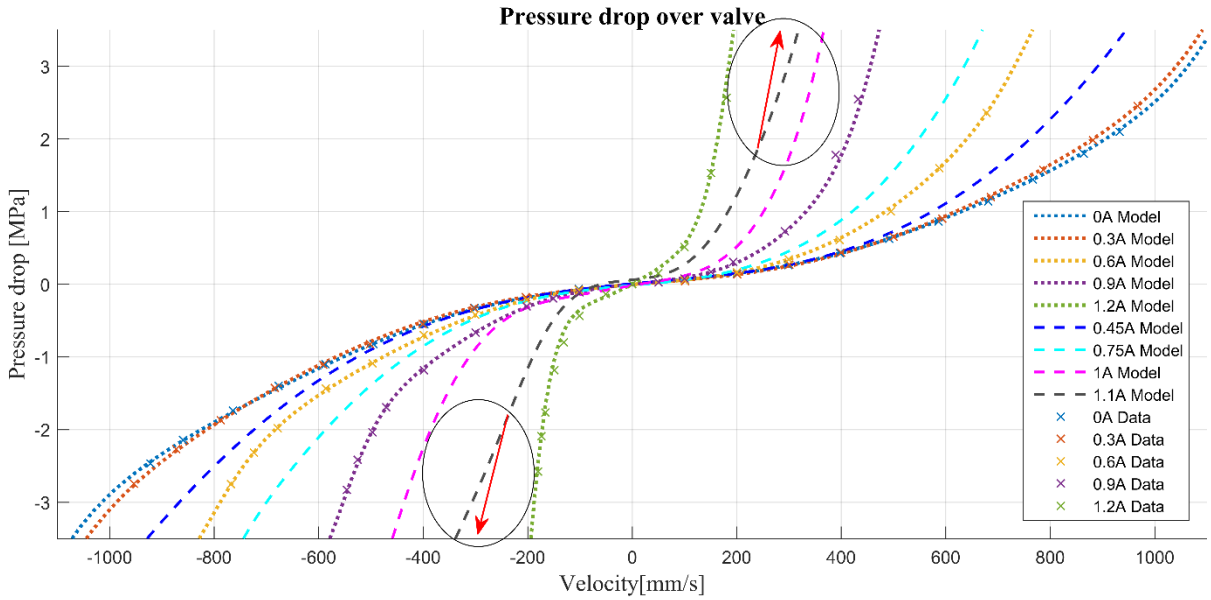


***Figure 4.3: Model and data pressure drop over valve***

## 4.4 Response time

Section 4.3 discussed the model that can determine the pressure drop over the valve for a given current and velocity combination. However, this is based on the experimental data extracted at a constant velocity and current setting. To capture the dynamic behaviour of how the pressure drop over the valve change, the response time, discussed in section 3.3.3, can be incorporated into the model.

The model only considers the velocity input at the given time step to determine the pressure drop. It therefore assumes that previous velocity inputs doesn't affect the current pressure drop calculation. For example, when the previous iteration's velocity input to the model is 100mm/s and the most recent input is 300mm/s, the model output will only use the given input velocity to calculate the

pressure drop. This assumption is made based on the expectation that the velocity would change gradually if a small enough sampling time is used. If the model results in discontinuous or unrealistic force spikes in simulation, this assumption would have to be revised and would possibly require additional experimental data to accurately predict the behaviour.

Dynamic response would, however, be included in the model with regard to changing the valve's solenoid current. For example, when the current is changed from 0A to 1.2A (irrespective of the velocity) the pressure drop needs to gradually increase to the 1.2A level instead of a step increase. Since the model uses solenoid current as an input, the possible electrical instrumentation delay and current driver response time is not accounted for in the model. The electrical delay and the current driver delay can be used to model the demand signal and output current signal which is sent to the suspension model. However, for the purposes of this study, these were assumed to happen instantaneously. Although such delays were shown to be up to 10ms, they would have to be determined for the setup that would be used on the vehicle.

Section 3.3.3 stated that the response time of the valve was influenced by factors such as pressure differences before and after switching, the magnitude of the current step, as well as the input velocity or flow rate. This complex system would require a comprehensive set of experimental data or a physics-based model to accurately predict the response time. In order to simplify the model the dynamic behaviour is therefore taken into account empirically.

The model is developed based on the response time results presented in Figure 3.20 and Figure 3.23. Whenever the current changes, the pressure drop is calculated based on a fraction, $P_{frac}$ between zero and one as:

$$\Delta P_{valve} = \Delta P_{valve,i} + P_{frac}\,(\Delta P_{valve,f} - \Delta P_{valve,i}) \qquad \textbf{(4-8)}$$

where $\Delta P_{valve,i}$ is the pressure drop calculated by the damping model before the current has been changed, $\Delta P_{valve,f}$ is the pressure drop calculated by the damping model for the most recent current and velocity input. This allows the pressure drop to gradually increase to that of the new current and velocity combination. The model uses the response time, $t_{res}$, to determine when the pressure drop changes 5%, 63%, 95% and 100% respectively, as shown in Table 4.1. This was based on experimental response time data such as shown in Figure 3.23. In between these points, Matlab's smoothing spline interpolation with a smoothing parameter of 0.99999 is used to calculate the fraction, as illustrated in Figure 4.4. Two additional data points were added for a fraction of zero and one to improve the shape of the spline.

To simplify the model, a constant response time can be used. Results showed that 0A to 1.2A took up to 50ms for certain conditions, while smaller steps showed responses faster than 30ms. Based on these results, 40ms is was used as the response time for current changes in the empirical model. This is a relatively conservative approach, since all the smaller current changes would happen much faster, however, the more extreme cases could take slightly longer than 40ms. This reduced the amount of variables and ambiguities when analysing the performance in simulation. With this method the effects of the response time can also be analysed effectively by simply increasing or decreasing the response time that is used to calculate the fraction.

This method of modelling the dynamic response could be modified to include the response time dependence on the current step or the difference in the pressure drop before and after switching, $(\Delta P_{valve,f} - \Delta P_{valve,i})$. This was not included in the current model and could be considered in future.

*Table 4.1: Fraction data points for changing pressure drop*

| Fraction $P_{frac}$ | Time | For $40ms$ response time |
|---|---|---|
| 0 | $-0.25 \times t_{res}$ | $-10ms$ |
| 0 | 0 | $0ms$ |
| 0.05 | $0.25 \times t_{res}$ | $10ms$ |
| 0.63 | $t_{res}$ | $40ms$ |
| 0.95 | $1.25 \times t_{res}$ | $50ms$ |
| 1 | $1.5 \times t_{res}$ | $60ms$ |
| 1 | $1.65 \times t_{res}$ | $66ms$ |

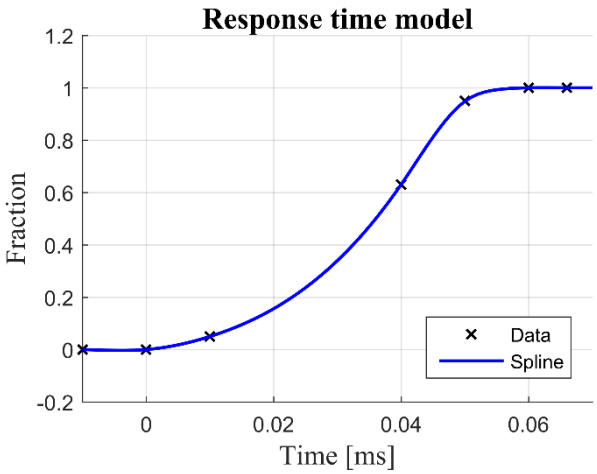


*Figure 4.4: Interpolation to calculate fraction*

## 4.5 Friction

Van Den Bergh (2014) showed that friction force has a significant effect on the simulation results of hydropneumatic suspension systems. However, he concluded that the accuracy gained by using a complex model over a rudimentary look-up model based on experimental data does not justify the additional computational demand. Therefore, to include the frictional force in the model, the friction force is modelled according to the experimental results previously shown in Figure 3.25, rather than a complex physics-based model. Piecewise cubic Hermite interpolation of the data points was used to calculate the frictional force for a given velocity input. The results indicated that the frictional force remains constant at higher velocities. Consequently, an additional data point is added at -1000mm/s and 1000mm/s with the force equal to what was measured for -300mm/s and 300mm/s respectively. The resultant model, along with the experimental data, is presented in Figure 4.5.

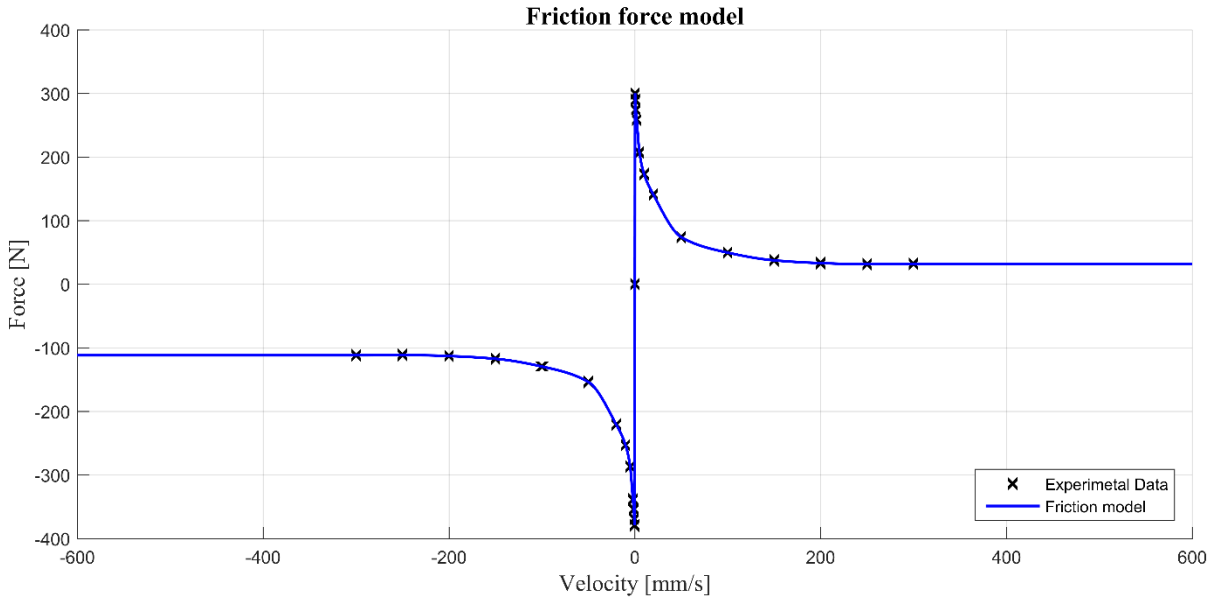


*Figure 4.5: 4S₄CVD friction model*

## 4.6 Model validation

After each part of the single-accumulator 4S₄CVD based on eq. (4-2) had been modelled, the next step was to validate the output of the model and to analyse its accuracy. The model was validated according to tests conducted to characterise the 4S₄CVD, as well as an additional dynamic road input.

### 4.6.1 Hydropneumatic spring

To validate the pneumatic spring or accumulator pressure and friction model the same 1mm/s triangular displacement input used during experimental testing to produce Figure 3.14 is used as input. Due to the noise of the measured actuator input, the digital command signal was used as the model input. When the noisy measured displacement signal is used as input, it results in a similarly noisy velocity signal. The noise in the velocity signal is used as input to the damping model which then leads to inaccurate damping and friction forces.

The displacement input, load-cell measured force and model-predicted force responses are shown in Figure 4.6. The measured and model-calculated forces correlate extremely well for this input. Figure 4.7 shows a force-displacement comparison of the measured force and model-calculated force. For more focus on the pneumatic spring model, the force derived from the measured and calculated accumulator pressure times in the piston rod area is also shown. The force output of the model includes the friction model, while the accumulator pressure output is the pneumatic spring model only. Due to uncertainties regarding accumulator volume and initial accumulator charge pressure, these variables were tuned iteratively until a good correlation was achieved. This could be justified to some extent, as other factors such as compliance in the test bench weren't accounted for and there could be a temperature difference between filling and testing. The estimated accumulator volume was 0.19$l$ and the pressure gauge read 6.9MPa after filling, however, the best fit was achieved with 0.16$l$ and a charge pressure of 6.6MPa. From Figure 4.7, it is evident that, after tuning, the model is capable of accurately predicting the accumulator pressure for the given displacement input. Furthermore, the force output, including the friction for a $\pm$1mm/s velocity input, correlates very well with the measured force output. It is also proved that the model accurately compensates for the compressibility of the oil, which would otherwise have resulted in an overestimated force output at higher pressures. The hysteresis with regard to heat transfer between the environment and the unit is also accurately included. Higher velocity inputs, however, results in more heat generated. This needs to be investigated to further validate the model in terms of heat transfer. The stability and accuracy of the hydropneumatic spring model is evaluated at higher velocity inputs in the next section as the force output is then not only function of the hydropneumatic spring, but also a damping model.

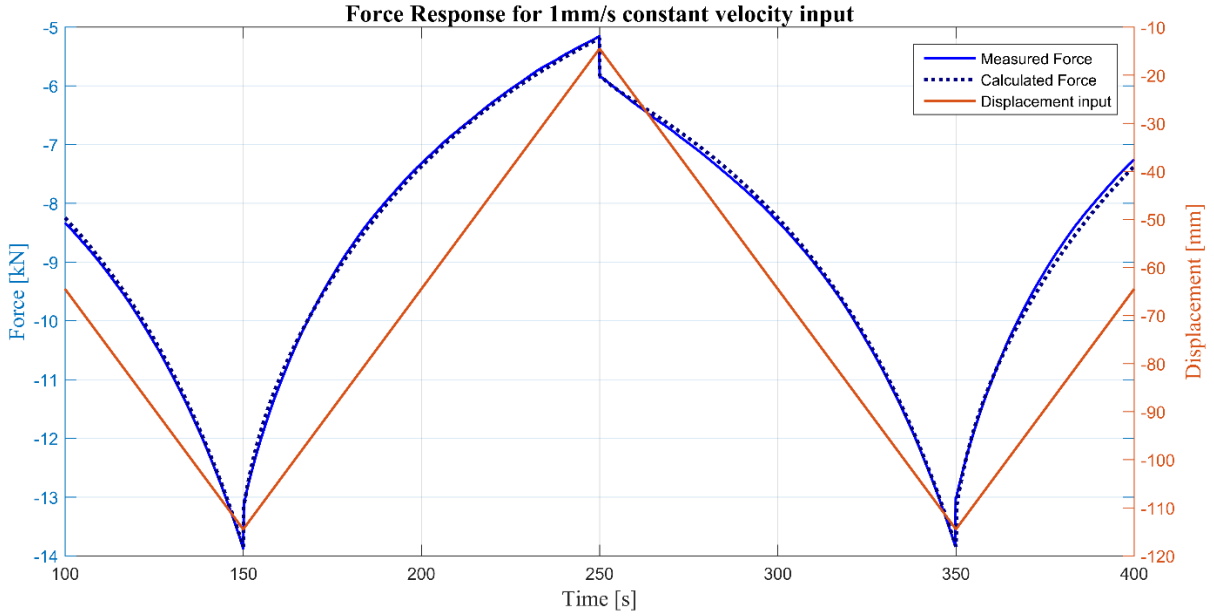


***Figure 4.6: Measured and calculated force response with no damping***

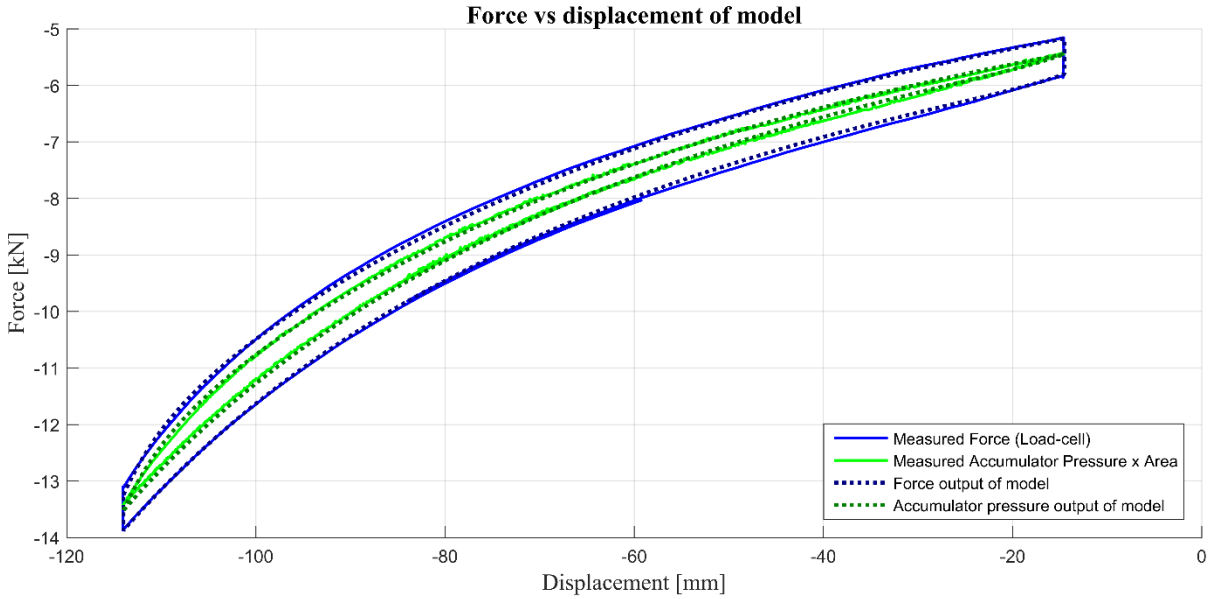


***Figure 4.7: Measured and calculated force versus displacement with no damping***

### 4.6.2 Damping

To validate the damping force calculation of the model, similar triangular displacement inputs can be used, but requires higher velocities to generate significant damping. The pressure drop or damping calculated by the model is essentially equivalent to the output presented in Figure 4.3. The pressure drop versus velocity is therefore not presented, but rather the pressure and force response as well as the force displacement.

The measured 800mm/s constant velocity input, along with the measured force and calculated force for 0A solenoid current, are presented in Figure 4.8. Figure 4.9 shows the measured and calculated accumulator and strut pressure for the same input. The corresponding force-displacement graph is presented in Figure 4.10. The model-calculated and the measured force generally correlates well, while the pressures correlates even better. The initial force offset can be ascribed to the residual force due to stiction, which disappears as the actuator displaces the strut. Some force discrepancies can be noted when the input or actuator changes direction, however, the model returns to the measured force within 20ms. This can possibly be attributed to not taking into account the inertial properties of the piston rod, bearing and mounting that has mass of more than 10kg. During full-vehicle simulation these properties can be accounted for by combining them with the unsprung mass so that the dynamic effects are taken into account by the multibody dynamic vehicle model. It is could also possible that the friction model, which was developed with constant velocity inputs, does not accurately predict the force in such dynamic situations. Since the damping model was developed using constant velocity inputs, there were some concern that it would not be capable to accurately calculate the pressure drop in dynamic situations where the velocity changed abruptly. However, as the calculated pressure responses correlate so well, it can be concluded that the model accurately predicts the pressure drop even in these dynamic conditions.

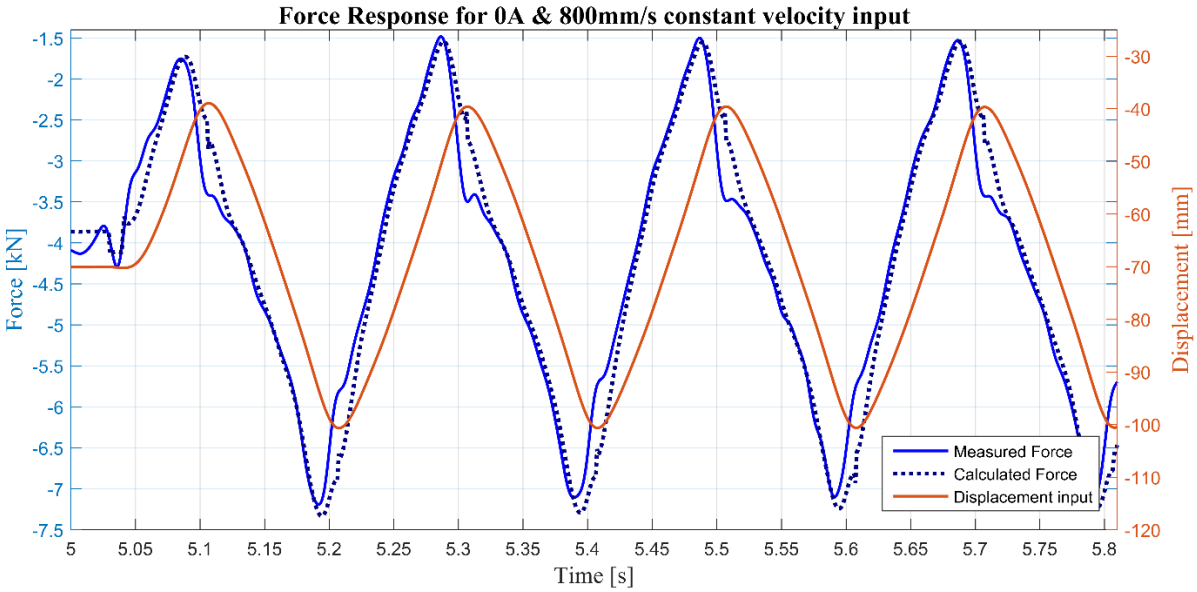


*Figure 4.8: Measured and calculated force response with 0A damping*

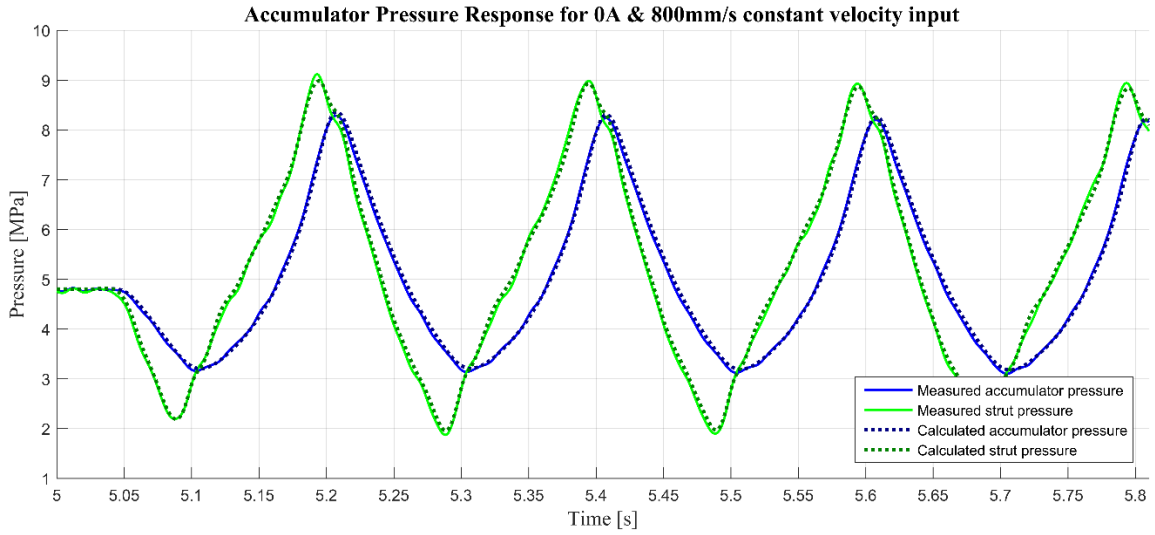


*Figure 4.9: Measured and calculated pressure response with 0A damping*

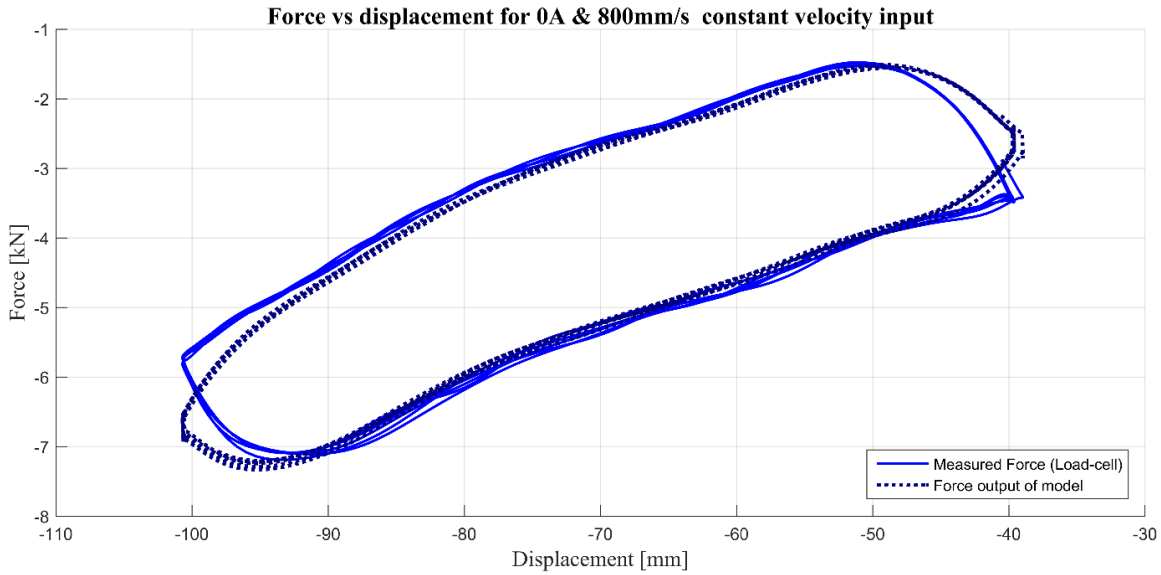


*Figure 4.10: Measured and calculated force versus displacement with 0A damping*

To validate the model for other damping settings, a solenoid current of 0.6A with a 600mm/s constant velocity input was used. The measured and calculated force response, along with the displacement input, are presented in Figure 4.11. The corresponding pressure response is shown in Figure 4.12 and the force displacement in Figure 4.13. The model produces a similar output to the 0A current setting where the pressure responses correlate very well. The measured and calculated force also show good correlation, but includes the same discrepancy after the input underwent a change in direction. Comparing measured and calculated output for these two cases show that the model can accurately predict the force output.

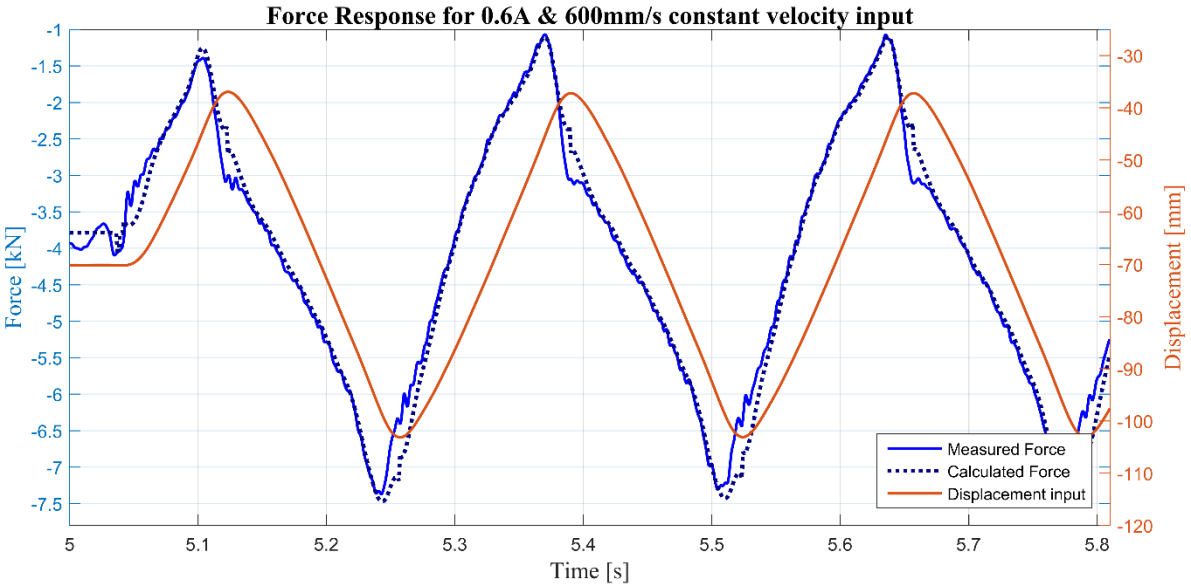


***Figure 4.11: Measured and calculated force response with 0.6A damping***

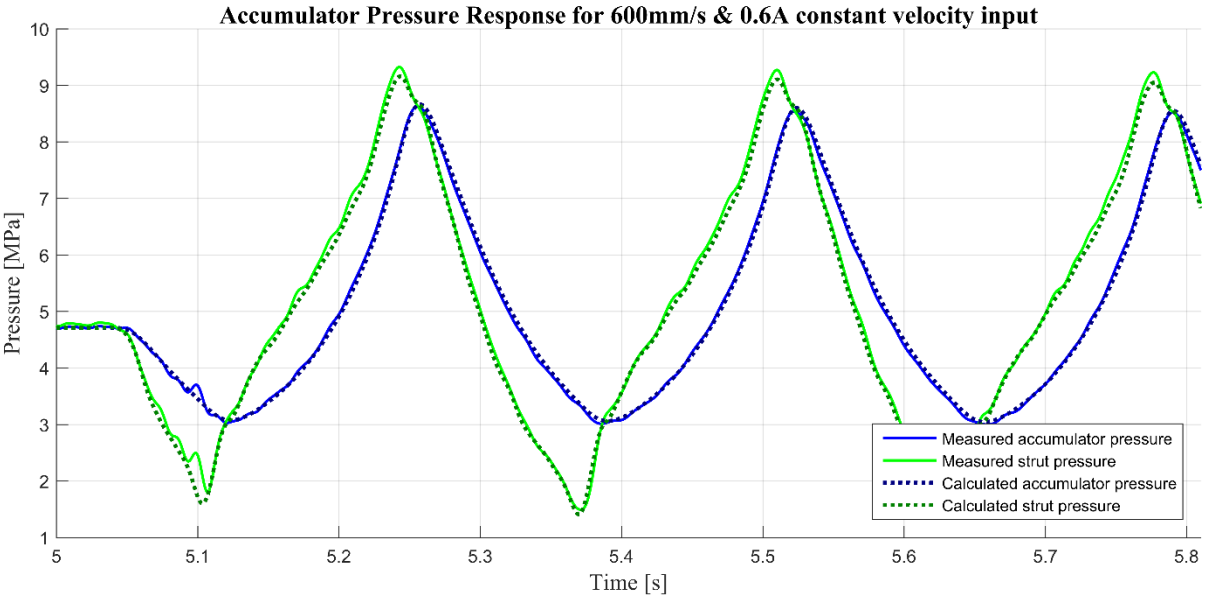


***Figure 4.12: Measured and calculated pressure response with 0.6A damping***

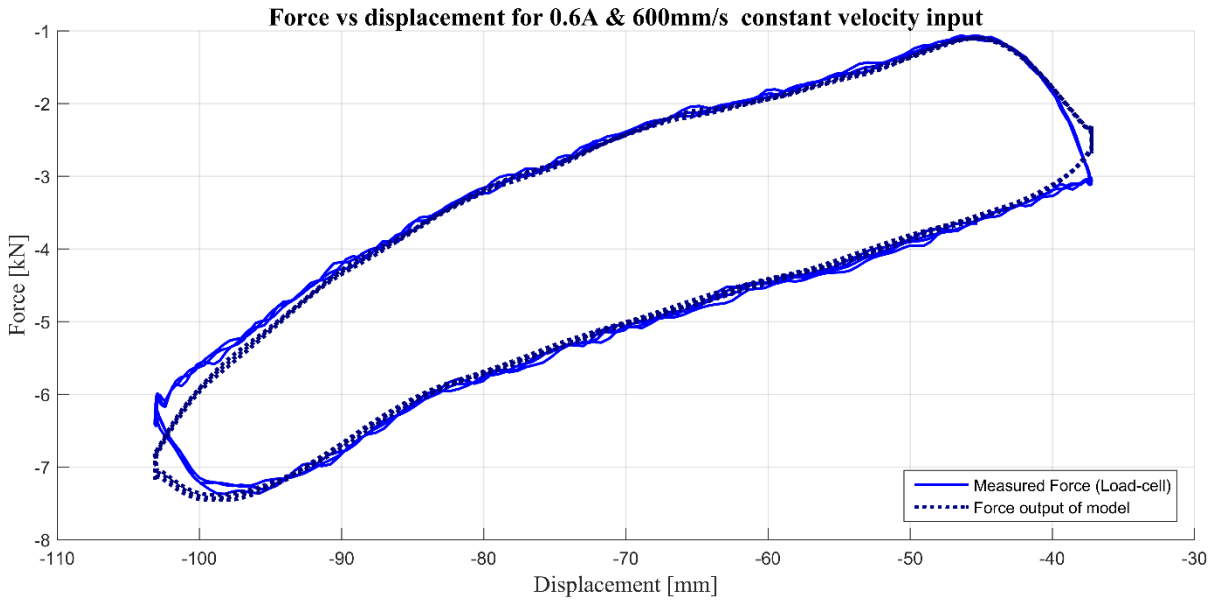


***Figure 4.13: Measured and calculated force vs displacement with 0.6A damping***

### 4.6.3 Response to a road input with constant damping

For further validation, the decision was taken to use a dynamic input based on an artificially generated class-D road, based on the ISO 8608 standard (International Organization for Standardization, 1995). The road has a total displacement of 180mm, which exceeds the stroke length of the $4S_4$CVD used during testing. This was then reduced to 80mm by scaling the total displacement input by a factor of 0.44, i.e. it is not a true representation of a class D road anymore. The decision was taken to apply a constant current to the solenoid to avoid possibly damaging the unit when high current is applied with high velocity. This also reduces complexity and possibly remove ambiguity in the results. The scaled road profile in the spatial domain is converted to the time domain, based on the speed a vehicle would drive over it. Although the displacement would remain unchanged, increasing the "vehicle speed" results in the input signal being at a higher velocity. A vehicle speed was determined iteratively so that the maximum input velocity does not exceed the tested velocity for the chosen solenoid current. For a 0.9A solenoid current, a vehicle speed of 10km/h was selected as it results in a maximum input velocity of 400mm/s. This is within the parameters used during the characterisation tests and would generate adequate damping while not producing damaging damping forces. Due to the above-mentioned limitations, this input is not necessarily appropriate for actual usage, however, the aim is to have some dynamic input which can be used for further validation.

An extract of the measured and calculated force, along with the displacement input, are presented in Figure 4.14. The sudden "steps" or discontinuities in the force response are caused by friction in the system. The suspension is fixed while forcing it with a specific input and as the direction of the input velocity changes the direction of the frictional force changes, resulting in a discontinuity. In reality the actual actuation of the suspension would be different due to the filtering effects of the tyre and the vehicle body being able to translate vertically, however, this can still be used to validate the model. Overall, the model-calculated force output correlates well with the measured force. The largest offset can be noted at large displacements where the force predicted by the model is marginally higher than what was measured, as can be seen at 5.3 seconds in Figure 4.14. It is estimated that this could be due to the pressure dependence of the frictional force as mentioned in section 3.3.4. At 5.3 seconds the piston is extended, resulting in a positive friction force. Because the pressure is higher than what was used to develop the friction model, the frictional force is therefore larger than what the model

calculates which would explain the slight offset. A pressure dependent friction model could be investigated for improved accuracy in future.

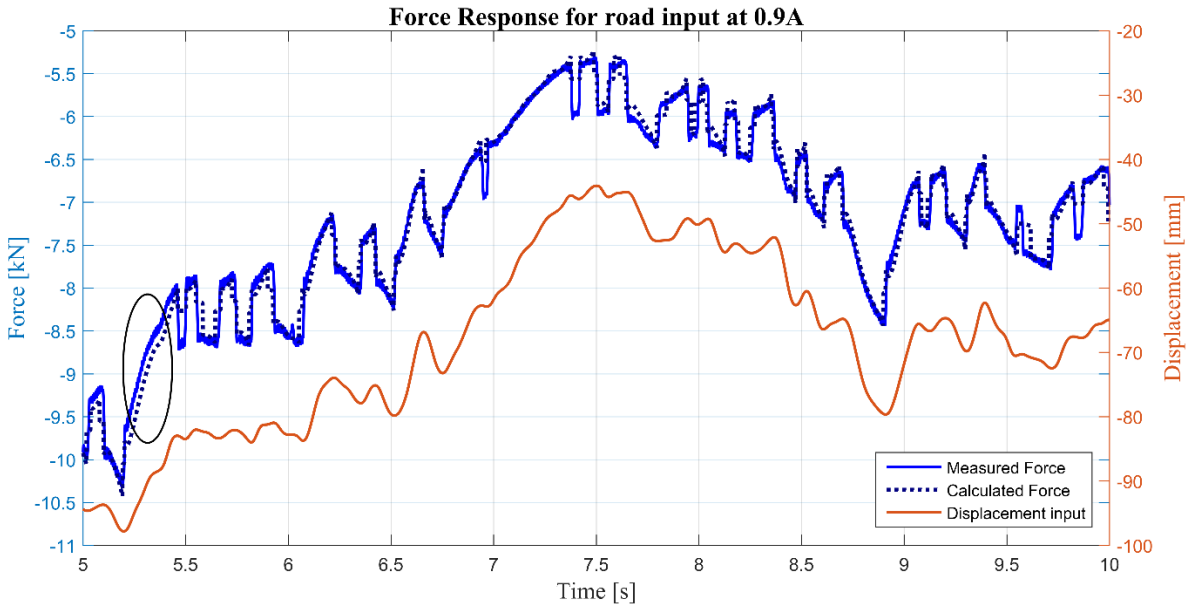


***Figure 4.14: Measured and calculated force for an artificial road input***

### 4.6.4 Response time

As a final step in the validation process, the dynamic response of the model when changing the solenoid current is analysed. The decision was taken to validate the model according to experimental data that focused on extracting the response time, as presented in Figure 3.20 and Figure 3.21. As previously mentioned in section 3.3.3, the response time tests had to be conducted at low velocities in order to allow sufficient time to accurately extract the response time and to reduce the actuator overshoot. Evidently, a very low pressure drop over the valve is created. Figure 4.15 and Figure 4.16 show the measured and calculated pressure drop when switching the current from 0A to 1.2A at 100mm/s and 0A to 0.9A at 150mm/s respectively. The model output for using the default 40ms response time and the experimentally determined response time is included. In order to create comparable results, the measured input signal was again used as input to the model. The noise was reduced by using a smoothing spline function.

Overall, the model-produced pressure drop correlates fairly well with the measured pressure drop. However, the model does seem to produce a slightly larger pressure drop for the 1.2A damping in Figure 4.15 and for both damping settings in Figure 4.16. Upon further inspection of the pressure drop model on a finer resolution (Figure 4.3), it was noted that the pressure drop model is responsible for this offset. The damping or pressure drop model was developed by focusing more on the broad data set, which effectively biases the higher velocities and pressure drops. Consequently, the model does not predict the very low pressure drops accurately in some cases.

In an attempt to improve the model, the lower velocity data points were also weighted, however, this causes the high velocity and large pressure drop predictions to become inaccurate. More experimental data points would allow for a better fit and possibly solve this compromise, alternatively a low velocity and a high velocity damping model could be utilized. Although the model could be refined further in various ways, the decision was taken that the current model can sufficiently calculate the pressure drop for the current application. Future research initiative could investigate other methods, e.g. artificial neural network, to model the damping and response time.

In terms of the response time, the model uses 40ms for all cases. As expected, the model responds slightly faster than the measured data for 0A to 1.2A damping in Figure 4.15, but marginally faster than 0A to 0.9A damping in Figure 4.16. Increasing the response time of the model to 55ms for the 0A to 1.2A case, the pressure drop rate follows the measured pressure drop extremely accurately. The same can be done for the 0A to 0.9A case by decreasing the response time to 30ms. This proves the model is capable of accurately calculating the pressure drop when changing current. Evidently, a slight compromise is made by choosing the response time to be 40ms for all cases. It does, however, reduce uncertainty when investigating the effects of the response time in simulation. The model could clearly be improved by adapting the response time based on, for example, the pressure drop or the current step size. These improvements did not form part of this study and the current method was deemed sufficient.

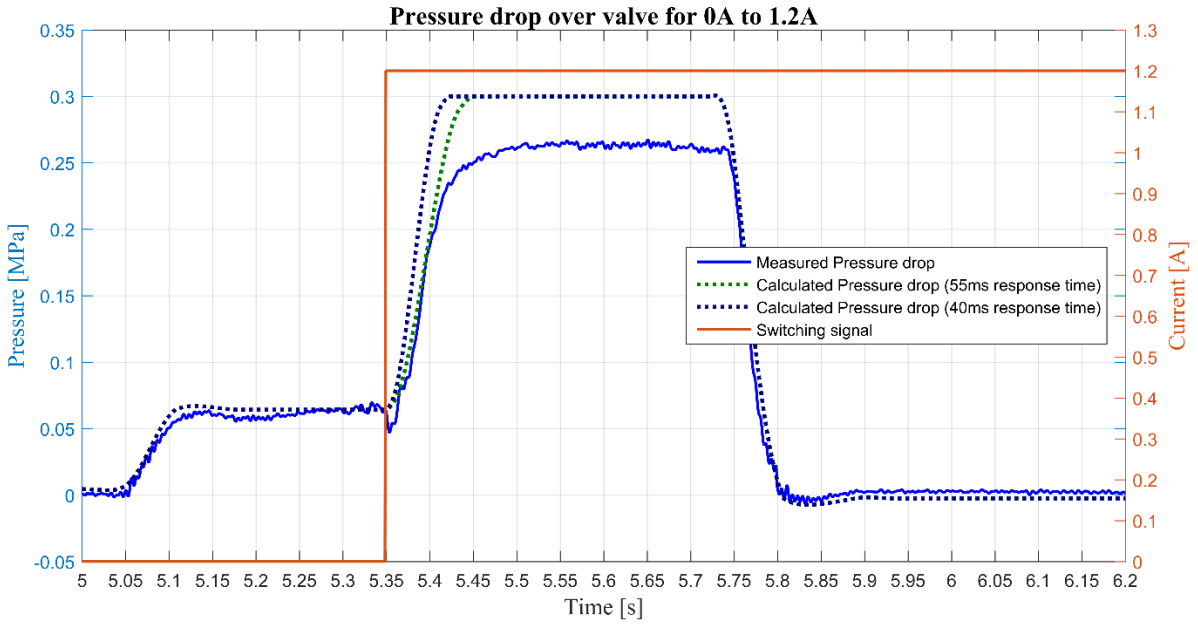


***Figure 4.15: Measured and calculated pressure drop response time for 0A to 1.2A damping***

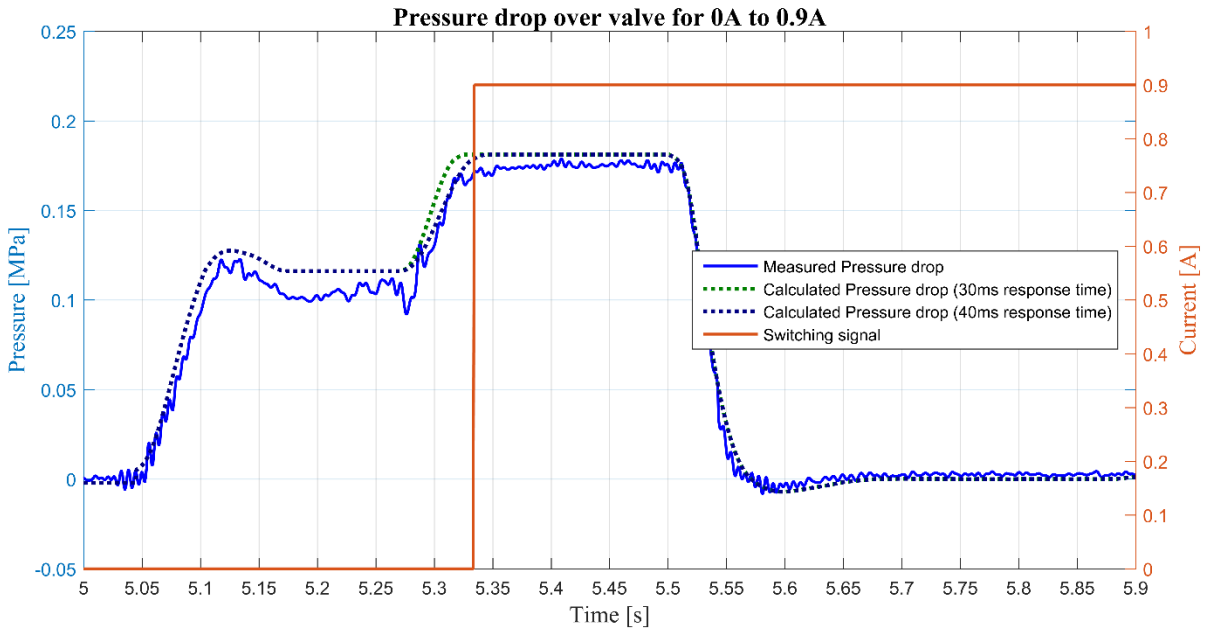


***Figure 4.16: Measured and calculated pressure drop response time for 0A to 0.9A damping***

## 4.7 Full 4S$_4$CVD model

After validating the single-accumulator and valve model according to experimental data, the model can be extended to the full, two-accumulator model of the 4S$_4$CVD intended for vehicle implementation. Experimental testing of the full, two-accumulator 4S$_4$CVD did, however, not form part of this study, and can therefore not be validated. However, as mentioned in section 2.4.4, Theron and Els (2007) developed a model that predicts the flow split between the two accumulators. Good correlation between the predicted force output and measured experimental results of the 4S$_4$ demonstrates that the incorporation of flow-split modelling is a suitable and accurate strategy.

The full 4S$_4$CVD model consequently consists of the same validated pneumatic spring and damping model. The input to these models is determined by the fraction of fluid flowing along each respective path, as indicated in Figure 2.14. The fluid flow caused by displacement of the piston rod, $Q_3$, and the equivalent flow split can be described by eq. (2-16):

$$Q_3 = A_{piston}\dot{x} = Q_1 + Q_2$$
$$Q_3 = \left[\left(Q_{frac} \times Q_3\right) + \left(1 - Q_f\right)Q_3\right] \quad \textbf{(2-16)}$$

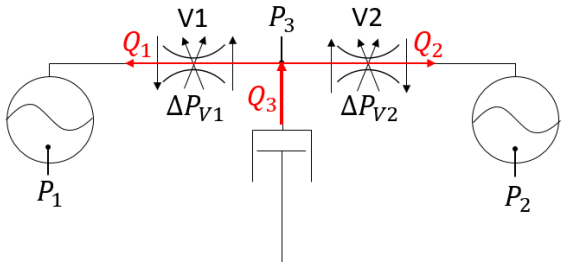


***Figure 2.14: Fluid flow model***

$Q_1$ and $Q_2$ is the flow rate through the valve to accumulators 1 and 2 respectively. $Q_{frac}$ is the fluid-flow fraction where 1 would mean that all the fluid flows to accumulator 1 and 0 that all of it goes to accumulator 2. The correct flow split will result in the system being in equilibrium, so that there is no pressure differential. For the system to be in equilibrium, the accumulator pressure and pressure drop over the valve needs to equal the strut pressure which can be described by previously presented eq. (2-17). This equation can be rewritten in terms of both the accumulator pressures and pressure drop as in eq. (4-9). The flow split is then calculated by using Matlab's fminbnd function, a minimiser function that iteratively changes the flow split (starting at 0.5, limited between 0 and 1) until it finds the minimum for eq. (4-9). The maximum allowed iterations for the minimiser function was set at 500 and the threshold or tolerance for allowed minimum set at 10Pa.

$$P_3 = P_1 + \Delta P_{V1} = P_2 + \Delta P_{V2} \quad \textbf{(2-17)}$$

$$\left(P_1 + \Delta P_{V1}\right) - \left(P_2 + \Delta P_{V2}\right) \approx 0 \quad \textbf{(4-9)}$$

Accumulator pressures, $P_1$ and $P_2$, are calculated with the hydropneumatic spring model discussed in section 4.2 and the pressure drop over valves 1 and 2, $\Delta P_{V1}$ and $\Delta P_{V2}$, are calculated with the damping model discussed in section 4.3. For a compressive input, increasing the flow fraction would therefore increase accumulator 1 pressure, $P_1$, as more fluid flows to the accumulator decreasing the volume. The pressure drop over valve 1, $\Delta P_{V1}$, would also increase due to the increased flow. However, the pressure of accumulator 2, $P_2$, would decrease and the pressure drop created over valve 2, $\Delta P_{V2}$, would also be lower. The opposite would happen if the fraction were to be decreased. The minimiser function determines the split for each time step before the force output can finally be determined by eq. (4-10):

$$F_{4S_4CVD} = \left(A \times P_3\right) + F_f \quad \textbf{(4-10)}$$

## Inter-accumulator flow error

When first analysing the output of the model, it was found that the model produces an unexpected pressure offset between the two accumulators after a given input. Figure 4.17 illustrates this in the pressure response sampled at 1kHz for an artificial triangular displacement, 400mm/s constant velocity input with 0.9A current supplied to both valves. The pressure differential between the two accumulators should be negligible after 1.1s, since there is no velocity input to create a pressure drop over the valves. After further investigation it was found that this offset is due to the model not being capable of accurately predicting the force output when given an artificial input where the velocity changes from 0 to 400mm/s in 1 time step. The problem arises from the model only considering fluid flowing from the strut and accumulator, but not from one accumulator to the other. With a 400mm/s input there is fluid flow and a pressure differential between the accumulators due to the different pressure drop over the valves. In the following time step the input could change to 0mm/s which equates to no fluid flow calculated in the model. This results in zero pressure drop over the valves, but there is still the residual pressure differential between the accumulators carried over from previous solve step, but now no flow to allow recalculation to satisfy equilibrium. This translates into an inaccurate prediction of the force output, which is clear when checking if the system satisfies equilibrium as defined in eq. (2-17). Figure 4.18 shows the corresponding error, which should be approximately 0 if equilibrium is reached.

The decision was taken to incorporate a strategy that allows flow between the accumulators when the piston velocity becomes low and equilibrium is not satisfied after the flow split has been calculated. After the appropriate flow split is calculated and the equilibrium error is more than 1Pa, a minimiser function is again used to iteratively change the amount of fluid flow between the accumulators, $Q_{2to1}$. The flow to each accumulator can then be defined by eq. (4-11).

$$Q_1 = Q_1 + Q_{2to1}$$
$$Q_2 = Q_2 - Q_{2to1} \qquad \textbf{(4-11)}$$

This flow is used to calculate the accumulator pressures and pressure drops within the respective models, which is then used to assess equilibrium with eq. (2-17). Figure 4.19 shows the pressure response of the model that includes this inter-accumulator flow strategy. After 1.1s the model now allows fluid flow from accumulator 1 to accumulator 2, even though there is no fluid flow caused by the piston displacement. Figure 4.20 shows the corresponding equilibrium error, which now is less than 0.1Pa. Evidently, incorporating this inter-accumulator flow strategy greatly increases the accuracy of the full 4S$_4$CVD model.

It is not clear whether Heymans (2017), or Theron and Els (2007) who previously employed the flow-split strategy, would have encountered the same flow split problem when their model is subjected to an artificial input where the input velocity abruptly reduces to zero between time steps. It is possible that their mathematical model is set up different so that it is still capable of reaching an accurate, equilibrium state without needing the proposed inter-accumulator flow strategy.

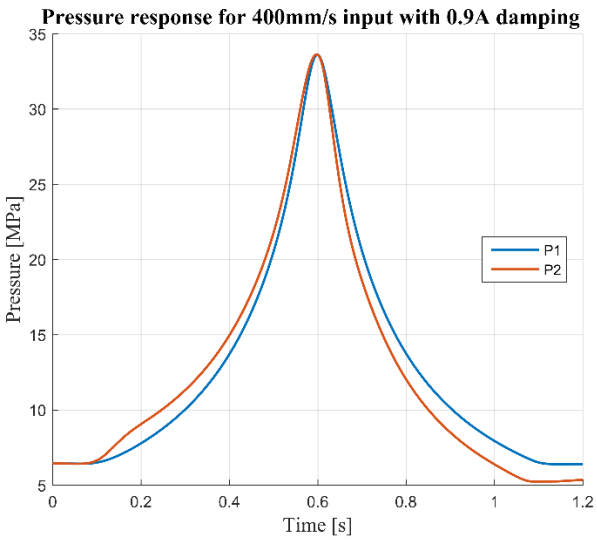


*Figure 4.17: Full model response error without inter-accumulator flow*

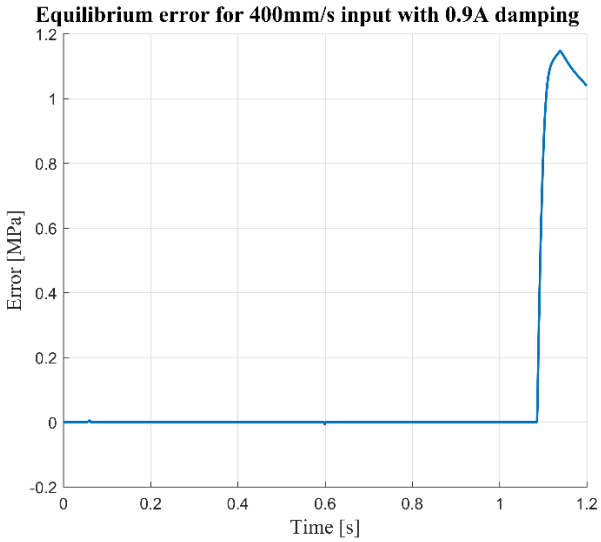


*Figure 4.18: Equilibrium error without inter-accumulator flow*

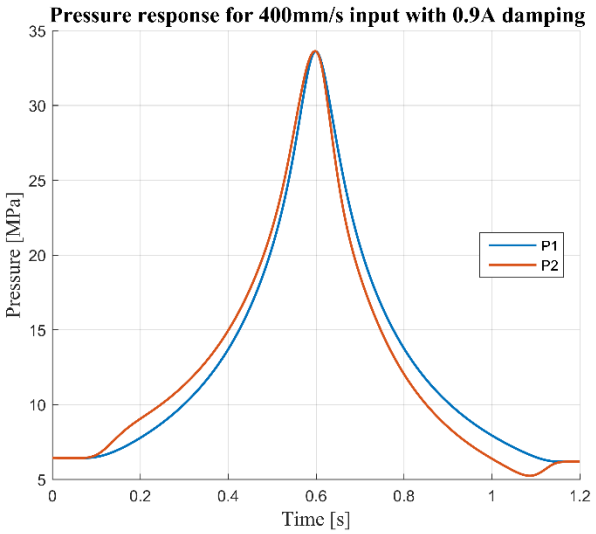


*Figure 4.19: Full model response with inter-accumulator flow*

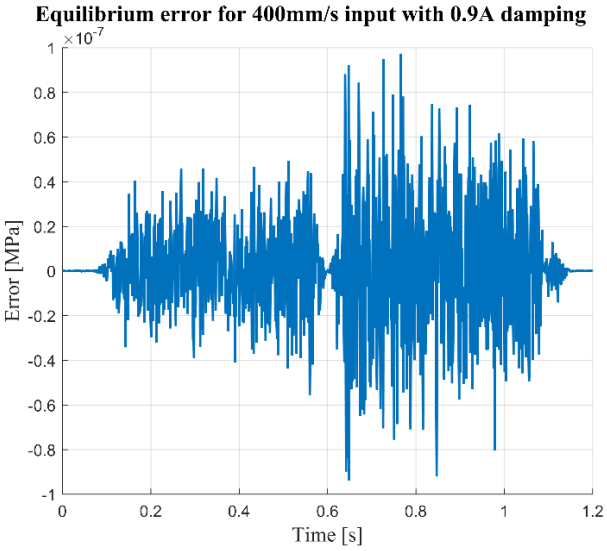


*Figure 4.20: Equilibrium error with inter-accumulator flow*

## Full 4S$_4$CVD characteristics

The optimisation study by Uys et al. (2007) determined that a total accumulator volume of 0.1$l$ and 0.5$l$ for the 4S$_4$ provided optimum ride comfort and handling performance. A similar study is required to investigate which accumulator volumes would be optimum for the 4S$_4$CVD. As a first estimate, the accumulator volumes and charge pressure of the full 4S$_4$CVD model is selected to produce similar stiffness characteristics as the already optimised 4S$_4$. After exploring different accumulator volumes and charge pressures with the full 4S$_4$CVD model, it was found that a total volume of 0.27$l$ at a charged pressure of 3.65MPa provides a similar soft spring characteristic, as shown in Figure 4.21. Any combination of the two accumulator sizes could essentially be used to make up the combined volume. Having two different size volumes does allow an additional stiffness characteristic. However, to achieve a similar hard spring characteristic of the 4S$_4$ an accumulator volume of 0.145$l$ is required, which requires the remaining accumulator volume to be 0.125$l$ to achieve the desired total volume. This effectively eliminates a 3$^{rd}$ stiffness setting as these volumes produce similar stiffness characteristics. Alternatively, volumes of 0.16$l$ and 0.11$l$ can be used, which produced a characteristic

that was both lower and higher than the hard $4S_4$ setting, as shown in Figure 4.21. It should however be noted that Els (2006) stated the hard stiffness of $4S_4$ to be sufficiently high. Therefore it might be better to increase the total volume, which decrease the soft stiffness of the $4S_4$CVD, but allows more freedom in selecting different accumulator volume combinations. Future research initiatives which focus on finding optimal volumes would address this problem.

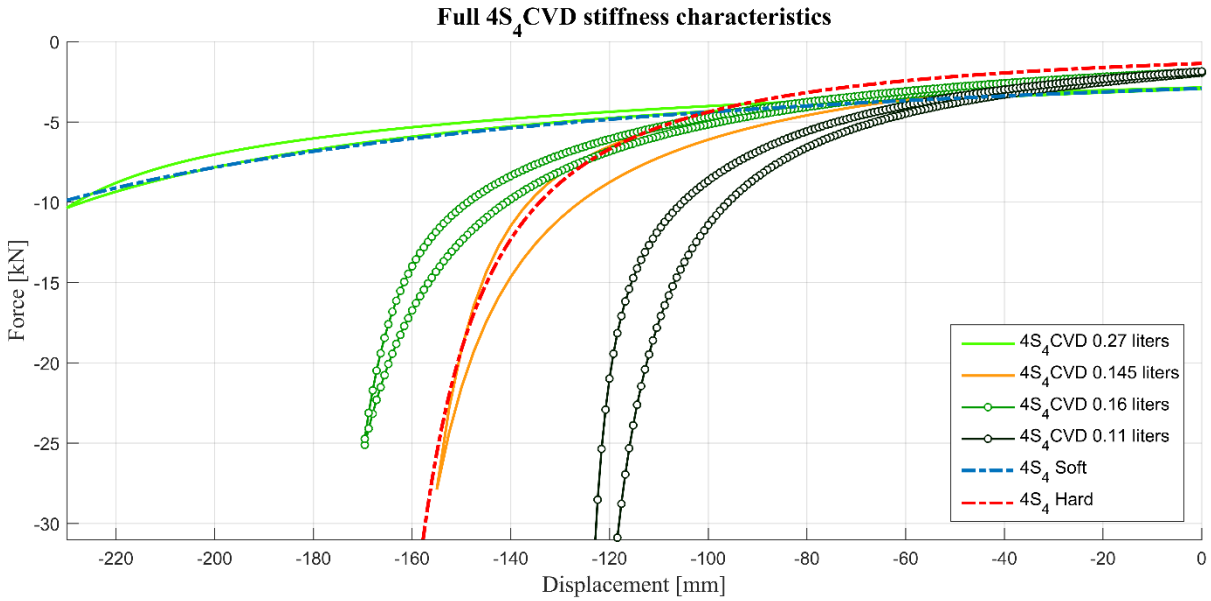


***Figure 4.21: Possible stiffness characteristics for the two-accumulator $4S_4$CVD***

The force output of the full $4S_4$CVD model is essentially always a combination of a spring, friction and a damping force. The damping or force versus velocity characteristics can however, be artificially extracted by determining them from the total pressure drop over the valves as calculated by the model. Figure 4.22 shows the possible damping characteristics of the $4S_4$CVD, along with the $4S_4$ damping characteristics and the stock or baseline damper for comparison. The characteristics were determined using a 100mm sine wave as input, with the frequency chosen to produce a reasonable damping effect. The soft spring allows fluid to flow to both accumulators, while the stiff spring blocks flow to one accumulator by supplying a 1.5A current. To simplify the process, it was assumed that there is no leakage past the valve, since tests presented and discussed in section 3.3.5 indicated it to be negligible. In the case of the soft spring, both valves were provided with the same current. When flow is allowed to both accumulators, the flow rate through each valve is reduced, which consequently reduces the damping. With the stiff spring, all the fluid is forced through one valve and the damping effect is therefore larger. The $4S_4$CVD would thus be capable of producing any damping characteristic from the lower 0A damping limit (when the fluid flow to one accumulator is blocked) up to and past 1.2A damping, until effectively blocking all flow.

From Figure 4.22 it is evident that the $4S_4$CVD is capable of producing much lower damping than the baseline and $4S_4$. Els (2006) stated that the $4S_4$ damping should be 50% less for significant ride comfort improvement. When comparing these characteristics, it could be concluded that the $4S_4$CVD soft spring is capable of producing around four times less damping than the soft $4S_4$. Based on this, the $4S_4$CVD would therefore already be capable of providing better ride performance. When considering how the $4S_4$CVD would affect the handling capabilities, the high damping (1.2A damping) can be compared to the $4S_4$ hard or handling setting. In Figure 4.22 it is evident that even with the stiff $4S_4$CVD setting it provides extremely low damping at velocities below 150mm/s. Although it is possible to increase the damping at low velocities by further increasing the current supplied to the solenoid valve, this would then have a knock on effect of then causing severe damping (effective lock-up) at velocities

below 200mm/s. It is expected that this will be detrimental to the handling capabilities of the vehicle. This problem arises from using flow control valves which causes an exponential increase in damping instead of a more linear increases as with the $4S_4$. Therefore, although the $4S_4$CVD would result in increased ride comfort, it would decrease handling due to negligible low speed damping.

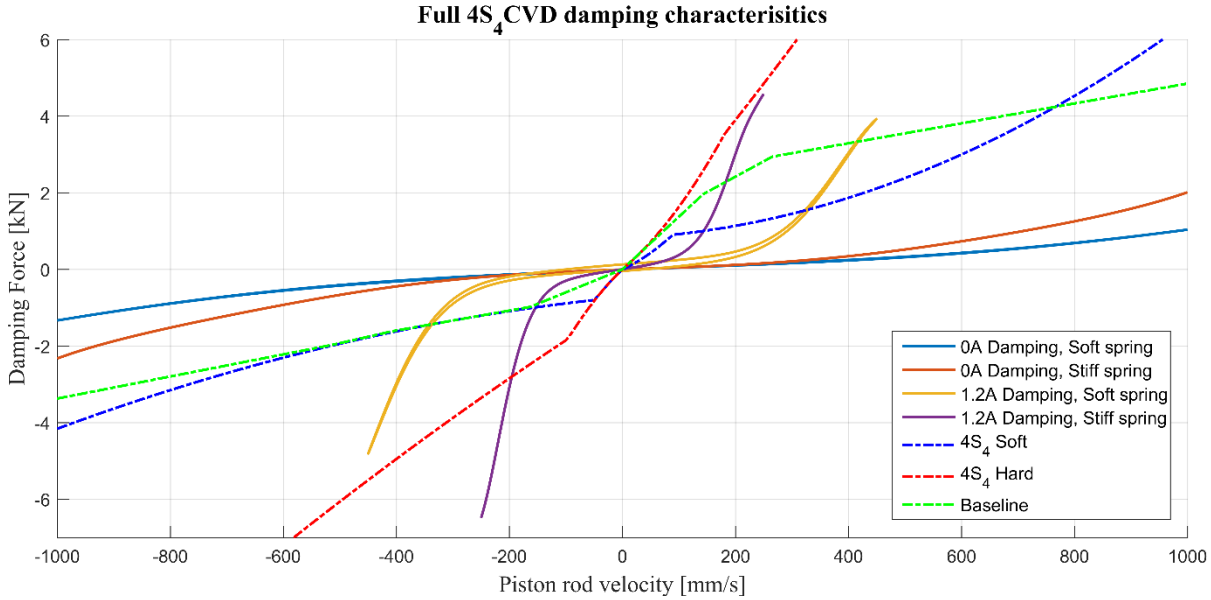


***Figure 4.22: Possible damping characteristics for the two-accumulator $4S_4$CVD***

## Computation time

Although optimisation of the computational efficiency or simplification of the model did not form part of the study, it was important to illustrate the computational demand of the current model. The time it takes to find a solution can be influenced by various factors, but is predominantly based on the computer's central processing unit. With a fairly capable 3.2GHz processor, the time required to solve 1s of simulation for various inputs is given in Table 4.2. The artificial road input used is equivalent to the one previously used and discussed in section 4.6.3

***Table 4.2: Solve time of the full $4S_4$CVD model***

| Model input | Suspension setting | Time [s] required to solve 1s of simulation at 1kHz | Time [s] required to solve 1s of simulation at 200Hz |
|---|---|---|---|
| 500mm/s triangular displacement constant velocity | 0A damping, soft spring | 25.6 | 5.39 |
| | 0.9A damping, soft spring | 26.1 | 5.49 |
| | 0A damping, stiff spring | 1.06 | 0.22 |
| Artificial road input | 0A damping, soft spring | 26.5 | 5.58 |
| | 0.9A damping, soft spring | 27.3 | 5.75 |
| | 0A damping, stiff spring | 1.09 | 0.23 |

The soft-spring setting took considerably longer to solve due to incorporating the highly iterative flow-split and inter-accumulator flow strategies, while these strategies are not required for the stiff spring setting. When comparing the various damping settings, it can be concluded that lower damping takes marginally less time to solve. This can be attributed to the higher damping in the model requiring more iterations converge to a solution that satisfies equilibrium. Decreasing the sampling rate of the model directly relates to a shorter solve time, however, this could decrease the accuracy of the model. It is estimated that the sampling time can safely be reduced to 200Hz, because the frequencies below 80Hz

predominantly effects ride comfort. The time required to solve 1s of simulation at 200Hz is also presented in Table 4.2. Decreasing the sampling frequency by 5 times decreased the solving time by a factor of about 4.75. However, the sampling rate is especially critical when the model includes a control strategy as it adds additional delay in the response and it was therefore kept at 1kHz for the remainder of this study.

## 4.8 Conclusion

This chapter presented the modelling and validation process of the single-accumulator $4S_4$CVD that was used in the characterisation testing. This model proved to be capable of accurately predicting the experimentally measured force and pressures for the various inputs considered. It also accurately models the dynamic behaviour when changing the solenoid current by gradually changing the pressure drop at the specified response time.

The validated model was further developed according to the final design layout that consists of two accumulators and two continuously variable valves. This model incorporates both an iterative flow split and an inter-accumulator flow strategy that determines the flow to each accumulator. However, this model has yet to be validated according to test data and, as a result, there is some uncertainty regarding the accuracy thereof. The computation time of the full $4S_4$CVD model is was also investigated, which highlighted the computational demand of the model when passively controlled.

# Chapter 5:
# SIMULATION AND CONTROL

This chapter investigates the dynamic response and control of the 4S$_4$CVD through simplified quarter-car simulations. Passive control simulations are conducted to evaluate the 4S$_4$CVD's capabilities and to establish how the characteristics can be changed to influence the response. These results can be used as a baseline in a comparison to the performance of an active skyhook-controlled 4S$_4$CVD. The effects of response time and controller gain on the skyhook control algorithm are also investigated. This investigation should indicate whether the 4S$_4$CVD and active skyhook control can provide improved ride comfort performance and support further investigation. All simulations are performed at a rate of 1kHz.

## 5.1 4S$_4$CVD simulation model

A model of the single-accumulator 4S$_4$CVD has successfully been developed and validated. This model was extended to the final design layout consisting of two accumulators and valves that have yet to be validated according to experimental data. However, including the flow-split and inter-accumulator flow greatly increased complexity and computational demand. The control strategy has to control both valves, while taking the ever changing flow split and inter-accumulator flow into consideration. Including these additional variables could obscure the results and make it difficult to draw definitive conclusions. Furthermore, including a control strategy exponentially increases the computational demand. Actively controlled simulations conducted with the single-accumulator model, as presented in Figure 5.12, took longer than 30 minutes to solve. Since this study focused on evaluating the possible performance and feasibility of the 4S$_4$CVD, the decision was taken to conduct simulations with the validated single-accumulator model as defined in eq. (4-1). Although the accumulator volume of the validated model can be modified to match the soft, medium and hard spring settings, all the fluid flow passes through one valve as shown in Figure 5.1. The simulation model would therefore have slightly higher damping than the full model.

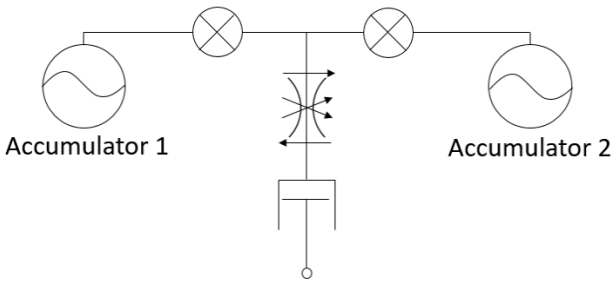


***Figure 5.1: 4S$_4$CVD simulation model***

## 5.2 Single degree of freedom model

After the vehicle modelling literature review, as discussed in section 2.5, the decision was taken to use a simplified quarter-car or single degree of freedom model to conduct a simulation based investigation of the 4S$_4$CVD. The study focused on the vertical dynamics associated with ride comfort. Including additional dynamics, such as vehicle roll, pitch or yaw, would complicate the model without really adding value to the validity of the investigation. Furthermore, a full quarter-car model includes the unsprung or wheel resonance that is important for analysing the road-holding capabilities of the wheel, but not necessarily the ride comfort. A simplified quarter-car or single degree of freedom model would therefore be capable of producing acceptably accurate results to highlight the 4S$_4$CVD's capabilities and could possibly justify a more detailed investigation.

The single degree of freedom model is illustrated in Figure 5.2. The model consists of an input or excitation displacement, $x_1$, which results in the displacement response, $x_2$, of the sprung mass, $M_s$, due to the force applied by the 4S$_4$CVD. For this study a sprung mass of 400kg was used, since the total body and chassis (sprung mass) of the Land Rover Defender was determined to be 2025kg (Uys et al., 2006). The relative motion between the input and sprung mass determine the suspension deflection, $x = x_2 - x_1$ that is used as input to the model to calculate the force output. The equation of motion describing the system can therefore simply be defined by eq. (5-1) as*:*

$$M_s\ddot{x}_2 = F_{4S_4CVD^*} \quad \textbf{(5-1)}$$

The single-accumulator force output can ultimately be described by the sub-model model inputs as:

$$F_{4S_4CVD^*} = f(x, \dot{x}, V_0, P_0, T_s, I, t_{res})$$

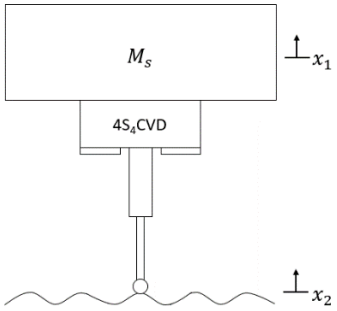


***Figure 5.2: 4S$_4$CVD single degree of freedom model***

The model therefore only considers vertical motion only and neglects any suspension kinematics. However, the suspension would be mounted vertically, which reduces the inaccuracy that would arise from the road input not being in the same plane as the suspension deflection. Furthermore, the model does not include any bump stops. Care should thus be taken when subjecting the system to harsh excitations, since it could cause the suspension to deflect outside its operating range.

## 5.3 Passive control analysis

Multiple passive control simulations were conducted to investigate the effect of different damping and stiffness settings on the ride comfort. The simplified quarter car model is subjected to a frequency sweep and an artificially generated road profile. The sprung mass dynamics are evaluated and can be used as a baseline for the active-controlled simulations. The effect of friction in the suspension on the ride comfort performance was also investigated.

### 5.3.1 Effect of damping and stiffness on ride comfort

#### Frequency sweep

The dynamic response of the sprung mass with different suspension settings was investigated with a sinusoidal frequency sweep or chirp input. The input changes from 0 to 30Hz at a 20 seconds/Hz, resulting in a 600 second simulation time. The frequency was slowly increased to allow sufficient time for the system to essentially reach a steady-state condition for the excited frequency range. The input was set up to approximate an acceleration between -1m/s$^2$ and 1m/s$^2$ throughout the frequency. This could then be used to approximate the frequency response of the sprung mass acceleration. Figure 5.3 shows the input displacement and acceleration used to excite the mass, along with the response for 1.2A damping.

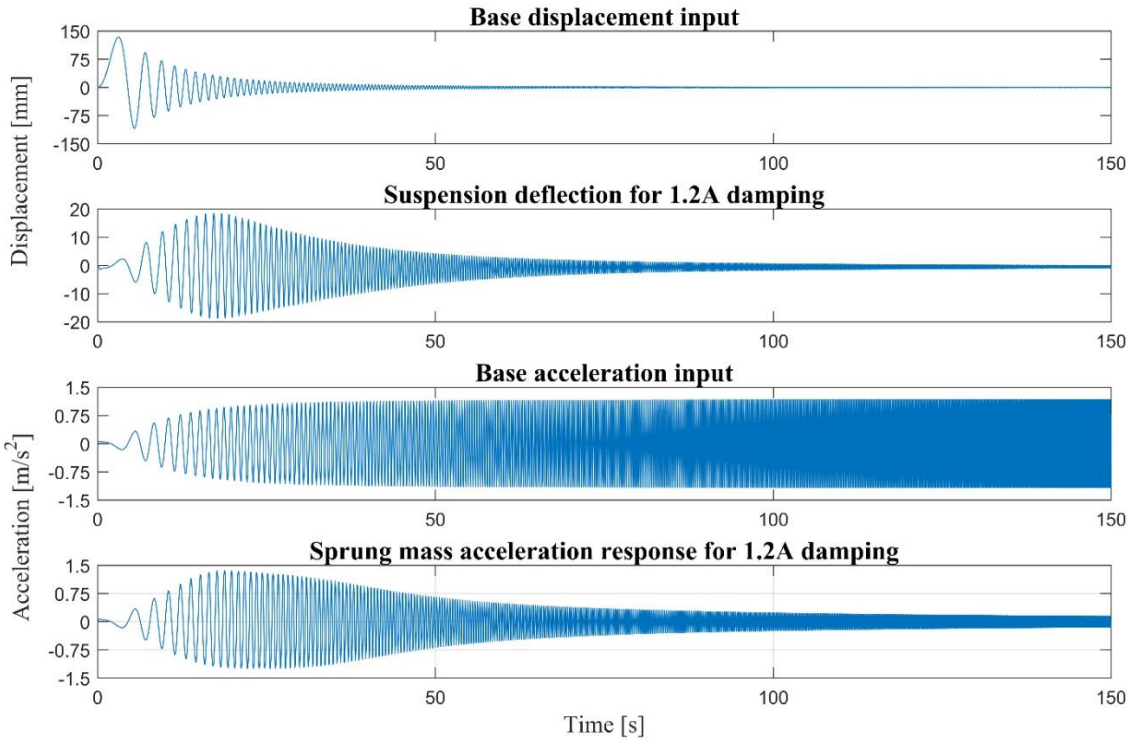


***Figure 5.3: Example of frequency-sweep excitation and response in time domain***

The corresponding unweighted frequency response of the sprung mass for different damping is shown in Figure 5.4. Despite the slow sweep, the sprung mass frequency response was still noisy at some frequencies. This is due to the excitation frequency changing before the sprung mass reaches a steady state. Although further increasing the sweep would reduce the noise this was assumed to be sufficient to make meaningful conclusions.

Although the force displacement relationship of the hydropneumatic spring is non-linear, it can be linearized by considering a specific displacement range. With a sprung mass of 400kg, the soft, 0.27$l$ 4S$_4$CVD needs to deflect about 120mm to support this mass. The stiffness coefficient can then be determined by considering a range around 120mm deflection. The stiffness coefficient of the soft 4S$_4$CVD, linearized across specific ranges, is listed in Table 5.1, which is based on the force displacement characteristic previously shown in on Figure 4.21. Due to the progressive increase of force per displacement, the stiffness also increases as the on the displacement range increases. The stiffness can be used to calculate the natural frequency of the sprung mass using eq. (5-2) is also included in Table 5.1 for each stiffness.

$$f_n = 1/2\pi \times \sqrt{k/m} \qquad \textbf{(5-2)}$$

***Table 5.1: Stiffness coefficient of the soft 4S$_4$CVD***

| Linearized range about 120mm [mm] | Stiffness, $k$ [kN/m] | Natural frequency, $f_n$ [Hz] |
|---|---|---|
| +-10 *(110 to 130)* | 20.5 | 1.14 |
| +-20 *(100 to 140)* | 21.25 | 1.16 |
| +-60 *(60 to180)* | 24.17 | 1.24 |
| +-100 *(20 to220)* | 30.17 | 1.38 |

The natural frequency of the sprung mass therefore depends on the deflection range in which the suspension is operating. The natural frequency of the sprung mass can be see with the amplitude spike at 1.2Hz irrespective of damping setting in Figure 5.4. This correlates to the natural frequencies

presented in Table 5.1, which would suggest that the suspension is operating at +-50mm deflection about 120mm to result in a similar natural frequency. The invariant or crossover point, where the magnitude of the response remains the same irrespective of damping, can be noted at about 1.85Hz. It was evident that increasing the damping decreased the amplitude response at frequencies below the invariant point, but slightly increased the response at higher frequencies. However, the lower frequencies carried less weight compared to the higher frequencies, based on the weighting function shown in Figure 2.1 of the BS 6841 standard (British Standards Institution, 1987). This illustrates how a passive damper has to make a trade-off between damping out the resonant frequency and high frequency filtering. Figure 5.5 shows the unweighted frequency response of the sprung mass for accumulator volumes of $0.27l$, $0.16l$ and $0.11l$, which represents the soft, medium and hard settings respectively. The natural frequency at 1.2Hz can be seen shifting to higher frequencies with increased amplitude as the stiffness was increased. Evidently, the increased amplitude and higher natural frequency would lead to decreased ride comfort. Interestingly, Figure 5.5 also shows 2 amplitude spikes (2Hz and 3.4Hz for the hard setting) which would suggest multiple natural frequencies. However, due to using a single degree of freedom model it expected to only have 1 natural frequency. The bulk modulus of the fluid that's incorporated into the model could result in an additional natural frequency, however, the "spring stiffness" due to the compressibility of the oil is so high that the natural frequency would be higher than the 15Hz range considered. The multiple natural frequencies can therefore be attributed to the stiffness of the $4S_4$CVD not being linear and as the deflection range changes so does the natural frequency as illustrated in Table 5.1.

Investigating the response of a frequency-sweep excitation demonstrates how the $4S_4$CVD can change it characteristics to influence the amplitude and natural frequency of the sprung mass. Fundamentally it is already possible to see how changing the characteristics according to the excitation frequency can be used to reduce the amplitude of the response.

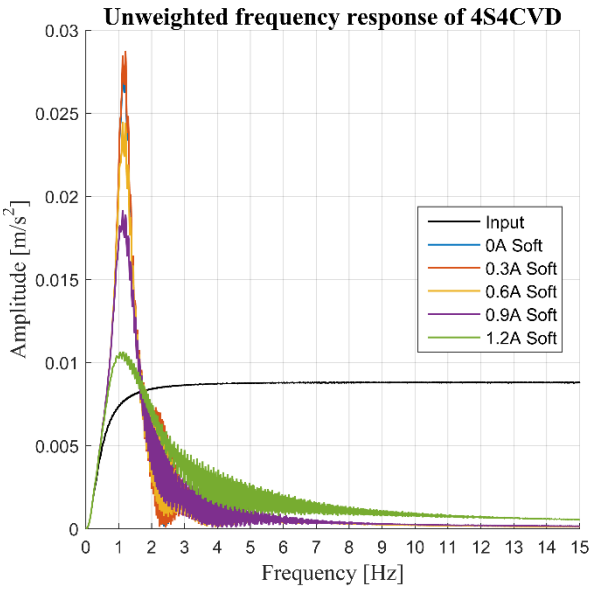


*Figure 5.4: Frequency response of sprung mass for changing damping*

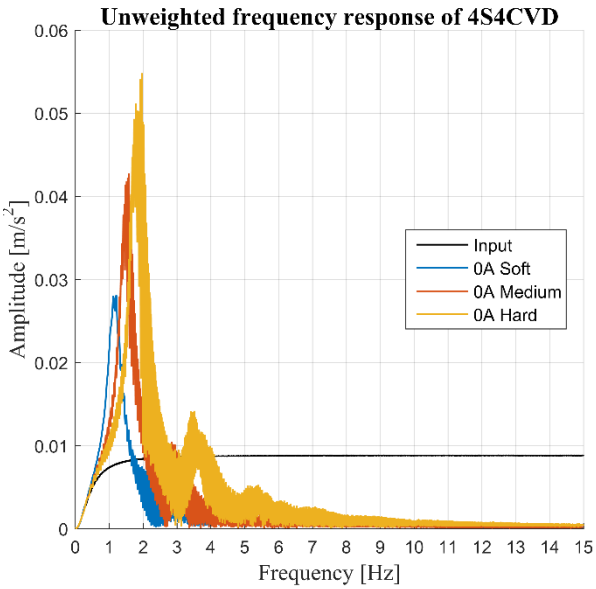


*Figure 5.5: Frequency response of sprung mass for changing stiffness*

## Road

In order to quantify the effect of different damping and stiffness settings, the decision was taken to subject the single degree of freedom model to a road input. The weighted RMS of the sprung mass acceleration can then be used to objectively evaluate the ride comfort according to the BS 6841 standard. The road input derived from a class-D road based on the ISO 8608 standard (International

Organization for Standardization, 1995), as depicted in Figure 5.6 which shows the profile in the spatial domain. A class-A road would be classified as smooth while a class-H road would be extremely rough. The profile was converted to a time-domain input based on the speed of the vehicle travelling over it. By using a single degree of freedom model, the sprung mass connects directly to the input and there is no filtering effect of the tyre. This, combined with the use of a point follower model, as opposed to more complex tyre model which includes the enveloping dynamics of the tyre going over obstacles, results in extremely harsh inputs. For example, using an input based on a vehicle speed of 80km/h results in an extremely harsh input with velocities exceeding 2m/s. As the goal was to compare the response across a range of damping settings, such a harsh input falls outside the validated range of the high, 1.2A damping setting. To reduce the harshness and allow stable, accurate simulation across different damping and stiffness settings, the road input was based on a vehicle speed of 10km/h. Although this is not necessarily a practically relevant simulation, due to limitations previously mentioned, it can be used to compare and evaluate the different damping settings. An extract of the 170s long road input and typical sprung mass displacement response is shown in Figure 5.7. As the tyre is not included in the model, the results do not represent the true capabilities of the $4S_4$CVD, however, it can be used to investigate the robustness of the model and used as a baseline to evaluate control strategies.

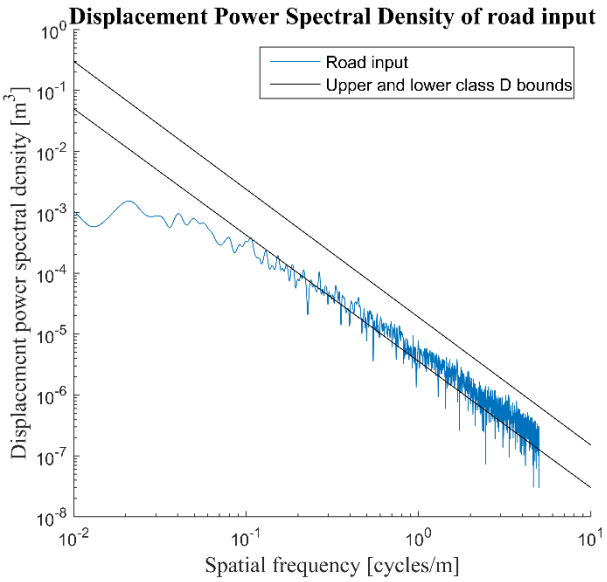


***Figure 5.6: Classification of road input***

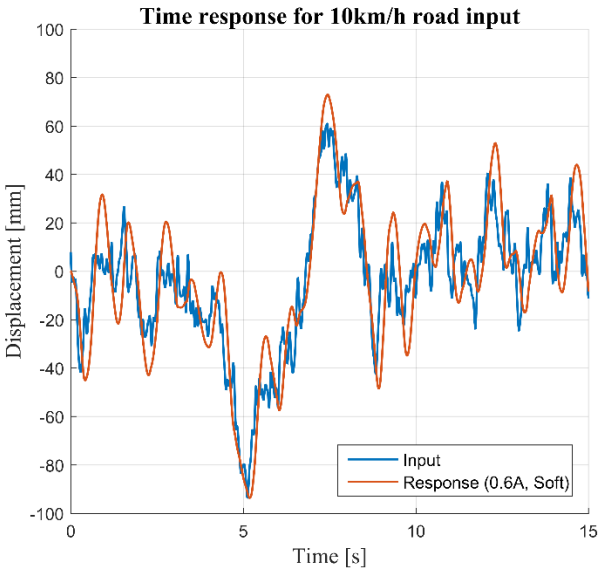


***Figure 5.7: Time response of road input***

Simulation of various $4S_4$CVD damping and stiffness combinations subjected to this road input were conducted. The frequency-weighting function, shown in Figure 2.1, could then be applied to the sprung mass acceleration response of each simulation as per the BS 6841 standard. The RMS of these weighted sprung mass accelerations and the ride comfort ranges according the standard are shown Figure 5.8. This clearly indicates how the $4S_4$CVD's damping and stiffness characteristics influence the ride performance when subjected to a typical road input. The lowest damping and stiffness setting provided the best ride comfort and could be used as a baseline for optimum passive-controlled ride comfort. This degraded as the stiffness or damping was increased. A fairly uncomfortable ride was the optimum that could be achieved with the soft stiffness and low damping. Medium stiffness was only able to achieve an uncomfortable ride, while the hard stiffness achieved a very uncomfortable ride. As the damping between 0A and 0.3A is negligible, the ride comfort also remains unchanged, however, as the damping was further increased the ride comfort also degraded. The 1.2A damping clearly produces excessive damping, since it resulted in an extremely uncomfortable ride irrespective of the stiffness.

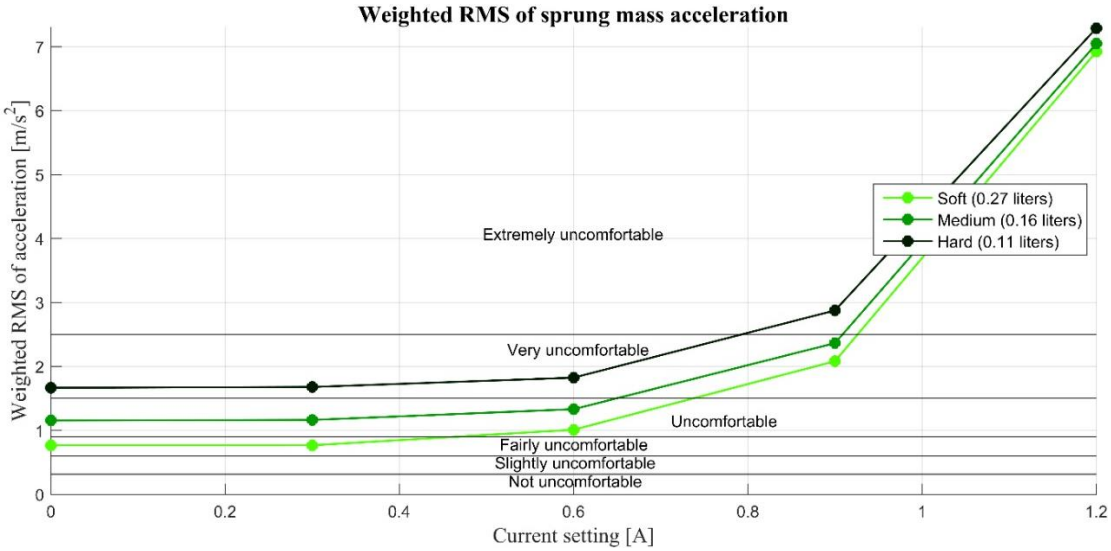


***Figure 5.8: Weighted RMS acceleration of sprung mass for different damping and stiffness settings***

## 5.3.2 Effect of friction on the ride comfort

The model with 0A damping and soft setting was then subjected to the same road input used in section 5.3.1. To analyse how the model responded with the effective discontinuity at zero velocity or when crossing zero velocity, the friction force versus the suspension deflection velocity is shown in Figure 5.9. From this it is clear that due to how the model is set up, the velocity input sometimes jump for -30mm/s to +30mm/s. This results in the friction force to jump from -0.2kN to 0.1kN between time steps, effectively cutting out some of the higher friction force spikes. The way the simulation is set up this is unavoidable, but increasing the sampling rate (currently, 1kHz) would decrease discontinuity and smoothen out the friction force output.

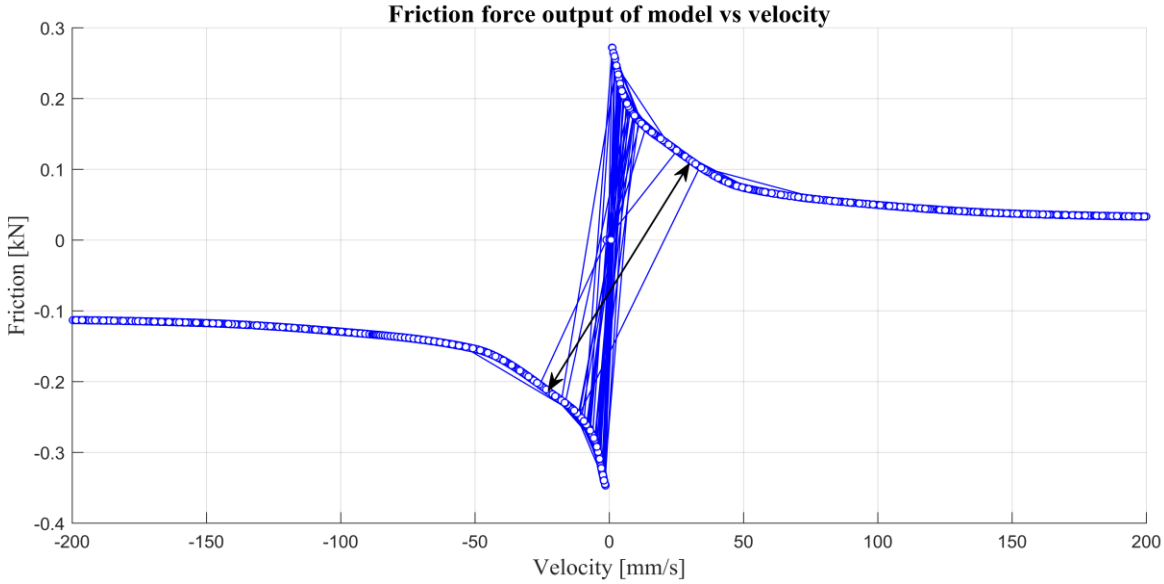


***Figure 5.9: Zero-crossing response of model***

Stiction in a suspension causes the system to be less responsive to smaller inputs and is expected to degrade the ride comfort performance. The characterisation results, discussed in section 3.3.4, indicated that the 4S$_4$CVD has reduced friction (50% less for compression and 30% less for rebound compared to its 4S$_4$ (Els, 2006) predecessor. To assess the improvements and effect of friction on the ride comfort, the friction in the model was artificially changed. The weighted RMS acceleration sprung

mass was used to quantify the effects, as shown in Figure 5.10. Figure 5.9 illustrated that the model produces somewhat unnatural frictional force where the friction doesn't necessarily smoothly transition between time steps, therefore, the results shown in Figure 5.10 shouldn't be considered as a good indication rather than a true representation of real world results.

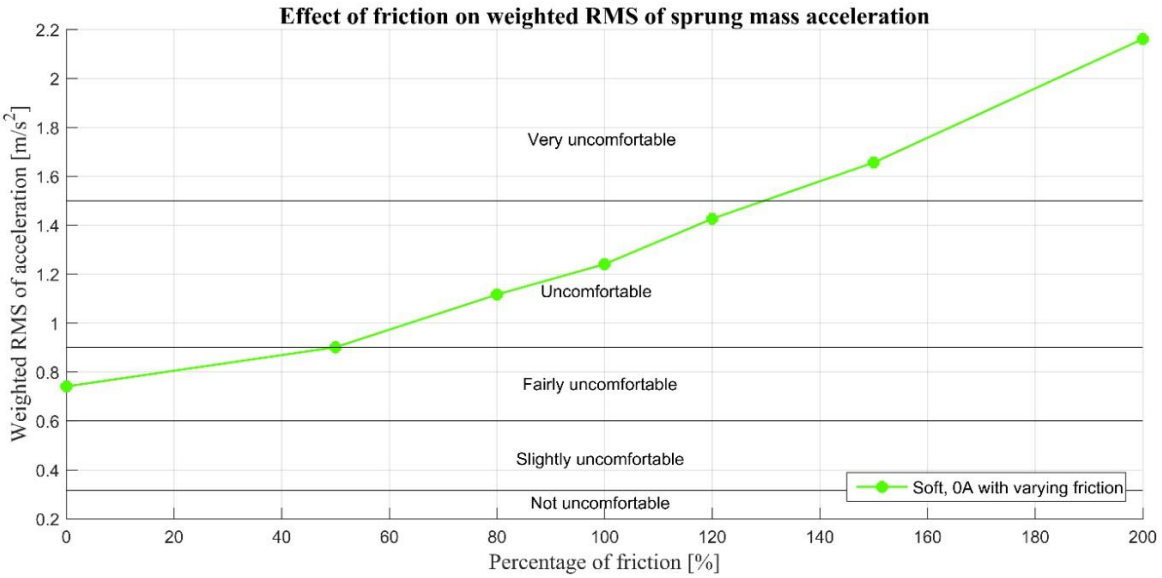


***Figure 5.10: Weighted RMS acceleration of sprung mass for different percentage of friction***

As expected, the ride did degrade as the friction was increased. Based on the input given, completely removing friction in the model reduced the weighted RMS acceleration by up to 40%. This is a fairly large improvement and therefore there is some uncertainty regarding the validity of this. The friction model used, produces discrete force spikes for every small alternating velocity. The data used to develop and validate the model was from long constant velocity inputs, therefore it did not take into account any compliance in the system that was expected to play a dominant role for small alternating displacements.

In an attempt to quantify the improvements made by using the rolling-diaphragm design $4S_4$CVD, the 100% and 120% friction can be compared, where 120% would represent the floating-piston $4S_4$ design. Decreasing the friction by 20%, according to the $4S_4$CVD's model, reduced the weighted RMS acceleration by 0.185m/s$^2$. This represents a decrease of about a 15%, which constitutes a fairly large improvement. This also suggest that a simplistic friction model, based only on the deflection velocity, might not be an accurate or reliable method of quantifying these improvements. It is therefore suggested that a more sophisticated friction model should be developed if the improvements were to be accurately quantified. Using this friction model with noisy measured displacement inputs could therefore cause inaccuracies in the model. For such a case it might be better to remove the friction model as majority of the forces are created by the damping and spring model. However, it could still be concluded that the reduction of friction in the $4S_4$CVD with the rolling-diaphragm design would produce better ride comfort performance.

## 5.4 Active skyhook control analysis

The passive control simulation showed how the response could be influenced by changing the $4S_4$CVD's damping and stiffness characteristics. It therefore further indicated that the $4S_4$CVD damping characteristics could actively be controlled to produce better ride comfort. For this study, the actively controlled capabilities of the $4S_4$CVD was investigated through the use of basic skyhook control. Since

the focus was on ride comfort, all the active-controlled simulations used the model with a 0.27liter accumulator volume (soft spring).

The skyhook control theory was discussed in section 2.6.1 and illustrated in Figure 2.17. It essentially changes the damping characteristics to approximate a system where a passive damper is connected between a fixed point in the sky and a sprung mass. The control logic controlling the force output of such a system can be described as in eq. (2-19):

$$F_{Sky} = \begin{cases} c_{sky}\dot{x}_1 & \dot{x}_1\dot{x} > 0 \\ 0 & \dot{x}_1\dot{x} \leq 0 \end{cases} \quad \textbf{(2-19)}$$

The desired skyhook damping force, $F_{sky}$, is therefore a function of the damping coefficient of the figurative damper that can be calculated by using the damping ratio, $\zeta$, as in eq. (2-20).

$$c_{sky} = 2\zeta\sqrt{k_s M_s} \quad \textbf{(2-20)}$$

This damping ratio is a tuneable parameter that determines the amount of damping the control strategy will try to add to the system. Determining the optimal skyhook parameters is no trivial matter. Poussot-Vassal et al. (2006) developed a reduced order observer model combined with a suitable cost function to implement optimal skyhook control in simulations with great success. Such complex control strategies does however not form part of the study. The decision was taken to run each skyhook controlled simulation with constant parameters which would still indicate possible performance of the 4S$_4$CVD. A ratio below 1 would reduce the amplitude of sprung mass oscillations (underdamped), while more than 1 eliminates oscillations (over damped). The effects of these parameters will be further investigated in section 5.4.1. The damping force of the 4S$_4$CVD, $F_{d_{4S_4CVD}}$ can calculated by:

$$F_{d_{4S_4CVD}} = dP_{valve} \times A \quad \textbf{(5-3)}$$

where the model calculates the pressure drop over the valve as a function of solenoid current and suspension deflection velocity respectively, $dP_{valve} = f(I, \dot{x})$. To control the valve in the model according to the skyhook control theory a minimiser function was utilised. It finds a solenoid current that results in the minimum difference between the desired skyhook damping force, $F_{Sky}$ and the actual damping force, $F_{d_{4S_4CVD}}$. The solenoid current would therefore continually be changed for the 4S$_4$CVD's damping force to best approximate the desired skyhook damping force. Test data used to develop the damping model ranged from a 0 to 1.2A solenoid current. The decision was therefore taken to also limit the maximum allowed current for the control strategy to a range of 0 to 1.2A.

## 5.4.1 Skyhook damping ratio

The skyhook damping ratio of eq.(2-20) determines the damping coefficient of the figurative skyhook damper. It therefore directly influences the magnitude of damping force in the control logic. To effectively analyse the possible ride comfort performance of an actively controlled 4S$_4$CVD, the effect of damping ratio was first investigated.

### Step input

In order to illustrate how the skyhook control logic changed the response, the model was first subjected to a step input. The decision was taken to use a 200mm upward step at a velocity of 400mm/s. Figure 5.11 shows the sprung mass displacement response for a skyhook damping ratio ranging from 0.2 to 2 for a 0ms and 40ms valve response time. 40ms was used as it corresponded to the 4S$_4$CVD's response time. The input step and sprung mass response with passive control and 0A damping is also presented for comparison.

Considering the response with no delay, it is evident that the amplitude of oscillations reduces as the damping ratio increases. Interestingly, even though the damping ratio was more than 1, the sprung mass still oscillated. After further investigation it was determined that this can be attributed to the $4S_4CVD$ having extremely low damping at low velocities as indicated on Figure 4.22. Because the damping model was restricted to operate within 0 to 1.2A, damping it wasn't possible to generate the required damping, resulting in an underdamped system as seen by the constant oscillation (even with $\zeta = 2$). To prove this, the damping model was allowed to extend to a 1.5A limit and also presented alongside in Figure 4.22. With the damping model now able to produce higher damping, it is possible to restrict oscillation, resulting in an overdamped system as to be expected. Note that the damping model was only created with experimental data up to 1.2A, therefore the 1.5A is based on how the model was extrapolated past 1.2A. In real life 1.5A would simply mean that the flow would be blocked, however this data wasn't included in the damping model as it causes it to become inaccurate at velocities leading up to 1.2A. Additional experimental data and possibly a different method of modelling the damping is required to accurately model the entire operating range (0 to 1.5A) which would allow the damper to produce the damping required by skyhook control strategy at low velocity.

When comparing the zero delay to the 40ms time response, it is clear that the amplitude of oscillations increases for the same damping ratio. This is to be expected, since the sprung mass moves further before the additional damping force is applied to restrict the oscillations. Although the amplitude still reduces as the damping ratio became larger, the reduction is much less in comparison to the 0ms response time. The frequency of the oscillations are also slightly lower the higher the skyhook damping ratio becomes.

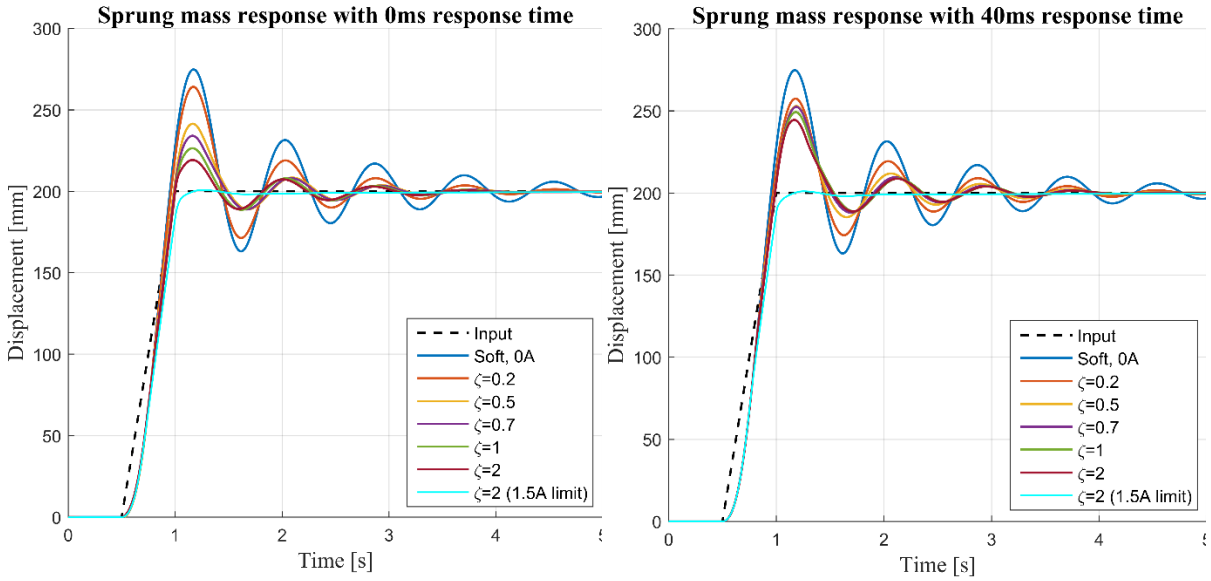


***Figure 5.11: Step input and sprung mass response for different skyhook damping ratios 0ms response time (left), 40ms response time (right)***

The step input displaces and disturbs the sprung mass causing it to oscillate at its natural frequency. The step input highlights how the natural frequency is influenced by active control without considering other excitation frequencies. In order to understand the total effect, a frequency sweep or a road input can be used to excite the sprung mass across a range of frequencies.

## Frequency sweep

As a further investigation, a frequency sweep at 20seconds/Hz was conducted with the same 0 to 30Hz input as used in Figure 5.4. Figure 5.12 shows the unweighted frequency response of the sprung mass acceleration for various skyhook damping ratios. Simulations were conducted for a response time of both 0ms and 40ms. Although the frequency range of interest exceeds the 15Hz presented, the 10-15Hz range essentially already indicated what the rest of the frequency response would be. The frequency response was therefore limited to 15Hz for clarity. The 0A and 1.2A passively controlled solenoid current responses are also presented for comparison. Since the control logic was limited between 0A and 1.2A, the actively controlled responses are expected to fall mostly within the 0A and 1.2A passively controlled response.

From Figure 5.12 it is evident that increasing the skyhook damping ratio decreases the amplitude of the natural frequency response for both response times considered. This is to be expected as a larger skyhook damping ratio relates to a larger damping force. Comparing the different 0ms and 40ms time responses, it could be noted that, for the same damping ratio, the 0ms response time reduced the amplitude more than the 40ms response time. The difference became more prominent at higher damping ratios. This correlates to what was noted in Figure 5.11. For frequencies above 3Hz it can be seen that a higher skyhook damping ratio leads to a larger response compared to lower damping ratios. The larger response time also produces slightly larger responses for the equivalent damping ratio at these higher frequencies. Note that the 4 to 8Hz frequency range is critical for ride comfort, as these frequencies are perceived as most uncomfortable and also carry a larger weight according to the BS 6841 standard (British Standards Institution, 1987). Therefore, the higher damping ratios that produced an amplitude close to the 1.2A level, rather than the lower 0A level for this range, would not produce good ride comfort.

Higher damping ratios generally moved the frequency response to the 1.2A passively controlled response, while lower damping ratios moved the response to the 0A passively controlled response. Therefore, some sort of a trade-off still existed between filtering out the lower natural frequency or high frequency responses. However, the lower damping ratios still seemed to follow the 0A damping response well at higher frequencies, while reducing the lower natural frequency response. This could produce improved ride comfort over passively controlling the solenoid valve at 0A.

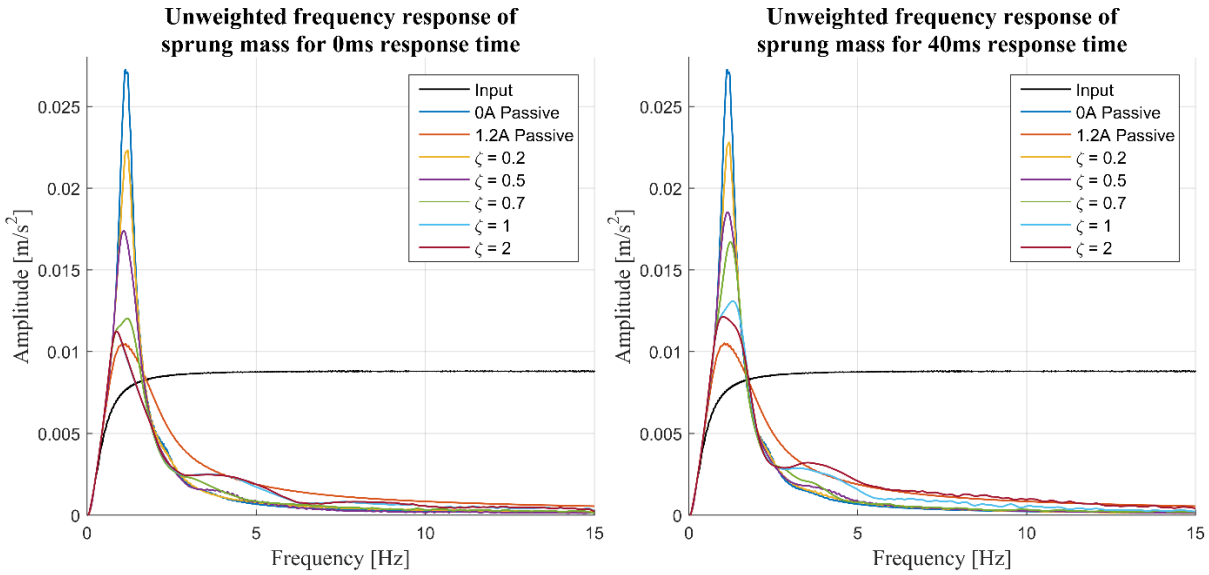


***Figure 5.12: Unweighted frequency response of sprung mass for frequency sweep 0ms response time (left), 40ms response time (right)***

### 5.4.2 Response time

After investigating the effect the skyhook damping ratio had on the sprung mass response, the influence of the valve response time was investigated. In an attempt to quantify and compare the performance of the suspension unit, it was subjected to the road input used in section 5.3.1, as shown in Figure 5.6. Based on the findings of Figure 5.12, the decision was taken to focus on the lower skyhook damping ratios as they showed the most potential. Figure 5.13 shows the weighted frequency response of sprung mass accelerations for a skyhook damping ratio of 0.2 and 0.4 for various valve response times. The corresponding RMS of the sprung mass acceleration for different valve response times are presented in Figure 5.14. For clarity, only the weighted frequency response of specific response times are presented.

For a skyhook damping ratio of 0.2, the reduction of the response at the natural frequency (1.3Hz) was negligible compared to passively controlling the valve with 0A. However, the amplitude of the response at higher frequencies was noticeably lower for response times lower than 10ms. The improvements of actively controlling the suspension with a response time of 40ms indicate some improvement, although less than the faster response times, while with a response time of 100ms improvements seem marginal.

For a skyhook damping ratio of 0.4, the amplitude of the response at the natural frequency is significantly reduced. With a 5ms response time the peak amplitude response is reduced by 14%, while 12.6% for 10ms, 7% for 40ms and 4% for 100ms response time respectively. As expected, the improvement depreciates with increased response time. Actively controlling the suspension with 5ms and 10ms response times seem to decrease the response at the higher frequencies. For 40ms and 100ms response times the amplitude of the response seem smaller at the more critical low frequencies, but generally larger, at higher frequencies than passively controlling the solenoid valve at 0A.

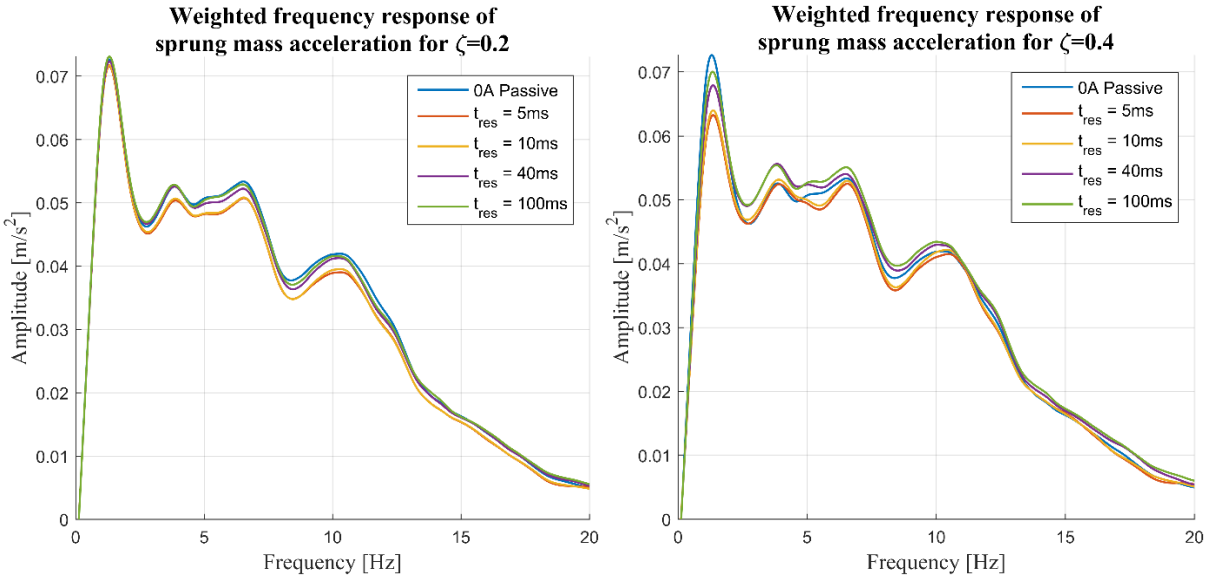


***Figure 5.13: Actively controlled weighted sprung mass acceleration of sprung mass for road input Skyhook damping ratio of 0.2 (left), Skyhook damping ratio of 0.4 (right)***

When comparing the response with damping ratio of 0.4 and 0.2, it can be noted that the response is a function of the response time as well as damping ratio. To quantify the frequency response in terms of perceived ride comfort, the RMS of the weighted sprung mass acceleration can be used. Figure 5.14 shows the unweighted, weighted and optimum passively controlled RMS of sprung mass accelerations

for various response times and damping ratios. The unweighted RMS of sprung mass accelerations are included to aid understanding of how the system responds and can justify the validity of the results.

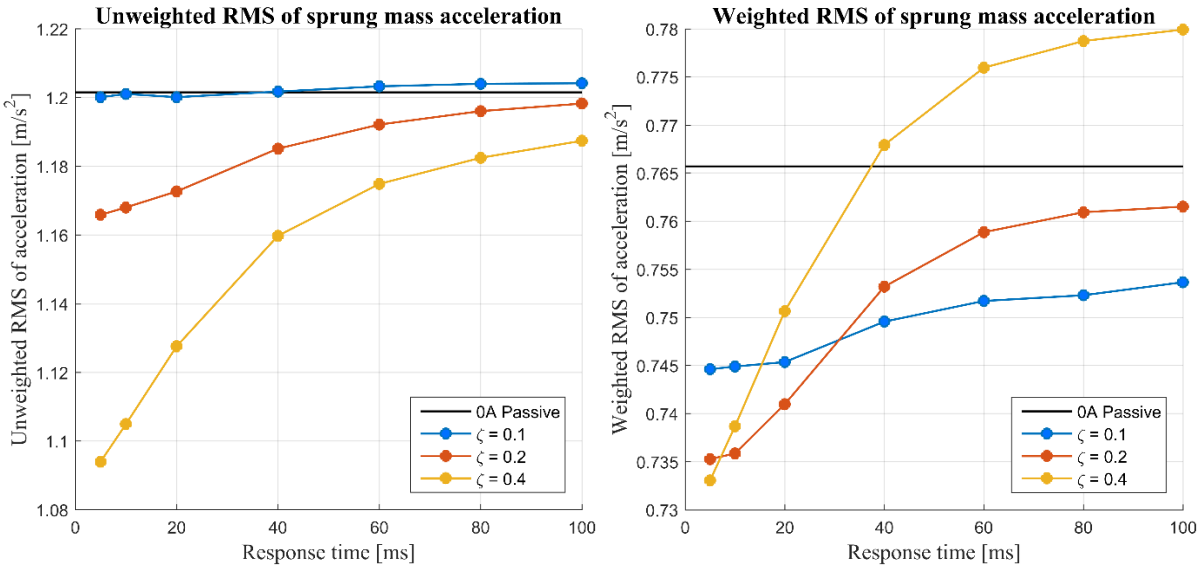


***Figure 5.14: Actively controlled RMS acceleration of sprung mass for road input Unweighted (left), Weighted (right)***

In the unweighted case, the higher 0.4 skyhook damping ratio was capable of producing the lowest RMS of sprung mass acceleration. As the response time increase, the acceleration response also increases for each damping ratio. The higher the damping ratio is, the more it is affected by an increasing response time. By increasing the skyhook damping ratio in the control logic, the 4S$_4$CVD consequently produces a larger damping force. Because the system is underdamped, adding additional damping would decrease the natural frequency acceleration response of the sprung mass. However, as the response time increased, the control logic was incapable of applying the damping force effectively, which caused the RMS of the sprung mass acceleration to rise. In the unweighted case, the natural frequency responses greatly influence the magnitude of the RMS value.

The frequencies between 4Hz and 8Hz are perceived as most uncomfortable and carry the most weight when applying the BS 6841 weighting function. Reducing the natural frequency therefore becomes less critical. This is evident when analysing the weighted RMS values, since the 0.4 damping ratio produced the best ride comfort only when the response time was 5ms. Furthermore, it produced the worse ride comfort with a response time of 40ms than what was possible with passive control.

From the weighted RMS values it can be concluded that, the lower the response time is the better ride comfort the skyhook control strategy is able to provide. Furthermore, the optimum skyhook damping ratio is dependent on the response time of the suspension. The lower the response time, the larger the damping ratio in the control logic should be to achieve optimum ride comfort performance. However, even with a response time of 100ms some ride improvement could be obtained if a low damping ratio was used in the control logic.

Section 4.4 discussed how the response time of the 4S$_4$CVD has been simplified to 40ms. Based on this, from the results it can be concluded that actively controlling the 4S$_4$CVD according to the skyhook logic with a damping ratio of 0.1 would provide improved ride comfort. The optimum actively controlled weighted RMS of acceleration achieved was 0.733m/s$^2$ with a response time of 5ms and $\zeta = 0.4$. For a response time of 40ms, 0.7496m/s$^2$ was achieved using $\zeta = 0.1$. With the optimal passive suspension the weighted RMS of acceleration achieved was 0.7657m/s$^2$, this means that active

control with 5ms resulted in 4.3% improvement and with 40ms only 2.1%. Based on these results the magnitude of improvements are rather insignificant. Passively changing the damping to the road input, rather than using an active sky-hook control strategy is effectively be just as good, especially with a higher response time.

## 5.5 Conclusion

This chapter investigated the performance and capabilities of the $4S_4$CVD through single degree of freedom model simulations. Passive simulations showed how the different damping and stiffness characteristics of the $4S_4$CVD could influence the response of the sprung mass. The effect of friction was also investigated and it was concluded that the $4S_4$CVD's reduced friction through the use of rolling diaphragms would translate into improved ride comfort. Active-controlled ride comfort performance of the $4S_4$CVD was investigated through the use of skyhook control logic. It was found that fast response times, combined with a suitable controller damping ratio, could produce improved ride comfort performance. Active control of the $4S_4$CVD could provide better ride comfort than what was achieved with passive suspension, however, the magnitude of improvements which includes a suitable response time doesn't seem significant when compared to optimum passive suspension.

# Chapter 6:
# CONCLUSIONS AND RECOMMENDATIONS

The suspension characteristics required for vehicle ride comfort and handling are on opposite sides of the design spectrum. Generally, a soft and compliant suspension is required for good ride comfort, while stiff suspension with a low ride height is required for improved handling. A passive suspension system therefore has to make a compromise. Controllable suspension attempts to negate this compromise by changing its characteristics to suit the dynamic state of the vehicle. Although a fully active controllable suspension is able to add additional energy to the system, it is much more expensive, energy intensive and complex than a semi-active suspension. A newly designed semi-active hydropneumatic suspension system was proposed that is expected to provide improved ride comfort and handling performance. The suspension is equipped with two proportional solenoid valves that can provide continuously variable damping. In addition, the valves are able to completely close off flow to one of two compressible gas volumes to provide discrete stiffness characteristics. This study set out to characterize and model this newly developed $4S_4$CVD.

As the $4S_4$CVD is based on the previously developed $4S_4$, a great deal of previous research and investigation relating to the $4S_4$ is also applicable to the $4S_4$CVD. Previous investigations proved that the $4S_4$, combined with a suitable control strategy, could successfully eliminate the ride comfort versus handling compromise. It was concluded that significant ride comfort improvements were possible if the lower damping limit could be reduced by as much as 50%. A high amount of friction was noted, which could be attributed to the floating-piston design. This causes the suspension to be unresponsive to smaller inputs and reduces ride comfort. Further simulation-based analysis indicated that the optimum suspension characteristics for ride comfort differ based on the road undulations. Therefore, a single set of ride comfort suspension characteristics would still not be able to always produce optimal ride comfort. Active control strategies were also investigated, however, it was found that the $4S_4$ was unable to utilise them for improved performance. This could be attributed to the discrete damping characteristics.

This led to the development of the $4S_4$CVD that aims to address these shortcomings. The variable flow-control valves aims to produce a lower damping limit for ride comfort. Furthermore, the valves were capable of continuously varying the damping, which could enable active control for improved performance. The rolling diaphragm aims to eliminate the friction associated with the floating-piston design. This study presented the process followed to investigate these aspects and the feasibility of the $4S_4$CVD.

## 6.1 Conclusions

### 6.1.1 Characterisation

The suspension was successfully characterised by actuating the unit on a test bench, as outlined in Chapter 3. A single accumulator version of the unit was used for characterisation to ensure that the valve dynamics could accurately be captured without having to account for two flow paths. The spring and damping characteristics, friction, response time and the flow-block ability of the $4S_4$CVD were extracted by subjecting the unit to various inputs while controlling the valve.

Results indicated that the unit is capable of producing the desired spring and low damping characteristics. The $4S_4$CVD was capable of producing continuously variable damping based on the

current supplied to the solenoid valve. The extracted damping characteristics indicated that the $4S_4$CVD is also capable of producing the desired low damping, which is less than 50% of the $4S_4$. It was noted that the $4S_4$CVD provides very low damping at low velocities even with high current (1.2A) supplied to the solenoid valve. It is possible to increase the damping at low velocities by further increasing the current supplied to the solenoid valve, however this would then have a knock-on effect of causing severe damping (effective lock-up) when the velocity is slightly increased. This problem arises from using flow control valves which causes an exponential increase in damping instead of a linear increase.

Accurately determining the full response time profile of the valve proved to be challenging. Initial testing indicated that the manufacturer-supplied current driver responds too slowly to allow extraction of the valve response time. A dual-channel power supply, combined with a fast-switching circuit, was developed to investigate the valve response time. The dynamic performance of the test setup directly influences the efficacy of extracting the response time. Without being able to precisely control the pressure drop and flow, it was not possible to extract a full and accurate response time profile. However, even with the limitations, valuable results were obtained. The response time was found to be dependent on the current step and the change in pressure drop created due to the changing solenoid current. Except in the extreme cases, the results confirmed that the valve is capable of responding within 40ms.

In comparison to the $4S_4$, the rolling-diaphragm design successfully reduced the suspension friction by about 50% for compression and 30% less for rebound. It can be concluded that the rest of the frictional force is due to the piston rod and strut seal. Although the friction of floating piston in the $4S_4$ is eliminated with the $4S_4$CVD design, the higher operating pressure limits the magnitude of improvement realised. Results also showed that the valve is capable of sufficiently blocking flow. It is expected that, at the very least, it would able to provide the dynamic stiffness required for handing manoeuvres. However, further testing is required to accurately quantify the amount of leakage. Consequently, satisfactory results were extracted to warrant developing a model for further simulation-based investigations.

### 6.1.2 Suspension modelling

The experimentally extracted characteristics were used to develop a validated mathematical model, as discussed in Chapter 4. Using a combined physics-based and empirical approach the $4S_4$CVD model consists of various sub-models responsible for mathematically incorporating each characteristic. The spring model or force due to displacement was accurately predicted by a BWR real gas model, combined with the energy equation. To model the damping or force due to velocity and solenoid current, a thin-plate surface spline was fitted to the experimental data. The valve response time is also incorporated in the model by ensuring that the calculated pressure drop gradually changes at the specified response time. A friction model that uses the deflection velocity as input is also included.

A single-accumulator $4S_4$CVD model was developed and successfully validated by comparing it to experimental data. This model was extended to the final design layout of two accumulators and two continuously variable valves. The model successfully incorporated the proven iterative flow-split and inter-accumulator flow strategies that determines the flow to each accumulator. Simulations of the full model were conducted to illustrate the possible damping and stiffness characteristics. Depending on the accumulator volumes, the $4S_4$CVD allows for a soft, medium and hard stiffness as well as a full lock setting compared to the soft and hard settings offered by the $4S_4$. This could be utilised when a medium setting would produce better ride comfort or handling performance than the hard or soft setting. The computation demand of the full $4S_4$CVD model was also investigated, which highlighted

the computational demand of the model when passively controlled. The computational demand of the 4S$_4$CVD model was also highlighted where passive control was found to take up to 30 seconds to solve 1 second of simulation.

Overall, the model proved to be capable of accurately predicting the force output for the various inputs considered. The model could therefore be used to further evaluate the possible performance of the 4S$_4$CVD through passive and actively controlled simulations.

### 6.1.3 Simulation and control

In Chapter 5 the mathematical model was used to investigate the passive and actively controlled performance of the 4S$_4$CVD through single degree of freedom simulations. Passive simulations showed that the 4S$_4$CVD can increase the damping to reduce the natural frequency response. However, this also increases the higher frequency response of the sprung mass. Using a stiffer suspension setting shifts the natural frequency response peak to frequencies which are critical for ride comfort. Consequently, optimum passively controlled ride comfort was achieved with the soft spring setting and low damping. Simulations investigating the effect of friction proved that the 4S$_4$CVD's reduction of friction through the use of rolling diaphragms translates into improved ride comfort.

Skyhook control was used to investigate if the 4S$_4$CVD could actively be controlled to improve ride comfort performance. The results proved that the lower the response time is, the better ride comfort the skyhook control strategy is able to achieve. Furthermore, the optimum skyhook damping ratio is dependent on the response time of the suspension. In order to achieve optimum ride comfort performance, it was found that the lower the response time was, the larger the damping ratio in the control logic should be. With a response time of 100ms, ride comfort improvement could still be achieved if a low damping ratio is used in the control logic. The 4S$_4$CVD, with a response time of 40ms, could actively be controlled with the skyhook control logic to provide better ride comfort than what was achievable with passive control. However, the magnitude of improvements with a response time of 40ms doesn't seem significant when compared to optimum passive suspension.

### 6.1.4 Final comments

The research proved that the 4S$_4$CVD successfully incorporated continuously variable damping in the proven vehicle-implemented 4S$_4$. It can actively be controlled with the skyhook control logic to further increase ride comfort. The new design also reduced the inherent friction and lower damping limit that increases ride comfort performance. Furthermore, the 4S$_4$CVD allows for an additional stiffness setting that could be utilised for improved performance. It was however noted that due to the flow control valves the 4S$_4$CVD's damping is extremely progressive, i.e. the damping at low velocities are very low, which exponentially increases at higher input velocities. It is possible that a control strategy could compensate for low damping at low velocities by increasing the current as this don't necessarily require such a fast response (low velocity damping usually associated with controlling the sprung mass roll and pitch). This was not investigated further and recommended for future work. Although the 4S$_4$CVD improved various aspects of the 4S$_4$, further investigation and possible refinements are required to determine whether it is a suitable successor to the 4S$_4$.

## 6.2 Recommendations for future research

As this was the initial investigation of the newly designed 4S$_4$CVD, future research is critical for successful development and implementation. The following key areas were identified and are recommended for future investigation:

### 6.2.1 Characterisation

- During testing of the high damping setting it was found that a small increase in velocity can lead to an exponential increase in pressure drop over the valve. This can be attributed to the flow-control valves. It was also found that, due to inherent delays, the actuator exceeds the force limits before switching off. Therefore, to protect structural integrity, valves and pressure transducers a safety valve could be added in the testing unit. It could also be beneficial to incorporate a blow-off damper characteristic in the design where if a specific pressure is exceeded, the damping force increases at a greatly reduced rate per increase in velocity.
- To accurately determine the full response time profile of the valve, further testing would be required. The response time results were dependent on the test setup and limited the results. Possible solutions could include a flow-control test bench, including a model of the actuator's response or increase the bandwidth of the actuating test setup. However, this would be a resource intensive investigation and the current tests results could be sufficient.
- The final design or two-accumulator layout should also be tested accordingly and these results could then be used to experimentally validate the full $4S_4$CVD mathematical model.

### 6.2.2 Modelling

- The fairly simplistic damping in the $4S_4$CVD model is based on interpolation of experimental data points. 0.3A increments were used, therefore a finer resolution would improve accuracy model throughout its operating range. This is especially important for high damping where the valve operates close to completely blocking flow, which is currently only accurately modelled up to 1.2A. Alternative methods of modelling the damping can be investigated, e.g. artificial neural network, which can be compared based on accuracy, controllability and computational demand.
- The $4S_4$CVD model is computationally demanding. Real-time simulation is not currently possible and therefore also experimentally implementing the active skyhook control strategy. Optimising or simplifying the model to allow real-time simulation would need to be investigated in order to experimentally test active control strategies. It is recommended that hardware in the loop testing is conducted to investigate experimental implementation of the model and control strategy combination.
- The $4S_4$CVD's MATLAB-based model could also be incorporated into the Simulink-based full vehicle model to allow full-vehicle simulations.

### 6.2.3 Simulation and control

- The model could be used to determine accumulator volumes, which would result in the optimal three stiffness settings for ride comfort and handling. A optimisation study similar to what was used to determine the $4S_4$ accumulator volumes could be conducted (Uys et al., 2007).
- This study only investigated possible ride comfort improvements through active skyhook control. Other ride comfort orientated strategies could therefore also be investigated to evaluate which strategy, combined with the $4S_4$CVD, delivers the best ride performance.
- The model should also be used to investigate possible handling performance combined with a suitable control strategy, such as groundhook, for improved handling or road-holding performance. This would consequently require a more complex vehicle model, such as a quarter-car model. The suspension model can be incorporated in the full vehicle model already developed and used with the $4S_4$. The possible handling performance of the $4S_4$CVD can then evaluated by simulating handling manoeuvres and compared to the $4S_4$.

- The ride comfort and handling strategies could be integrated in a global strategy that would continuously determine the optimum suspension characteristics based on the dynamic state the vehicle is in. For example, skyhook and groundhook control logic could be combined or integrated into the 4S$_4$'s proven RRMS strategy. Damping would thus always be actively controlled, while the 4S$_4$'s RRMS strategy would determine the optimal stiffness setting.
- Another consideration would be to incorporate model predictive control in the control strategy. Model predictive control could improve the performance as it could reduce or eliminate the negative effects associated with increased response time and also determine optimal suspension characteristics.
- Having the 4S$_4$CVD modelled and incorporated in a full vehicle model allows various vehicle dynamic investigations which can utilise the changing suspension characteristics to improve performance. For example the suspension characteristics can be changed to decrease stopping distance or incorporated in other control system such as stability control.

### 6.2.4 Vehicle implementation

The ultimate goal is to implement the 4S$_4$CVD on the vehicle. However, simulations only approximate the possible performance of the actual system as it is based on an ideal environment. Therefore, to evaluate the actual active controlled performance of the 4S$_4$CVD, hardware in the loop testing is recommended as it includes important aspects such as the noisy measurements used as input to the model and additional electrical delays. Experimental testing would also require a continuously variable current driver with a fast response time and a model that could be solved in real time.

If active control should not yield performance increases, passive control of the 4S$_4$CVD could still be investigated. The 4S$_4$CVD's additional stiffness setting and continuously variable damping combined with a suitable passive control strategy could be able to produce better ride comfort and handling compared to the 4S$_4$.

### 6.2.5 Alternative 4S$_4$CVD concept

This study developed an accurate model and active control thereof in simulation but did not investigate experimental implementation. During the simulation-based investigations, it became clear that the success of an active control strategy relies on accurately controlling the additional damping force. To control the solenoid valves to produce the desired damping force, the fluid flow though the valve needs to be known. Furthermore, with two flow paths, the different flow rates would need to be calculated first. However, requiring complex calculations at each time step to determine the flow through each valve is computationally demanding. Although further investigation would be required for confirmation, it might not be feasible to implement real time. It would be possible to have two accumulators of the same volume that yields equal flow rates. However, that would eliminate the third stiffness setting and also impose limits on the hard and soft stiffness combination.

An alternative 4S$_4$CVD concept is presented in Figure 6.1, which could reduce computational demand and greatly simplifies the control. This concept replaces the flow-control valves of the 4S$_4$CVD with two state valves that is only responsible for blocking flow and change stiffness characteristics. A pressure compensated flow control valve, or rather, a valve capable of producing variable damping, would then control the damping before the flow split between each accumulator. Due to the flow control valve not producing sufficient damping at low flow rates, a different valve design (such as a poppet-type valve) could be investigated which produces a more linear force vs velocity profile.

This would simplify the control as fluid flow through the valve is can be calculated and the control input can simply be selected to produce the desired damping. With the current 4S$_4$CVD design the

control input to each valve influences the flow split. If the fluid flow through the one valve is known, the control input needed to achieve the desired damping force can be determined. However, if that input is given that changes the flow through that valve (due to flow going through path of least resistance) and therefore that input won't achieve the desired damping force. To solve this problem the system could iteratively be solved until the control input would result in the desired damping force. This increases computational demand and possibly decreases accuracy due to iterative solving process when compared to the alternative $4S_4$CVD concept. This alternative concept could also reduce or possibly eliminate the need for flow-split calculations, if the damping over the two state valves due to small flow rate differences would be negligible. For comprehensive model, it would however need to calculate the flow-split during switching of the two-state valves (which could take up to 100ms) as that would generate significant damping. This setup would still allow three stiffness settings and continuously variable damping.

Results suggested that a single valve that was characterised would still produce sufficiently low damping to improve ride comfort. However, the additional valve adds flow restrictions, which could increase the damping. This could be compensated for by including a bypass valve, a larger valve or two valves in parallel.

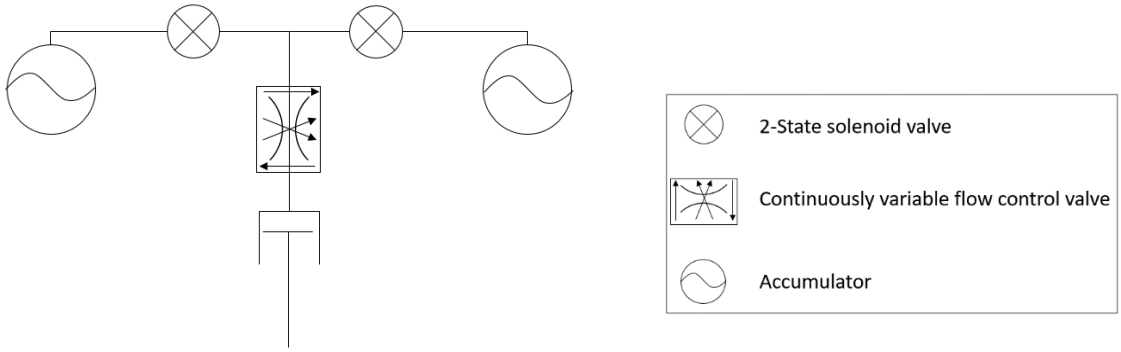


***Figure 6.1: Alternative $4S_4$CVD concept***

# REFERENCES

André, S. 2013. *Optimization of Valve Damping*, Masters Thesis, [Online]. Availible: http://www.diva-portal.org/smash/record.jsf?pid=diva2%3A699726&dswid=9525/ [Accessed 20 January 2018], Linköping University, Linköping, Sweden.

Armstrong-Hélouvry, B., Dupont, P. & De Wit, C. C. 1994. *A survey of models, analysis tools and compensation methods for the control of machines with friction*. Automatica, Vol. 30, pp. 1083-1138.

Breytenbach, H. 2009. *Optimal vehicle suspension characteristics for increaased structural fatigue life*, Unpublished M.Eng Masters, , University of Pretoria, South Africa, Pretoria.

British Standards Institution. 1987.*British Standard Guide to Measurement and Evaluation of Human Exposure to Whole Body Mechanical Vibration and Repeated Shock*, BS 6841.

Canale, M., Milanese, M. & Novara, C. 2006. *Semi-active suspension control using "fast" model-predictive techniques*. IEEE Transactions on control systems technology, Vol. 14, pp. 1034-1046.

Dorling, R., Smith, M. & Cebon, D. 1995. Achievable dynamic response of active suspensions in bounce and roll. *Advances in Automotive Control 1995.* Ascona, Switzerland: Elsevier.

Els, P. S. 2005. *The applicability of ride comfort standards to off-road vehicles*. Journal of Terramechanics, Vol. 42, pp. 47-64.

Els, P. S. 2006. *The Ride Comfort vs. Handling Compromise for Off-Road Vehicles*, PhD Thesis, [Online]. Availible: https://repository.up.ac.za/handle/2263/26302 [Accessed 10 July 2017], University of Pretoria, Pretoria, South Africa.

Els, P. S. & Grobbelaar, B. 1993. *Investigation of the Time-and Temperature Dependency of Hydro-Pneumatic Suspension Systems*. SAE Technical Paper Series no. 930265, pp. 55-65.

Els, P. S. & Van Niekerk, J. L. 1999. *Dynamic Modelling of an Off-Road Vehicle for the Design of a Semi-Active, Hydropneumatic Spring-Damper System*. Procedings of the 16th International Association for Vehicle System Dynamics (IAVSD), Pretoria, South Africa. August 30 to September 3, 1999.

Freudenberg. 2017. *Freudenberg Sealing Technologies* [Online]. Available: https://ecatalog.fst.com/seals/all/diaphragms/bfa/2198/bfa-70-60-70-0-253-diaphragm-standard---bead-type-a-with-fa/ [Accessed 10 July 2017].

Gillespie, T. D. 1992. *Fundamentals of Vehicle Dynamics,* Warrendale, PA, Society of Automotive Engineers.

Goncalves, F. D., Koo, J.-H. & Ahmadian, M. 2003. *Experimental approach for finding the response time of MR dampers for vehicle applications*. Procedings of ASME 2003 International Design Engineering Technical Conferences and Computers and Information in Engineering Conference, Illinois, USA. August 2 to September 6, 2003, pp. 425-430.

Grobler, J. F. 2016. *Multi-State Hydro-Pneumatic Suspension System Through the Use of Magneto-Rheological (MR) Valves*, Unpublished M.Eng Masters, , University of Pretoria, Pretoria, South Africa.

Guglielmino, E., Sireteanu, T., Stammers, C. W., Ghita, G. & Giuclea, M. 2008. *Semi-active suspension control: improved vehicle ride and road friendliness*, Springer Science & Business Media.

Harty, D. 2003. *Branding vehicle dynamics*. Automotive engineering international, Vol. 111, pp. 53-66.

Heymans, G. S. 2017. *Development Of A Magneto-Rheological (MR) Equipped Semi-Active Suspension System For Off-Road Vehicles*, Unpublished M.Eng Masters, [Online]. Availible: https://repository.up.ac.za/handle/2263/66204 [Accessed 12 July 2017], University of Pretoria, Pretoria, South Africa.

Hydraforce. 2013. *Electro-Proportional Valves* [Online]. Available: http://hydraforce.com/Proport/Prop_html/2-602-1_ZL70-30/2-602-1_ZL70-30.htm#view9 [Accessed 11 July 2017].

International Organization for Standardization. 1995.*International Standard ISO 8608: Mechanical vibration – Road surface profiles – Reporting of measured data*, ISO 3888-1:1999(E).

International Organization for Standardization. 1999.*International Standard ISO 3888-1: Passenger cars – Test track for a severe lane-change manoeuvre – Part 1: Double lane-change*, ISO 3888-1:1999(E).

Jacobsen, R. T. & Stewart, R. B. 1973. *Thermodynamic properties of nitrogen including liquid and vapor phases from 63K to 2000K with pressures to 10,000 bar*. Journal of Physical and Chemical Reference Data, Vol. 2, pp. 757-922.

Karnopp, D., Crosby, M. J. & Harwood, R. 1974. *Vibration control using semi-active force generators*. Journal of engineering for industry, Vol. 96, pp. 619-626.

Koo, J.-H., Goncalves, F. D. & Ahmadian, M. 2006. *A comprehensive analysis of the response time of MR dampers*. Smart materials and structures, Vol. 15, pp. 351.

Mathworks. 2015. *MATLAB and Simulink* [Online]. Available: http://www.mathworks.com/ [Accessed 20 July 2016].

Meeser, R. F. 2015. *Magneto-rheological (MR) Damper design for off-road vehicle suspensions with flow blocking ability.* University of Pretoria.

Msc Software. 2016. *Adams* [Online]. MSC Software Corporation. Available: http://www.mscsoftware.com/product/adams [Accessed 15 January 2017].

National Highway Traffic Safety Administration. 2010. *Rollover Fatalities* [Online]. Available: https://www.safercar.gov/Vehicle-Shoppers/Rollover/Fatalities [Accessed 31 January 2018].

Öhlins Racing. 2018. *Öhlins CES history* [Online]. Available: https://www.ohlins.com/products/ces/ohlins-ces-history/ [Accessed 10 January 2018].

Otis, D. & Pourmovahed, A. 1985. *An algorithm for computing nonflow gas processes in gas springs and hydropneumatic accumulators*. Journal of dynamic systems, measurement, and control, Vol. 107, pp. 93-96.

Paddan, G. S. & Griffin, M. J. 2002. *Evaluation of whole-body vibration in vehicles*. Journal of sound and vibration, Vol. 253, pp. 195-213.

Pourmovahed, A. & Otis, D. 1990. *An experimental thermal time-constant correlation for hydraulic accumulators*. Journal of dynamic systems, measurement, and control, Vol. 112, pp. 116-121.

Poussot-Vassal, C., Savaresi, S. M., Spelta, C., Sename, O. & Dugard, L. *A Methodology for optimal semi-active suspension systems performance evaluation*. Precedings of 49th IEEE Conference: Decision and Control (CDC). December 15 to December 17, 2010, IEEE, pp. 2892-2897.

Poussot-Vassal, C., Sename, O., Dugard, L., Ramirez-Mendoza, R. & Flores, L. 2006. *Optimal Skyhook Control for Semi-Active Suspensions*. IFAC Proceedings Volumes, Vol. 39, pp. 608-613.

Rs Components. 2018. *Multiple Output Linear DC Power Supply* [Online]. Available: https://docs-emea.rs-online.com/webdocs/156d/0900766b8156d936.pdf [Accessed 20 January 2018].

Sammier, D., Sename, O. & Dugard, L. 2003. *Skyhook and H8 control of semi-active suspensions: some practical aspects*. Vehicle System Dynamics, Vol. 39, pp. 279-308.

Savaresi, S. M., Poussot-Vassal, C., Spelta, C., Sename, O. & Dugard, L. 2010. *Semi-active suspension control design for vehicles,* Oxford, Elsevier.

Shell. 2016. *Shell Tellus S2 V 46* [Online]. Available: https://www.shell.co.za/business-customers/industrial-lubricants/lubricants-product-range/shell-tellus-hydraulic-fluids/_jcr_content/par/textimage_ff00.stream/1486050963469/a1c5fc9c1d6946d52f8000acd155f41f6d74f2b806e777518db6ca948f152875/shell-tellus-s2-v-46.pdf [Accessed 20 February 2018].

Spelta, C., Savaresi, S., Moneta, A., Tosi, F., Fabbri, L. & Nardo, L. *Semi-Active Control Strategies for High-Performance Motorcycles*. 17th IFAC World Congress. 2008, 4689-4694.

Spencer Jr, B., Dyke, S., Sain, M. & Carlson, J. 1997. *Phenomenological model for magnetorheological dampers*. Journal of engineering mechanics, Vol. 123, pp. 230-238.

Theron, N. J. & Els, P. S. 2007. *Modelling of a semi-active hydropneumatic spring-damper unit*. International Journal of Vehicle Design, Vol. 45, pp. 501-521.

Thoresson, M. J., Uys, P. E., Els, P. S. & Snyman, J. A. 2009. *Efficient optimisation of a vehicle suspension system, using a gradient-based approximation method, Part 1: Mathematical modelling*. Mathematical and Computer Modelling, Vol. 50, pp. 1421-1436.

Tsampardoukas, G., Stammers, C. W. & Guglielmino, E. 2008. *Hybrid balance control of a magnetorheological truck suspension*. Journal of Sound and Vibration, Vol. 317, pp. 514-536.

Uys, P. E., Els, P. S. & Thoresson, M. J. 2006. *Criteria for handling measurement*. Journal of Terramechanics, Vol. 43, pp. 43-67.

Uys, P. E., Els, P. S. & Thoresson, M. J. 2007. *Suspension settings for optimal ride comfort of off-road vehicles travelling on roads with different roughness and speeds*. Journal of Terramechanics, Vol. 44, pp. 163-175.

Van Den Bergh, J.-S. 2014. *Effects of friction and gas modelling on vehicle dynamics simulation*, Unpublished M.Eng Masters, , University of Pretoria, Pretoria, South Africa.

Van Der Westhuizen, S. F. & Els, P. S. 2015. *Comparison of different gas models to calculate the spring force of a hydropneumatic suspension*. Journal of Terramechanics, Vol. 57, pp. 41-59.

Van Rensburg, N. J., Steyn, J. & Els, P. 2002. *Time delay in a semi-active damper: modelling the bypass valve*. Journal of Terramechanics, Vol. 39, pp. 35-45.

Vaughan, N. & Gamble, J. 1996. *The modeling and simulation of a proportional solenoid valve*. Journal of dynamic systems, measurement, and control, Vol. 118, pp. 120-125.

Voigt, K. G. 2006. *Semi-active spring and damper control for ride comfort*, Draft copy of Masters degree thesis at University of Pretoria submitted to study leaders, Prof. N.J. Theron and Prof. P.S. Els, for review.,

Zwick Roell. 2018. *Zwick K7500 Electronics* [Online]. Available: http://www.kutlultd.com.tr/files/downloads/pdf/dynamic/servocontroller/K7500.pdf [Accessed 20 January 2018].

# APPENDIX

## A. BWR constants for Nitrogen

Constants for the BWR equation (Els and Grobbelaar, 1993):

$a = 0.115703387 \left[\left(\frac{m^3}{kg}\right)^3 \frac{N}{m^2}\right]$

$A_0 = 136.0474619 \left[\left(\frac{m^3}{kg}\right)^3 \frac{N}{m^2}\right]$

$b = 2.96625 \times 10^{-6} \left[\left(\frac{m^3}{kg}\right)^3\right]$

$B_0 = 0.001454417 \left[\frac{m^3}{kg}\right]$

$c = 7.3806143 \times 10^{-5} \left[\left(\frac{m^3}{kg}\right)^3 K^2 \frac{N}{m^2}\right]$

$C_0 = 1.0405873 \times 10^{-6} \left[\left(\frac{m^3}{kg}\right)^3 K^2 \frac{N}{m^2}\right]$

$\alpha = 5.863972 \times 10^{-9} \left[\left(\frac{m^3}{kg}\right)^3\right]$

$\gamma = 6.7539311 \times 10^{-6} \left[\left(\frac{m^3}{kg}\right)^2\right]$

$R = 296.797 \left[\frac{J}{kgK}\right]$

Constants for the calculation of the IG specific heat capacity for nitrogen (Jacobsen and Stewart, 1973):

$N_1 = -735.210$
$N_2 = 34.224$
$N_3 = -0.557648$
$N_4 = 3.5040$
$N_5 = -1.7339 \times 10^{-5}$
$N_6 = 1.7465 \times 10^{-8}$
$N_7 = -3.5689 \times 10^{-12}$
$N_8 = 1.0054$
$N_9 = 3353.4061$
$y = N_9/T$

## B. Pressure drop over valve modelling

Various methods were investigated and assessed to determine which method of curve-fitting would yield accurate results. The decision was taken to first investigate whether a basic surface fit could be applied to the limited data to approximate the pressure drop over the valve before trying other more complex techniques. Figure B.1 to Figure B.4 show the model and data comparison for linear interpolation, cubic interpolation, thin-plate spline interpolation and locally weighted scatterplot smoothing (LOWESS) respectively. The pressure, velocity and current surface plot of each model are shown alongside its pressure drop versus velocity for clarification.

As expected, all three interpolation methods approximate the test data given as input very well. However, when examining the pressure drop output for currents not tested at (especially between

0.9A and 1.2A) it is clear some methods fall short. The 1.05A pressure drop output given by the linear and cubic interpolation model can be seen to be biased to the 1.2A data and then abruptly changes when the velocity exceeds that of the 1.2A data. Evidently, this would not approximate the actual pressure drop accurately. The thin-plate spline method, on the other hand, shows a much smoother transition and yields a pressure drop closer to what is realistically expected. Although the shape at 1A and 1.1A can be seen to slightly deviate from expected results, it is within reasonable bounds. The LOWESS method, which is essentially a combination of a regression and nearest neighbour method, does show promising results as it preserves the shape fairly well. However, despite numerous iterations of tuning it remained unable to provide a smooth and also accurate pressure drop output. The discontinuities can clearly be noted in the surface plot around 1A and smoothing causes the fit to deviate from the test data.

It should be noted that, in each case, the inaccuracy appeared when there were large pressure differences between each of the recorded current settings, for example, between 0.9A and 1.2A at 200mm/s. For a more accurate fit, additional test data would therefore be required to obtain a more refined data set as input. The LOWESS and thin-plate spline methods both have the advantage of extending past the given data, which is advantageous in simulation that would otherwise be unsolvable when it falls out of bounds. Evidently, the thin-plate spline interpolation method results in superior pressure drop predictions. For this application the thin-plate spline method was deemed suitable to predict the pressure drop over the valve for a given velocity and current combination.

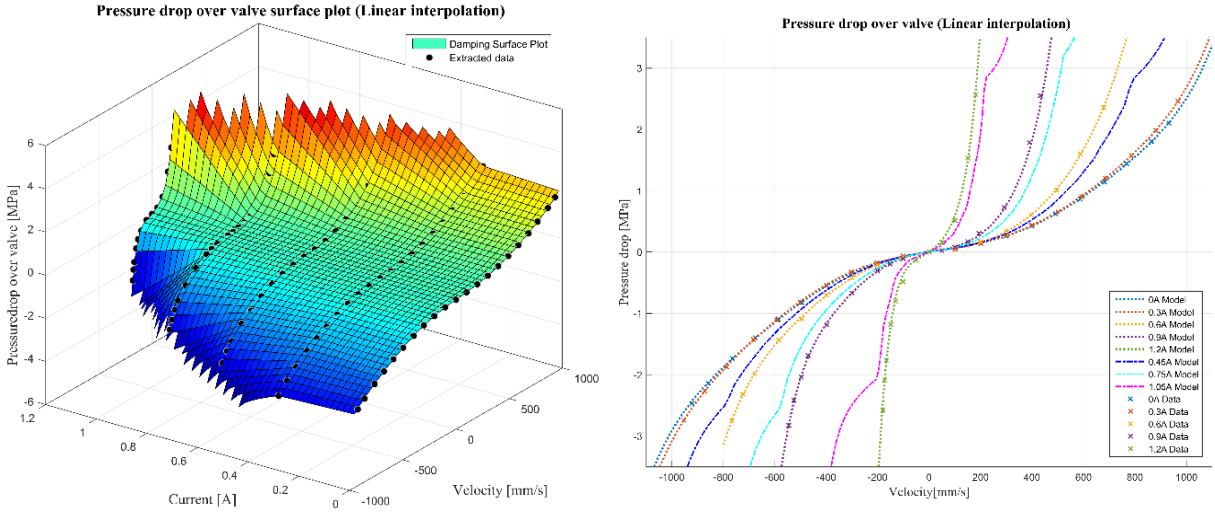


***Figure B.1: Linear interpolation pressure drop model***

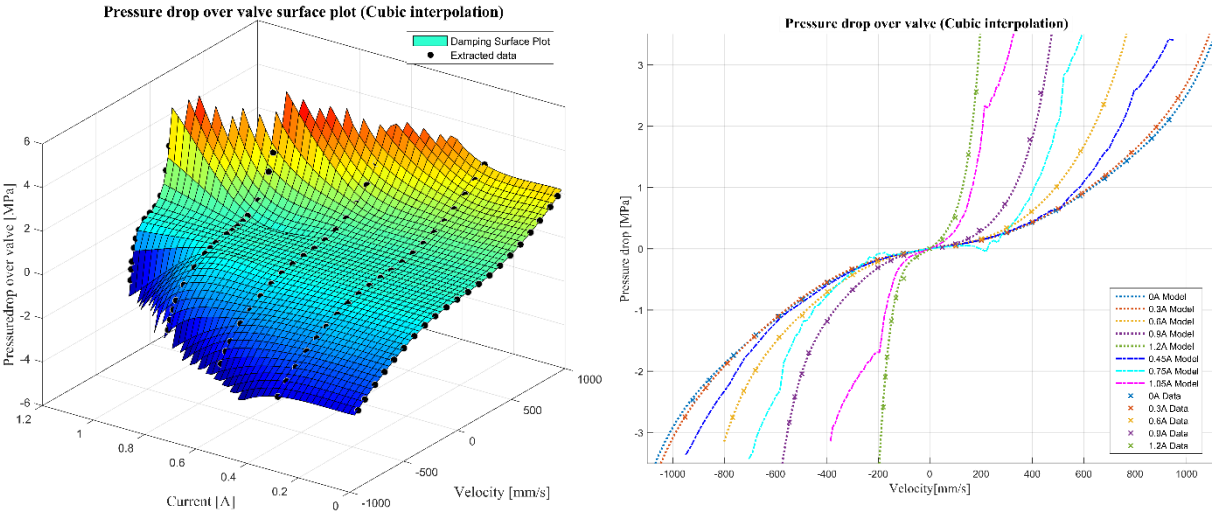

*Figure B.2: Cubic interpolation pressure drop model*

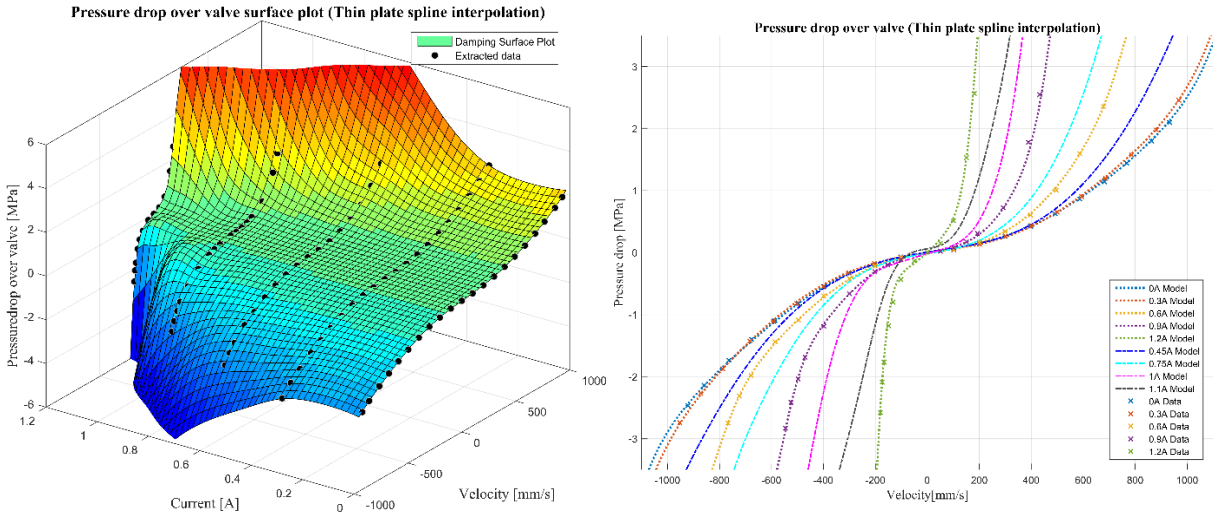


*Figure B.3: Thin-plate spline interpolation pressure drop model*

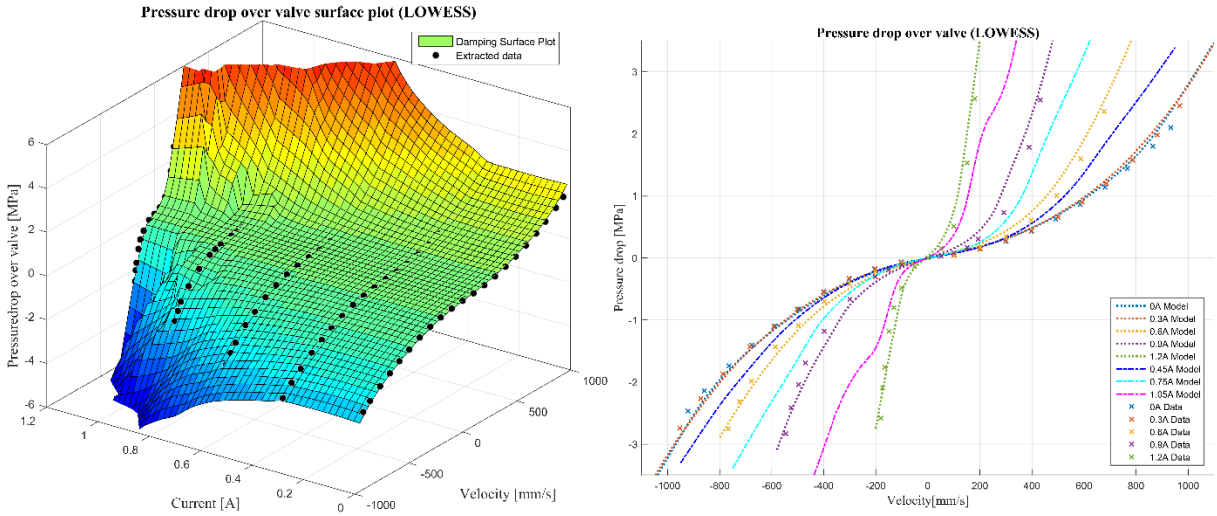


*Figure B.4: LOWESS pressure drop model*